Investigating the Effects of Methylmercury on Tetanus Induced Synaptic Plasticity in CA1 of Rat Hippocampus Using A Newly Developed MEA Protocol

by

Tony Fong

-

A thesis

presented to the University of Waterloo

in fulfillment of the

thesis requirement for the degree of

Master of Science

in

Public Health and Health Systems

Waterloo, Ontario, Canada, 2019

© Tony Fong 2019

Author’s Declaration

I hereby declare that I am the sole author of this thesis. This is a true copy of the thesis, including any required final revisions, as accepted by my examiners.

I understand that my thesis may be made electronically available to the public.

Abstract

Background: Methylmercury (MeHg) is a neurotoxicant that induces sensorimotor dysfunction at high levels. However, the majority of the world's populations are exposed at lower levels, at which the effects and mechanisms are less certain. Evidence from the past few decades suggests that low levels of MeHg may impair learning and memory. Long-term potentiation (LTP) in acute hippocampal slices is a cellular model of memory and learning. Hence, LTP may be a useful model to study the detrimental effects and mechanisms of MeHg on learning and memory. However, LTP studies often report large variability in potentiation magnitude between studies, making it difficult to consistently detect small effects. The large variability may be, in part, due to a disregard of the recording distance to the soma and the slice origin along the longitudinal axis.

Objectives: 1. To develop a more precise LTP protocol which incorporates the distance of the recording point to the soma and slice of origin along the longitudinal axis. **2.** Using the newly developed experimental protocol to investigate the effects of MeHg, at levels that do not affect basal transmission, on synaptic plasticity.

Methods: Evoked responses at different distances to the neuronal soma in the CA1 region of acute rat hippocampal slices stratified by pole of origin along the longitudinal axis were recorded using a multi-electrode array. LTP was induced with a tetanus protocol (2 trains at 100 Hz, intertrain duration: 20 s). Notable components of the evoked waveform across the experiment were identified using principal component analysis. In the toxicity study, different doses of MeHg (0, 0.1, 1, 5 μM) containing ACSF was perfused to the slice for 20 minutes before LTP induction. In addition, slices were exposed to APV (50 nM) as a positive control. All statistical analyses were conducted using a random intercept linear mixed model.

Results: Two components, the field excitatory post-synaptic potentiation (fEPSP) and the positive going aspect (PGA), were identified in the PCA. An fEPSP potentiation gradient in which the degree of potentiation was inversely proportional to the distance of the recording point to the soma was found more prominent in ventral slices but less in dorsal slices. In both dorsal and ventral slices, the PGA was potentiated at distal recording points while depressed at proximal recording points to the soma. In slices from both poles, both fEPSP and PGA changes post-tetanus were found to be mainly driven by NMDA receptors. Interestingly, fEPSP

potentiation in dorsal slices showed to contain an NMDA-independent component. Furthermore, preliminary results suggest that 5 μM MeHg may depress fEPSP potentiation and increase PGA potentiation post-tetanus.

Conclusion: The current study calls for the attention to record and analysis both the fEPSP and PGA in LTP studies. Most importantly, recording and analysis should be stratified by: i) recording distance to the neuronal soma and ii) origin of the slice along the longitudinal axis. Furthermore, the developed method is showing some promises in studying the effects of MeHg on learning and memory.

Acknowledgements

First, I would like to express my greatest gratitude to my supervisor Dr. Brian Laird for his continuous support during my MSc degree. I will always remember the moments where you have extended a helping hand during the hardships I encountered. I am and will forever be indebted to you for this degree. To my co-advisor, Dr. John Mielke, I thank you for allowing me to use the equipment and for providing feedback to my work. I would also like to sincerely thank my committee members, Dr. Laurie Chan and Dr. Diane Williams for donating their time and expertise to this thesis.

Taking this opportunity, I would also like to extend my gratitude to Dr. Paul Marriott and Dr. Reza Ramezan for patiently aiding and teaching me the analytical methodologies. I have learned a lot from both of you and gained many skills that will further my career. I also thank Dr. Reza Ramezan for acting as a mentor guiding me through the hardships in graduate school.

Finally, I would like to thank my friends and family for supporting me to pursue this degree. In particular to my parents, I would not have achieved the current accomplishment without the unconditional support and love you have shown me. I also thank my colleagues. It was incredible to have worked with you.

Table of Contents

List of Figures

List of Tables

List of Abbreviations

α-amino-3-hydroxy-5-methyl-4-isoxazolepropionic acid (AMPA)

Artificial cerebrospinal fluid (ACSF)

2-amino-5-phosphonovaleric acid (APV)

Cornu Ammonis (CA)

Cyanquixaline (CNQX)

Dentate gyrus (DG)

Docosahexaenoic acid (DHA)

Eicosapentaenoic acid (EPA)

Field excitatory post-synaptic potential (fEPSP)

Field inhibitory post-synaptic potential (fIPSP)

Gamma-Aminobutyric Acid (GABA)

Long-term potentiation (LTP)

Long-term depression (LTD)

Methylmercury (MeHg)

N-methyl-D-aspartate (NMDA)

Positive going aspect (PGA)

Principal component analysis (PCA)

Schaffer collateral (SC)

Sprague Dawley (SD)

Stratum lancunosum-moleculare (SLM)

Stratum oriens (SO)

Stratum pyramidal (SP)

Stratum radiatum (SR)

Wet Weight (ww)

1.0 Overview

Methylmercury (MeHg) is a hazardous organometal naturally produced as a result of inorganic mercury methylation by marine and freshwater microorganisms (Hong, Kim, & Lee, 2012). Globally, humans are primarily exposed through the consumption of contaminated seafood and, on occasion, via some grains, such as rice (Rothenberg et al., 2016). MeHg is particularly known for its neurotoxicity; at high levels it can cause widespread neuropathy. For example, large-scale MeHg poisonings in Iraq and Japan revealed that the symptoms of MeHg toxicity include motor disturbances and dysesthesia (Ekino, Susa, Ninomiya, Imamura, & Kitamura, 2007; Harada, 1995). Fortunately, brain levels of MeHg seen in cases such as in Minamata, Japan and Iraq are extremely rare. Even in populations around volcanic islands that regularly consume fish (e.g., such as those living in the Faroe Islands), MeHg levels in brain are still more than two-fold lower than what was seen in cases during the Minamata tragedy (Lapham et al., 1995). Therefore, for the majority of the world's population, concerns regarding lower exposure levels of MeHg are of far greater toxicological relevance. Evidence from epidemiological and toxicological studies have suggested that lower levels of MeHg may impair learning and neurological development in youth (Debes et al., 2016; Karpova et al., 2014).

Long term potentiation (LTP) is a model of synaptic plasticity and is widely accepted as a cellular and molecular correlate for learning and memory (Bliss & Collingridge, 1993). In essence, LTP is a long-lasting increase in transmission strength between neurons that has been observed following certain patterns of electrical stimulation. Studies are mostly conducted in the Schaffer collateral pathway of acutely prepared hippocampal slices (Nicoll, 2017). Considering MeHg may impair learning and memory at lower exposure levels, LTP may be an effective model to study the underlying physiology of its neurotoxicity. However, the degree of potentiation observed across

LTP studies varies greatly rendering results incomparable and inconsistent among studies. Hence, small effects on LTP magnitude cannot be consistently detected across studies. This variability may arise as a result of a disregard of where the slice is taken along the longitudinal axis and the recording position of the potentiation. Substantial evidence have suggested that synaptic plasticity expression are different in regions along the hippocampal longitudinal (dorsal-ventral) axis (Strange, Witter, Lein, & Moser, 2014). Moreover, there is currently no standardization or understanding of the effects of recording position in LTP studies. Therefore, I have developed a multi-electrode array protocol which measures LTP at various distances to the neuronal soma in slices stratified by pole of origin along the longitudinal axis of the hippocampus. Furthermore, LTP expression differences between male and female were investigated using this newly developed protocol as evidence suggested a difference in potentiation between the two sexes (Hyer, Phillips, & Neigh, 2018). Ultimately, this assay will be used to investigate the effects of low levels of MeHg exposure on synaptic plasticity.

2.0 Introduction

2.1 Implications from Chronic Exposure to Low Level Methylmercury

MeHg has been documented to induce a wide range of toxicity in the neurophysiology, neurodevelopment, and cardiovascular system. In the cardiovascular system, MeHg has been associated with increased risk for hypertension, ischemic events and myocardial infarction (Stern, 2005). With regards nervous system, MeHg is known and established to cause motor sensory dysfunction, speech impediment, seizures and tremors (Ekino et al., 2007). However, epidemiological evidence describing the effects of relatively low levels of MeHg on neurodevelopment has been inconsistent.

In contrast to high levels of exposure, the mechanisms and effects of chronic low levels of MeHg exposure in neurophysiology is less clear (Bradford et al., 2016). In adults, MeHg is well established to induce sensorimotor and epilepsy at high levels in adults (Ekino et al., 2007). At high levels, MeHg induced neurotrophy and cell death occurs. Current evidence presents the possibility that prolonged low levels of MeHg can interfere with normal neuronal development in neonate and children. As a result, MeHg leads to disruption in higher cognitive skills, such as learning and memory (Debes et al., 2016). However, the mechanism resulting in both neurotrophy or improper neuronal development are still under debate. Most importantly, it is unclear if there is an overlap of mechanisms in neurotrophy and neuronal development.

2.1.1 Epidemiological Studies

Results from epidemiological studies have been inconsistent to show adverse MeHg effects on neurodevelopment and learning. Large cohorts from New Zealand and Faroe Islands found that maternal hair mercury levels were correlated with decreases in a child's performance in cognitive

tests at a young age (Crump et al., 1998; Debes et al., 2016). More importantly, Debes et al. (2016) showed that, in the Faroe Island cohort, the decrease in cognitive performance still persist at later stages of life. In contrast, Myers et al. (2009) found no correlation between maternal hair mercury levels and a child's intelligence quotient between 6 months and 9 years of age in the Seychelles child development study.

One explanation for the inconsistent results among epidemiological studies is that essential nutrients in fish, such as DHA and EPA, may counteract, or dampen MeHg toxicity (Grandjean & Herz, 2011). A recent study by Rothenberg et al. (2016) found that associations of maternal hair mercury and offspring mental development in a population that rarely consumes fish were strengthened after adjusting for seafood consumption. The converse has also been found true, which further strengthens this explanation; that is, MeHg suppresses benefits of essential nutrients on neurodevelopment (Oken et al., 2016). One study found that neither maternal DHA, EPA, nor MeHg levels were correlated with offspring cognitive tests in a U.S population, which contradicts the widely accepted view that DHA and EPA are beneficial to neurodevelopment (Oken et al., 2016). These evidences suggest that the detrimental effects of low-level chronic exposure to MeHg are difficult to consistently detect.

2.1.2 Learning Deficits in Rodents

In the past decade, rodent studies have indicated that low levels of MeHg exposure at a young age can result in learning deficits that persist through adolescence and to young adulthood. A single subcutaneous injection of 0.6 mg/kg MeHg on postnatal day 7, which resulted in a brain level of approximately 0.5 µg/g (ww), was able to induce spatial memory deficits in Sprague-Dawley (SD) rats at postnatal day 35 (Falluel-Morel et al., 2007; Sokolowski et al., 2013). Other studies employing a more chronic paradigm have also found similar results. For example, postnatal

day 5 SD rats that received 0.4 mg/kg/day intraperitoneal injection of MeHg for 28 days were shown to have a higher escape latency in the Morris Water Maze (Tian et al., 2016). These data suggest that rodent models may be useful for studying the effects of MeHg on the nervous system in regards to development and function.

2.1.3 Hippocampus: A Target of Methylmercury Toxicity

Methylmercury induced impairments on memory and learning are likely as a result of its underlying effects on the hippocampus, given the critical role of the hippocampus in learning and memory (Neves, Cooke, & Bliss, 2008). Indeed, substantial evidence has shown that MeHg accumulates in the hippocampus and, in turn, may alter normal neurological functions (Falluel-Morel et al., 2007; Kakita et al., 2000; Sakamoto et al., 2004; Sokolowski et al., 2013). Further evidence also shows that the sensitivity of the hippocampus to MeHg can surpass all other brain regions at certain stages of neurodevelopment (Wakabayashi et al., 1995). During the postnatal period, MeHg exposure was shown to selectively decrease neuronal stem cell count in the hippocampus without affecting the cerebellum (Falluel-Morel et al., 2007). Interestingly, hippocampal neuronal stem cell generation still persists throughout adulthood and plays an important role in memory and cognitive function (Gonçalves et al., 2016), which may explain the effects of MeHg exposure on cognition extending from early life to later stages of life observed in both rodents and humans.

2.2 Hippocampus

The hippocampus is located within the medial temporal lobe of each hemisphere, and is involved in learning and memory formation across mammalian species (Bunsey & Eichenbaum, 1996). In addition to its functionality, its structure and morphology are generally well-conserved among mammals (Knowles, 1992). Components of the hippocampal formation include the dentate

gyrus (DG), subiculum, and the hippocampus proper (Cornu Ammonis; CA), which then can be further divided into CA1 and CA3 sub-fields (Knowles, 1992), as seen in Figure 2.1. Given its well conserved functionality and morphology, the hippocampus is therefore widely used for comparative neurological studies.

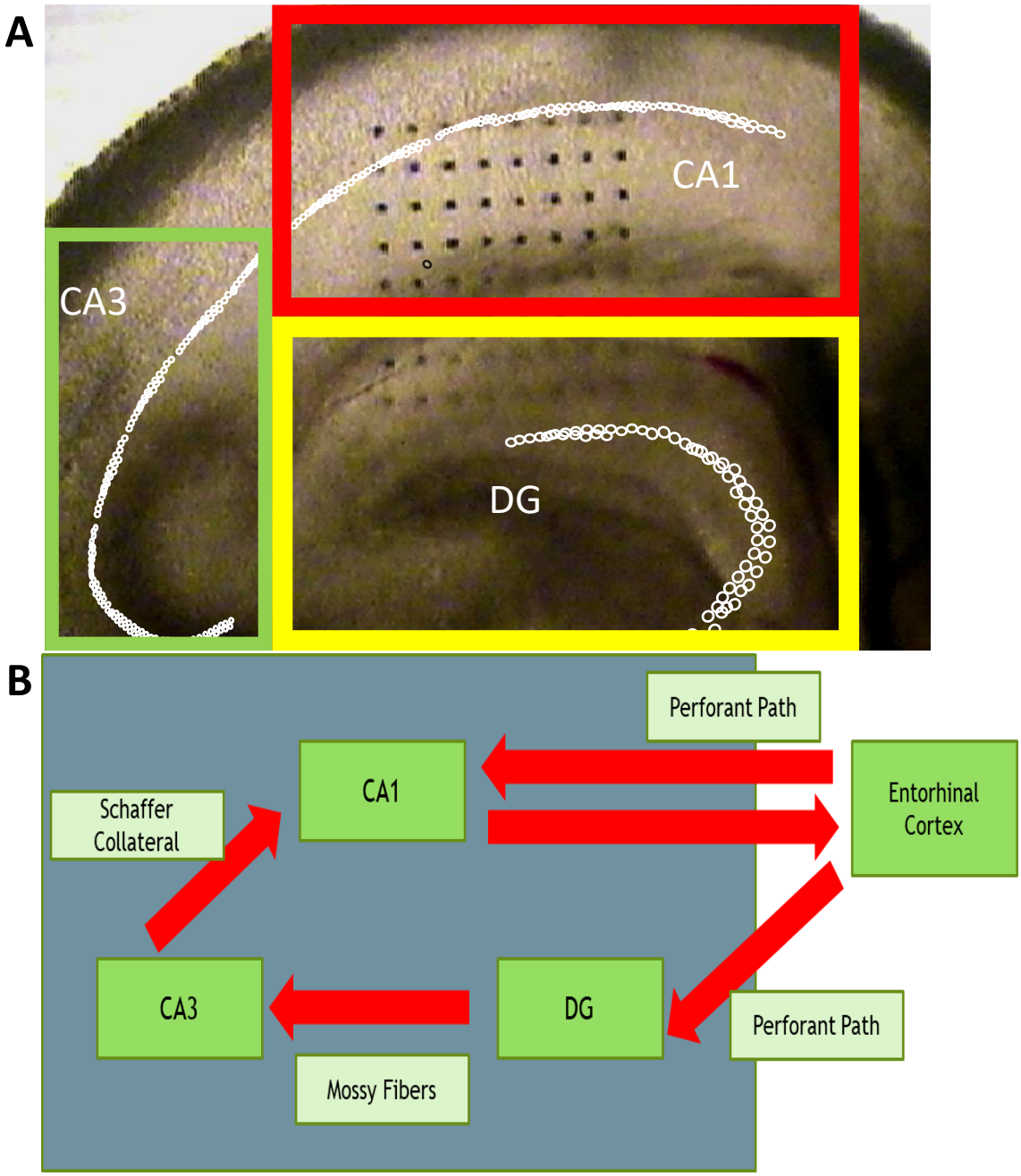

Figure 2.1 The Structure of the Hippocampus. A. An image of a transverse hippocampal slice on a multi-electrode array. Yellow: the DG region; Green: CA3 region; Red: CA1 region. B. A schematic representation of the connection between the subfields shown in A. Excitatory axons from the perforant pathway connect to the granule cells of the DG, which are then connected to the pyramidal cells of CA3. In turn, the excitatory connections via the Schaffer Collaterals synapse on the apical and basal dendrites of pyramidal cells of the CA1 subfield. The perforant pathway also directly synapses at the apical dendrites of the CA1 subfield. CA: Cornu Ammonis; DG: dentate gyrus.

2.2.1 Functional Segregation Along the Longitudinal Axis of the Hippocampus

It is now apparent that the hippocampus is not a unitary structure and that the contribution of the hippocampus to behavioral and cognitive tasks varies along the longitudinal axis (Strange et al., 2014). Lesion studies provided evidence for functional dissociation along the longitudinal axis (Dorsal-Ventral) of the hippocampus by showing that the dorsal hippocampus plays a crucial role in spatial learning and declarative memory, whereas the ventral hippocampus is involved in emotional responses such as anxiety, stress and depression (Fanselow & Dong, 2010). Figure 2.2 presents an illustration of the hippocampus in a rat brain with the dorsal and ventral poles.

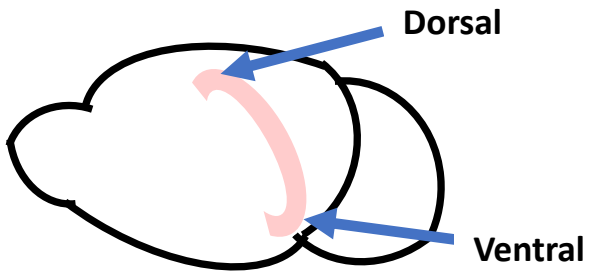

Figure 2.2 Hippocampus Orientation in a Rat Brain. Due to its orientation, the hippocampus can be sub-divided into dorsal and ventral poles.

Segregation in functionality is believed to stem from differences in biochemical, electrophysiological, and anatomical properties. Numerous receptors and channels, including NMDA and potassium channels, are unequally distributed along the longitudinal axis of the hippocampus (Dougherty et al., 2013; Dubovyk & Manahan-Vaughan, 2018). Consistent results across electrophysiological studies have indicated that pyramidal neurons are more excitable in the ventral hippocampus (Dougherty et al., 2013; Papatheodoropoulos, 2015a). Anatomically, the dorsal and ventral poles of the hippocampus differ with respect to their afferent connections to the

entorhinal cortex and their efferent connections to other cortical and subcortical structures (Dougherty et al., 2013).

Interestingly, susceptibility to specific pathologies and insults is also different between the dorsal and ventral poles. Ventral hippocampus has a higher susceptibility to epileptic activity. Papaheodoropoulos et. al. (2015) showed that slices from the ventral pole of the hippocampus are more likely to display epileptiform discharges than their dorsal counterparts. In contrast, the dorsal hippocampus is more susceptible to ischemic insults (Ashton, Van Reempts, Haseldonckx, & Willems, 1989). It is not yet known if such differences in susceptibility are also observed in MeHg toxicity.

2.2.2 Hippocampus Circuitry

In the hippocampus, unilateral excitatory synapses project and link the DG, CA3 and CA1 subfields forming the tri-synaptic circuit (Amaral, Scharfman, & Lavenex, 2007). Excitatory synapses from the entorhinal cortex project on to granule cells via the perforant pathway. From the granule cells, mossy fibers form synapses with pyramidal cells of the CA3 subfield. From the CA3 pyramidal cells, axons divide into two pathways. One path consists of the commissural fibers that project to the contralateral hippocampus, while the other forms the final connections of the tri-synaptic circuit involving the Schaffer collaterals and the apical and basal dendrites of the pyramidal cells in the CA1 subfield, which then send information back to the entorhinal cortex.

2.2.3 Hippocampal Slices

Acute hippocampal slices are an excellent tool for pharmacological and toxicological studies (Lein et al, 2011). Due to the orientation of the hippocampal neurons, large numbers of synaptic connections are preserved even after slicing at different orientations (Andersen et al., 1971). Hippocampal slices can be prepared and maintained with relative ease, but, at the same

time, maintain high similarity in neurophysiology to their *in vivo* counterpart (Lein et al., 2011). Most importantly, their structure and synaptic circuits are readily accessible for electrophysiological studies of specific pathways (Lein et al., 2011). In addition, experimental conditions can be precisely controlled. Thus, hippocampal slices have proven to be a powerful model for investigating changes in functional features of synaptic connectivity in the absence of many external factors that may contribute to inter-individual variability seen *in vivo*. In the case of methylmercury, acute hippocampal slices may control and test for effects of differential nutrient exposures which may cause the wide range of vulnerability of MeHg toxicity observed *in vivo*.

2.2.4 Lamina Structure of the CA1 Subfield

After slicing, hippocampal pyramidal cell dendrites and many of their connections lay in the same plane forming a highly organized lamellar structure. Within the CA1, pyramidal cells span the stratum oriens (SO; containing the basal dendrites), stratum pyramidal (SP; containing the cell body), stratum radiatum (SR; containing the proximal segment of the apical dendrites), and stratum lancunosum-moleculare (SLM; containing the distal segment of the apical dendrites) layers (Spruston, 2008). The regions are relatively recognizable under a dissecting microscope and act as hallmarks for electrode placement to stimulate designated pathways in electrophysiological recordings.

2.3 Synaptic Plasticity

Synaptic plasticity is the ability of neurons to modify their synaptic activities as a result of specific stimulation patterns (Bliss & Collingridge, 1993). The notion was first introduced by Donald Hebb, who postulated that repeated activation of one neuron by another induces long-lasting cellular changes that result in an increased synaptic connection between the two neurons (Hebb, 1955). The first experimental evidence for Hebb's postulate was discovered by Bliss and

Lomo in the hippocampus of anaesthetized rabbits. Specifically, they found that high-frequency electrical stimulation applied to the perforant pathway increased the field excitatory post-synaptic potential (fEPSP) measured in the dentate gyrus. The phenomenon was coined long-term potentiation (LTP). The view of LTP as a cellular mechanism for learning and memory formation has become widely held (Bliss & Collingridge, 1993).

2.3.1 Long-Term-Potentiation

Since its discovery, LTP has been found and described at many different synapses in the central and peripheral nervous systems, but the most well characterized synapse is that of the Schaffer collateral/commissural projection to the CA1 pyramidal cells (SC-CA1). The main reason being that CA1 pyramidal cell activity represents the primary output of the hippocampus (Spruston, 2008). Typically, LTP in this pathway is induced by repetitive high-frequency (100 Hz) trains of electrical stimulation applied in intervals (Bliss & Collingridge, 2013; Volianskis et al., 2015).

The degree of potentiation varies greatly among LTP studies and is often ignored as the typical approach involves intra-study comparisons. Differences in LTP magnitude of control samples (non-drug treated, or genetically modified) between studies can be as high as 100% (T. V. Bliss & Collingridge, 2013; Ko et al., 2014; Lei et al., 2016; Suárez, Bustamante, Orensanz, Martín del Río, & Solís, 2014). Most studies have investigated tetanus induced potentiation of evoked responses in the SC-CA1 pathway of acutely prepared hippocampus slices. The general framework of the procedure involves the quick extraction of a rodent brain into chilled salt solution, which is then sliced to 350-450 µm thickness with a vibratome, or a tissue chopper and preserved in warm oxygenated salt solution until use. During an experiment, a stimulating and a recording electrode are placed in the CA1 region of the hippocampus at the investigator/experimenter's discretion. Although the general framework is conserved in all

studies, various differences among experimental settings exist, such as the manner of slice preparation, slice maintenance, and recording. Hence, many investigators dismiss variations in LTP magnitude as of technical origin, as opposed to considering that such variation may also partly represent an underlying physiological phenomenon.

2.3.2 LTP Magnitude Variation Within the CA1 Stratum Radiatum

LTP magnitude, or expression within the SR is correlated with distance between the site of recording and the pyramidal soma. Kopanitsa et al. (2006) observed a clear LTP magnitude gradient within the SR in the hippocampus slices. The magnitude of LTP was seen to be highest near the soma with an average 100% potentiation over baseline, while potentiation in the distal SR reached only a 10% increase over baseline.

Recent evidence suggests that the dendrites in the SR are not homogenous and exhibit differences in synaptic connectivity. AMPA and dopamine receptors are shown to have a distance dependent gradient in distribution throughout the dendrites of the SR (Nicholson et al., 2006). A distance dependent gradient in innervation density is seen along the CA1 apical dendrites (Edelmann et al.,2017). In regards to AMPA receptors, the number of perforated synapses and AMPA receptor density increased within the SR in proportion with distance from the soma (Nicholson et al., 2006).

2.3.3 Glutamate Receptor Mediated Long-Term Potentiation

NMDA receptors allow for the influx of calcium ions. Excitatory transmission involves the release of glutamate from the presynaptic terminal and its binding to the α-amino-3-hydroxy-5-methyl-4-isoxazolepropionic acid (AMPA) and NMDA glutamate receptors at the post-synaptic terminal (Bliss & Collingridge, 2013; Volianskis et al., 2015). The activation of the AMPA receptors allows Na^+ influx causing depolarization, which contributes to the downward

deflection observed in the fEPSP. On the other hand, NMDA receptors allow for both Na^+ and Ca^{2+} influx, but are blocked by Mg^{2+} at resting membrane potential, and thus contribute little to the initial fEPSP response. However, sufficient presynaptic activation leads to the release of Mg^{2+} from the NMDA channels. Once the NMDA receptors are unblocked, the inward flow of Na^+ and Ca^{2+} occurs. Accumulation of intracellular Ca^{2+} acts as a secondary messenger for a range cellular cascades, which, in part, modify AMPA receptor properties, such as conductance, and numbers on the postsynaptic terminal. The resultant increase in AMPA receptor function mediates the elevated fEPSP slope, or amplitude observed in LTP.

The activation of N-methyl-D-aspartate (NMDA) glutamate receptors is essential for the induction of LTP at SC-CA1 synapses. The discovery of the essential role of the NMDA receptor dates back to 1983 (Collingridge et al., 1983). It was found that the addition NMDA receptor selective antagonist DL-2-Amino-5-phosphonopentanoic acid (APV) resulted in no LTP after tetanus application. Replication studies have been successfully conducted across multiple groups globally (Hansen et al., 2014; Nicoll, 2017). Recent evidence suggest a hetero-distribution of glutamate receptors, such as the NMDA receptor, across the longitudinal axis (Dubovyk & Manahan-Vaughan, 2018) and dendritic field. In the apical dendritic field (where the SC-CA1 pathway lies), NMDA receptors density decrease with distance from the soma among perforated synapses, the main excitatory synapses (Menon et al., 2013). From a functional perspective, NMDA-mediated currents also decrease with increasing distance to the neuronal soma (Stabel et al., 1990). It is then worthwhile to revisit the role of NMDA receptors on LTP expression at different recording distances to the soma and the longitudinal pole.

2.3.4 LTP Variation Along the Longitudinal Axis

A majority of past studies have indicated that dorsal hippocampal slices express a higher magnitude of LTP. Papatheodoropoulos and Kostopoulos (2000) were first to show higher LTP expression in dorsal hippocampal slices compared to ventral. In subsequent years, similar results were found (Dubovyk & Manahan-Vaughan, 2018; Maggio & Segal, 2007; Maggio, Stein, & Segal, 2015). Surprisingly, these results contradict evidence indicating that principal cells in ventral CA1 hippocampal have higher excitability compared to their dorsal counterpart (Cohen et al., 1999). Biochemistry studies have also shown that the ventral hippocampus has a higher distribution of excitatory NMDA glutamate receptor subunits while at the same time has less inhibitory GABA subunit expression (Dubovyk & Manahan-Vaughan, 2018). Furthermore, principal neurons in ventral hippocampal slices have a higher probability to fire an action potential compared to those in dorsal hippocampal slices when injected with the same current (Dougherty et al., 2012; Papatheodoropoulos, 2015a; Ruchi et al, 2016).

One possible reason for the contradictory phenomenon are the limits of the commonly-applied LTP induction protocols. Previous experiments have mostly used a single train of tetanus or the weaker protocol theta-burst stimulation pattern to induce LTP (Dubovyk & Manahan-Vaughan, 2018; Maggio & Segal, 2007; Papatheodoropoulos & Kostopoulos, 2000). Although experiments using strong induction protocols have also found similar results, these experiments may be compromised for the use of a vibratome to generate slices (Dubovyk & Manahan-Vaughan, 2018; Maggio & Segal, 2009; Maggio et al., 2015). Although vibratomes are known to be less traumatic on tissue and generate smoother/cleaner surface on slices, they may hinder the accuracy and precision of obtaining dorsal and ventral slices as the whole brain (hippocampus embedded in the hemisphere) is sectioned compared to a chopper where the extracted

hippocampus is sectioned. Therefore, it is worthwhile to investigate LTP expression in both poles at higher LTP induction protocols.

2.3.5 Sex Differences in Synaptic Plasticity

Sex differences in cognitive function have been found in both animals and humans. In particular, there are many studies on differences in hippocampal related functions among the two sexes. In many strains of rodents, males tend to exhibit superior performance in spatial learning and memory tasks such as having lower escape latencies in the Morris water maze (Berger-Sweeney, Arnold, Gabeau, & Mills, 1995; Hyer et al., 2018; Shah, Prados, Gamble, De Lillo, & Gibson, 2013). Similarly in human studies, males participants were shown to outperform female participants in spatial visualization tasks (Rizk-Jackson et al., 2006). Specifically, female participants had higher latency in locating objects in computer generated environment compared to their male counterparts. In contrast, female participants excel at episodic memory (Rizk-Jackson et al., 2006). Yonker et. al. (2005) found that women outclassed age and estradiol level matched male participants on verbal free recall and face recognitions tests. Furthermore, there is also evidence indicating that females are superior at processing semantic information (Xu et al., 2014).

Severity of pathology induced impairments in cognitive functions is also sex dependent (Cahill, 2006). In regards to hippocampal-dependent cognitive symptoms, females have greater severity in Alzheimer's disease and depression, while males have greater severity in schizophrenia. In addition, learning and memory-related function are more impacted by stress in females than males (Reich et al., 2019). Stress-induced learning deficits are also known to be sex dependent (Derks et al, 2016). Considering the evidence for sex differences in hippocampus related functions, difference in synaptic plasticity expression can be an underlying mechanism. In recent years, there is evidence suggesting that male rodents have a higher susceptibility to MeHg induced behavioral

(Björklund et al., 2007) and biochemical (Ruszkiewicz et al, 2016) alterations than their female counterpart.

Evidence has been found showing the DG region from male rodents express higher LTP magnitude (Maren, 1995). However, many studies have found inconsistent results in the CA1 region. For example, Qi et al (2016) found no differences in potentiation in CA1 region between slices prepared from male, or female rodents (Jain et al, 2019; Qi et al., 2016),while other studies (Hwang et al., 2010; Yang et al, 2004) have found that slices from male animals had higher LTP expression.

2.3.6 Principal Component Analysis

It is generally accepted that an evoked field response in an electrophysiological study includes multiple components. This is reflective of its nature as the aggregated electrical activity in a given area of tissue that consists of multiple cell types and, thus, in turn, different synapses (Bliss, Collingridge, Morris, & Reymann, 2018). For decades, neuroscientists have been mostly interested in studying aspects (slope, or amplitude) describing the negative deflection that occurs directly after the stimulus artifact as shown in Figure 2.3. The reason for the accumulated interest is that many studies have shown the negative aspect to be a reflection of the excitatory transmission and hence it has be coined field excitatory post-synaptic potentiation (fEPSP) (Bliss et al., 2018; Nicoll, 2017). As such, other aspects of the evoked response are not well characterized. Most importantly, it is unclear how many aspects or features there are and how much each contribute to the information of the signal.

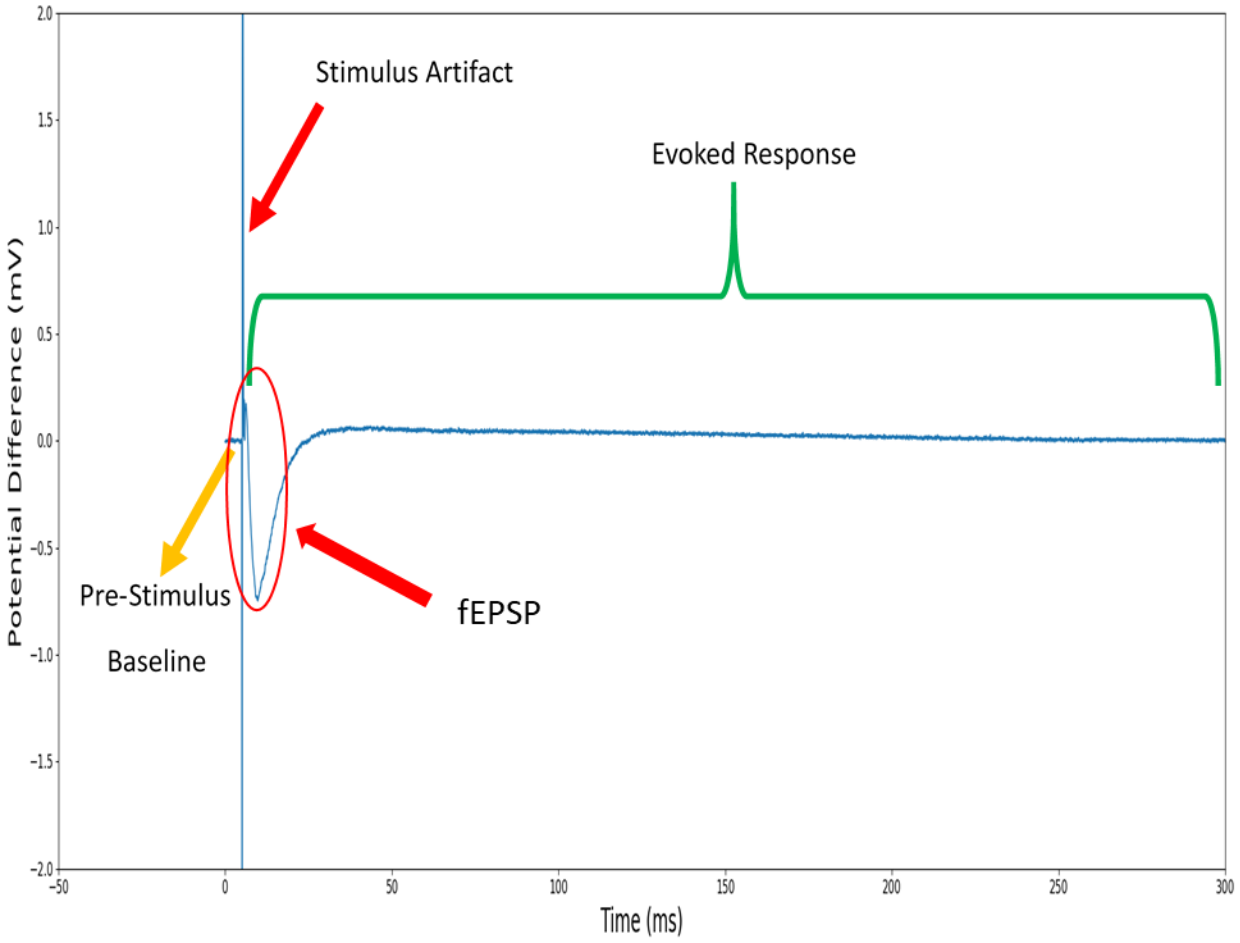

Figure 2.3. Sample Trace of an Evoked Waveform. A single trace contains: i) a 5 ms pre-stimulus baseline, ii) a stimulus artifact, and iii) the evoked responses induced by the stimulus. The fEPSP is the negative deflation observed directly after the stimulus artifact.

Identifying other components of the evoked waveform that may have physiological interpretations could enhance our usage and analysis of data in evoked potential experiments, in particular that of multi-electrode arrays (MEA). In recent years, the emergence and availability of MEAs have allowed multiple recording sites as opposed to one, or two points in acute tissue slices by traditional sharp electrode methods. Sadly, synaptic plasticity studies that employed MEA have not been able to fully utilize, or interpret data generated from multiple sites of recording. Generally, synaptic plasticity studies using MEAs have either used only a single point in their analysis or treated data from multiple sites as technical replica. To date, there is no standard or agreement on the analysis of MEA generated LTP data. PCA may identify additional features aside from the fEPSP which maybe unique to each recording point on the array and in turn could lead to formation of better analytical strategies. Most importantly, the additional features identified may also aid in the analysis to dissect the spatial anatomical relation presented by the increased number of recording points in MEAs.

Principal component analysis (PCA) is a multivariate analysis technique that reduces dimensionality of data sets by analyzing and capturing modes of variation (Chapman & Mccrary, 1995). In other words, the method detects features using a systematic approach which analyzes the variation across all waveforms in an analytical set. As a result, PCA always picks a smaller number of features to describe the signal as opposed to the full signal while at the same minimizing the amount of information lost. There are two main advantages in applying PCA to evoked responses: 1) ability to extract components of the waveform that vary across the experiment, but are uncorrelated with each other and 2) ability to quantify amounts of variability contributed by each identified component. Although there are studies that have employed principal component scores

in tissue evoked potential studies (Astrelin et al., 1998; Chapman & Mccrary, 1995), no study has interpreted the underlying physiology driving force to the identified components.

2.4 Synaptic Plasticity: A Potential Target of Methylmercury

2.4.1 Absence of Neuronal Death at Low Dose Methylmercury

In contrast to high exposure paradigms, low chronic levels of MeHg do not necessarily result in changes of brain tissue morphology. Autopsies of 32 Seychelles neonates did not reveal any histological changes in white, or grey matter in the brain despite having an approximate MeHg concentration of 0.3 µg/g (ww) (Lapham et al., 1995). Although the concentration is more than two-fold lower than that found in acute toxicity/to induce change tissue morphology, MeHg related learning deficits were still reported in the same population (Debes et al., 2016).

Consistent with epidemiological studies, no changes at the histological level were found in the rodent brain at 0.3 µg/g (ww). A 14-day daily post-utero oral exposure to 0.34 mg/kg MeHg daily did not show visible morphological changes , evaluated by light microscopy, in any region of the adult rat brain (Kung et al., 1989). A 50-day exposure paradigm during gestation and lactation in rats that resulted in a brain concentration of 1.45 µg/g (w/w) was found to produce no morphological alterations (Lindström et al, 1991). More importantly, deficits in learning can still be observed in the absence of histological changes. For example, mice exposed to 0.5 mg/kg MeHg during gestation and lactation did not display neuronal death despite subjects exhibiting degrees of learning deficits (Onishchenko et al., 2007). Therefore, MeHg-related learning deficits seen in rodents may be a result of changes in synaptic transmission, or connectivity, as opposed to neuronal loss. However, it is unknown whether these effects are of neurodevelopmental origins.

2.4.2 Methylmercury Effects on Basal Synaptic Transmission

Preclinical evidence suggests that MeHg induces hyperexcitability neuronal tissue. Yuan and Atchison (1993) found that 4 μM induced no noticeable change in the fEPSP measured in the SP; while, at higher concentrations, a complete cessation of the fEPSP response was observed (Yuan & Atchison, 1993). Interestingly, a transient increase of 20-40 % of fEPSP amplitude was observed at 100 and 500 μM MeHg perfusion before complete cessation of the response. Furthermore, it was shown that MeHg caused cortical slices from *in vivo* MeHg treated rats to exhibit epileptiform activity, a sign of hyperexcitability of cortical neurons (Dasari & Yuan, 2010). The exact mechanisms behind MeHg effects on synaptic transmission are still not well understood, but they are primarily believed to be a result of MeHg enhanced glutamate transmission and impairment of gamma-aminobutyric acid (GABA) signaling (Santos et al., 2016).

2.4.3 Methylmercury Enhanced Glutamate Mediated Synaptic Transmission.

One prime suspect for the MeHg induced increase in neuronal excitability is increased glutamate levels at the synaptic cleft. High levels of MeHg have been found to inhibit uptake and increase release of glutamate *in vitro*. For example, 5 μM MeHg (30 minutes preincubation) inhibits glutamate intake up to 46% in rat primary astrocyte culture (Albrecht, Talbot, Kimelberg, & Aschner, 1993). Reynolds and Racez (1987) found that 20 μM MeHg (50 minutes preincubation) increased glutamate release in mouse cerebellar slices. At the same time, it is important to recognize that these studies were conducted using extremely high dose levels, which are rarely seen in the general population. Therefore, it is important to recognize that these effects of MeHg on glutamate transmission may not be present at lower MeHg concentrations.

NMDA receptors play a role in induced toxicity of MeHg at high levels seen during the Minamata tragedy and low levels typically seen in the general populations of Canada and the

United States. The NMDA receptor antagonists memantine and MK-801 have been shown to consistently reduce neuronal damage and death from high level MeHg exposure *in vitro* and *in vivo* (Liu et al., 2017; Petroni et al., 2013; B. Xu et al., 2013; T. Yang, Xu et al., 2016). Interestingly, MeHg was found to induce expression of NMDA receptor subunits NR1, NR2A, and NR2B *in vivo*, which contributes to alterations in synaptic transmission (Gao et al., 2008). More importantly, these changes in NMDA receptor subunit expression coexisted with learning deficits in mice. Again, the exact role of the interaction between NMDA receptors and MeHg is still not completely clear.

2.4.4 Methylmercury Enhanced GABA Currents

GABA receptors are also a prime suspect for MeHg action in which the mechanisms are still elusive. Early evidence suggests that MeHg can inhibit uptake of GABA in cortical homogenates prepared from rats treated with 7mg/kg/day MeHg intraperitoneal injections for 7-10 days (Araki et al., 1981). Moreover, there is evidence suggesting that GABA is more sensitive to MeHg action as inhibition of cortical GABA uptake can be present without affecting glutamate uptake (O'Kusky & McGeer, 1989). Consistent with these early studies, high levels of MeHg (10-200 μM) has been now shown to increase GABA mediated currents in rodent cerebellum cortex preparations (Yuan & Atchison, 2003, 2007). Specificity was confirmed via the absence of effect in the presence of GABA antagonist (e.g., bicuculline). Interestingly, the effects of MeHg observed were biphasic, first excites before completely a complete inhibition GABA currents on postsynaptic membranes. Considering that higher dose can lead to cell death, which can lead to cessation of GABA mediated current, MeHg can be speculated to increases GABA currents at low doses while cell death at higher doses. Indeed, a recent study found that at 1-5 μM MeHg can potentiate GABA current without an after cessation in xenopus oocytes. Most importantly, these

effects seem to be mediated by $GABA_A$ α1 subunits. However, the mechanism regarding the mode of action of MeHg on GABA are still unclear (Huang & Narahashi, 1997; Yuan & Atchison, 2016).

3.0 Study Aims

3.1 Study Goals

The overall goal of this research document is to develop a more sensitive analytical strategy in acute slice LTP MEA assay to detect effects of MeHg. Therefore, the exact goals are twofold:

1. Develop a more sensitive assay in measuring LTP stratifying the tissue slice based on sex, pole of origin, distance of recording point to the neuronal soma or a combination of these factors.
2. Using the newly developed assay to analyze the effects of increasing doses of MeHg on synaptic plasticity.

3.2 Specific Research Questions

The research questions to be specifically answered are the following:

1. Does the origin along the longitudinal axis of the acute hippocampal slices affect components of the evoked response during LTP expression?

2. Does the recording distance to the neuronal soma affect components of the evoked response during LTP expression?

3. Does sex affect evoked response components differently during LTP expression?

4. Does NMDA receptor antagonist block LTP expression equally at all recording distance to the neuronal soma and in slice of different origin along the longitudinal axis (dorsal vs ventral)?

5. Does MeHg affect components of the evoked responses during LTP expression equally at all recording distance to the neuronal soma and slice of different origin along the longitudinal axis (dorsal vs ventral)?

4.0 Tetanus Induced Changes in SC-CA1 Evoked Responses

4.1 Overview

The main purpose of this chapter is to investigate tetanus (100 Hz x 2; intertrain duration: 20s) induced changes on evoked potential waveforms as a function of recording distance to the soma and origin of hippocampal slice along the longitudinal axis from both male and female rats. In addition to studying the standard evoked response fEPSP aspect (amplitude), this chapter will also explore and identify other aspects of the evoked response which may vary due to tetanus induction. The chapter is divided into three sections: 1. PCA to identify main components of the evoked field potential, 2. statistical modeling and testing of evoked response components, and 3. effect of NMDA receptor antagonist on the evoked response components.

4.2 Materials and Methods

4.2.1 Electrophysiology Experiments

Female and male SD rats (12-20 weeks old) were purchased from Envigo™ and housed in polypropylene cages with woodchip bedding and stainless-steel wire lids on a 12-hour dark/light cycle. After euthanizing with CO_2 and decapitation, brains were quickly removed and placed in ice cold oxygenated (95 %O_2:5 % CO_2) artificial cerebrospinal fluid (ACSF). ACSF composition was as follows: 127.0 mM NaCl, 2.0 mM KCl, 1.2 mM KH_2PO_4, 26.0 mM $NaHCO_3$, 2.0 mM $MgSO_4$, 2.0 mM $CaCl_2$, 10.0 mM glucose (pH 7.4; osmolality 300-320 mOsm). The hippocampus on the right hemisphere was extracted and 350 μm thick transverse slices were prepared using a McIlwain tissue chopper, sectioning the hippocampus from dorsal to ventral along the longitudinal axis. Slices generated from the approximate first 2 mm were defined as dorsal slices. Ventral slices were generated from tissue that was at least 4.55 mm away from the first 2 mm (dorsal) portion. In a typical experiment, 3 to 4 slices were generated from each pole. Slices were then transferred

to a custom holding chamber filled with oxygenated ACSF (35°C) and allowed to recover at interface (95 % O2:5 %CO2) for a minimum of 2 hours.

4.2.2 Field Excitatory Postsynaptic Potential Recording

Evoked responses were recorded using an 8 x 8 multi-electrode array probe (electrode size 20 x 20 μm, interelectrode distance of 100 μm). Responses were evoked at 0.167 Hz using the MED64 system (Alpha MED Scientific Inc., Osaka). Sampling rate of each evoked waveform trace was 20 kHz. The order of dorsal and ventral slice use was balanced between experiments, i.e., if a dorsal slice was used in one experiment, the next experiment used a ventral slice. The first row of the electrode probe had been consistently placed at the SP layer, or approximately 100 – 200 um away from the neuronal soma. Warmed and oxygenated ACSF (32°C) was perfused at a rate of 1-1.5 mL/min. Slices were allowed to rest on the probe for a minimum of 20 minutes following placement. Subsequently, a point of stimulation in the SR was selected in the CA1 region of each slice. Points of recording was up to 600 μm from the soma that are 100 μm away from the stimulating electrode on the horizontal axis (towards the subiculum), i.e., 6 points was be recorded per slice. If electrical noise was present, the adjacent channel that is 100 μm away along the horizontal axis was analyzed.

The fEPSP amplitude were extracted as the minimum value located between 6 to 15 ms of the evoked response. The positive going aspect (PGA) amplitude were extracted as the maximum value located between 15.5 to 70 ms. In other words, the fEPSP and PGA are the absolute amplitude difference to zero at 6 to 15 ms and 15.5 to 70 ms, respectively. For each slice, the average of the first twenty minutes served as a baseline to which all values were normalized for both fEPSP and PGA. The average increase over baseline in the last 10 minutes of recording after tetanus was taken as the degree of potentiation.

N indicates the number of animals whereas n indicates the number of slices (per animals or in total)

4.2.3 Imaging and Determination of Electrode Position in the CA1

Placement of the hippocampal slices on the multi-electrode array was recorded with a light microscope. Illustrative images of dorsal and ventral hippocampal slices are in Figure 4.1A and Figure 4.1B. However, evoked waveform shapes had been used as a gold standard to determine the location of the first row of electrodes, the 100 μm recording point to the neuronal soma. It has been revealed that the evoked responses can be identified according to distance to soma depending on the shape of the waveform (Kolta et al., 1995). Previous current-source density analysis study revealed that the observation of negative deflection of the evoked responses occurring after the stimulus artifact will decrease when approaching the soma and that at the soma the response will become a positive peak when an electrical stimulation is applied to the SR (Kolta et al, 1996). An illustrative sample is in figure 4.2A and 4.2B. In figure 4.2A, the neuronal soma was located within the MEA where the evoked response contained a positive deflation whereas in the other channels a negative deflation appeared at the same timing. In figure 4.2B, the neuronal soma was not located and the 100 μm to soma location was instead estimated by a decreased pattern of the negative deflation along the vertical axis of the MEA grid. The distance between the recording electrode and soma was then calculated and deduced from an inter-electrode distance of 100 μm.

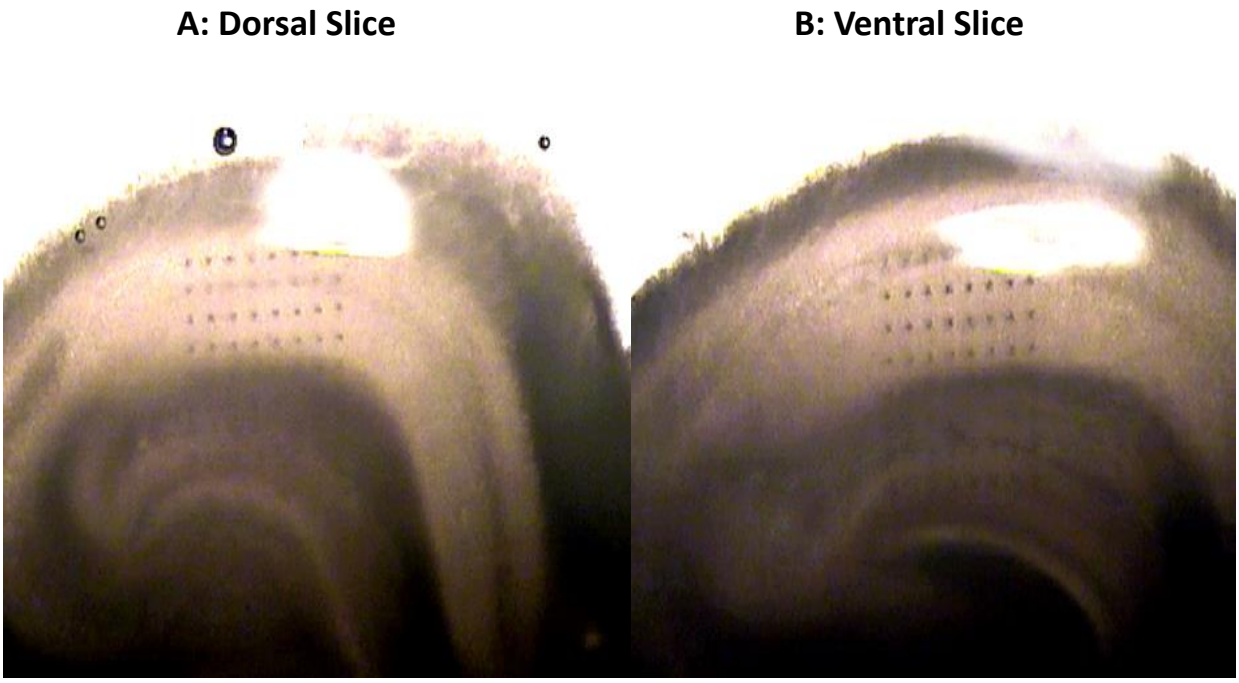

Figure 4.1. Dorsal and Ventral Hippocampus Slices. A. Illustration of a dorsal hippocampal slice on a MEA. B. Illustration of a ventral hippocampus slice on an MEA

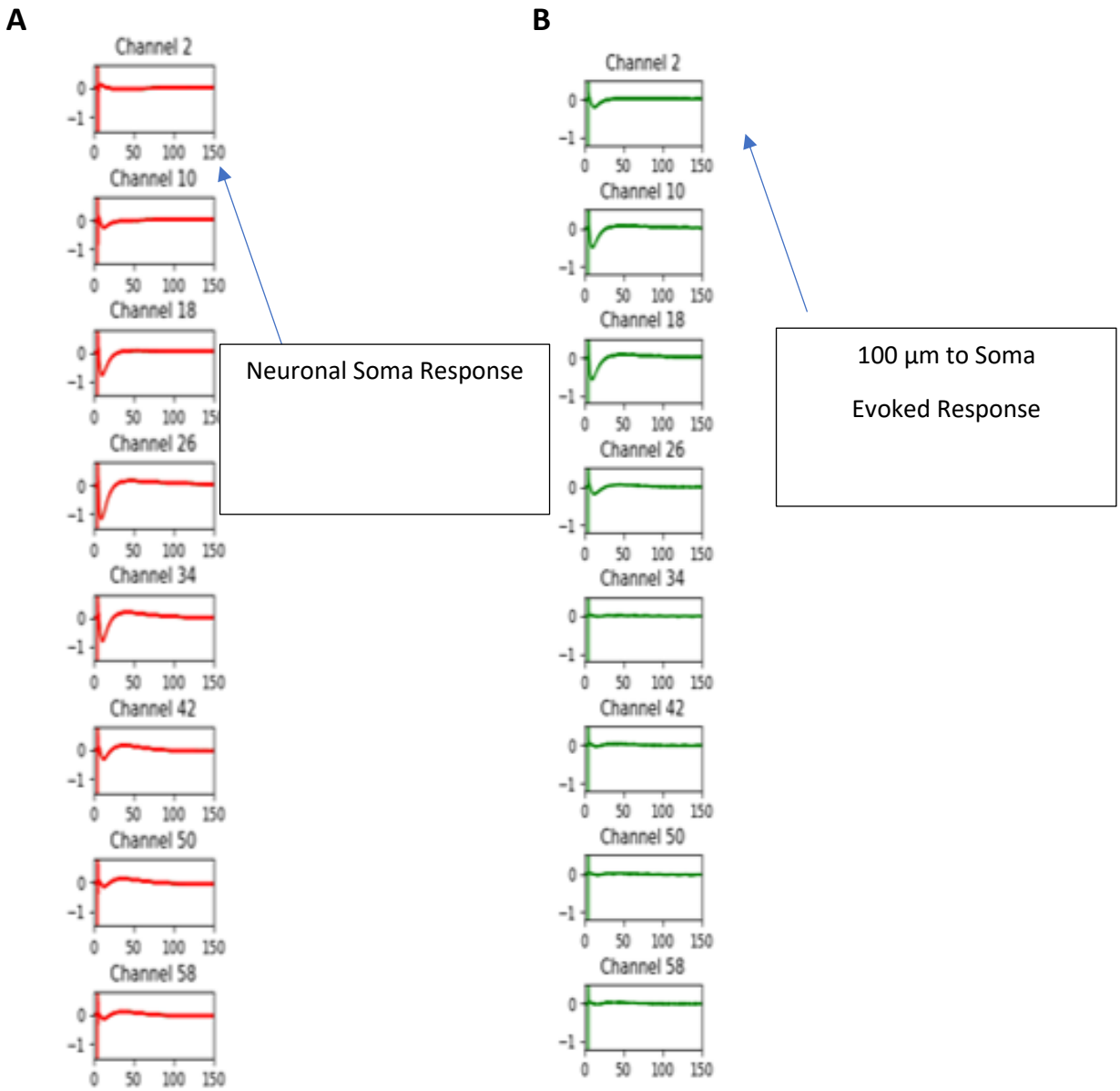

Figure 4.2 Determination of the 100 µm recording point. Somatic response was observed on the MEA and subsequent points were calculated based on inter-electrode distance. B. Somatic response was not observed on the MEA. The 100 µm point of recording was estimated by a decrease in the negative deflection of waveform.

4.2.4 Input/output Curve

An input-output curve was made to determine the test stimulation intensity needed to evoke a response eliciting 30-60% of the maximal fEPSP at the channel that was located 100 um horizontally from the point of stimulus towards the subiculum. To measure the input-output (IO) relationship, fEPSP amplitudes were recorded against increasing stimulation intensities at increments of 5 μA. Maximum fEPSP amplitude was defined as occurring immediately before the waveform showed contamination from other sources.

4.2.5 Long Term Potentiation/ Tetanus Protocol

Experiments were conducted in male and female animals. Stable baseline activity was recorded for a minimum of 20 minutes before application of tetanus (high frequency stimulation, HFS, two trains of 1 s, 100 Hz, 20 s apart). The full flow of the experiment is presented in Figure 4.3.

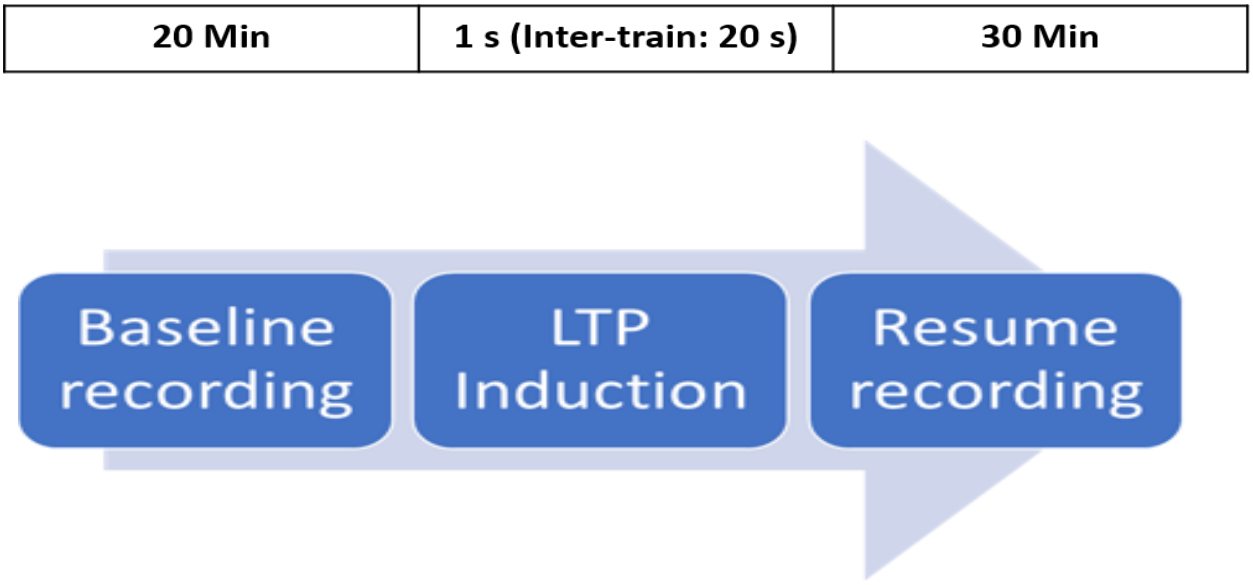

Figure 4.3. Tetanus Experiment Flow. Overall flow of an individual tetanus experiment. After establishing 20 minutes of stable baseline, tetanus was applied and recording was resumed for an additional 30 minutes.

Stability was defined by the two following criteria: 1. No more than 10% variation in amplitude to 100% baseline between each waveform sampled every minute during the first 20-minute period and 2. No more than 5 % difference between the average normalized amplitude of the first and last 10-minute period during baseline recording. fEPSP recordings was continue for at least 30 minutes post-tetanus. Magnitude of potentiation for both fEPSP and PGA was determined by taking an average of the last 10 minutes of recording and calculated as a percent increase over baseline average.

4.2.6 Long Term Potentiation/ Tetanus and APV Protocol

Experiments were conducted in male animals only. Stable baseline activity was recorded for a minimum of 20 minutes before application of 50 nM 2-Amino-5-Phosphonopentanoic acid (APV, Sigma-Aldrich) containing ACSF perfusion, which would last for the remainder of the experiment. Tetanus was applied 20 minutes after APV ACSF perfusion. Evoked responses were recorded for another 30 minutes post-tetanus. As a result, the experiment was divided into three phases in the proceeding order: 1. baseline, 2. APV, 3. APV-LTP. A schematic representation is illustrated in Figure 4.4. The average change over baseline in the last 10 minutes of baseline, APV, and recording was taken as baseline, APV, and APV-LTP phase.

Phase: Baseline	Phase: APV	Phase: NA	Phase: APV- LTP
20 Min	20 Min	Apply Tetanus (22s)	30 Min

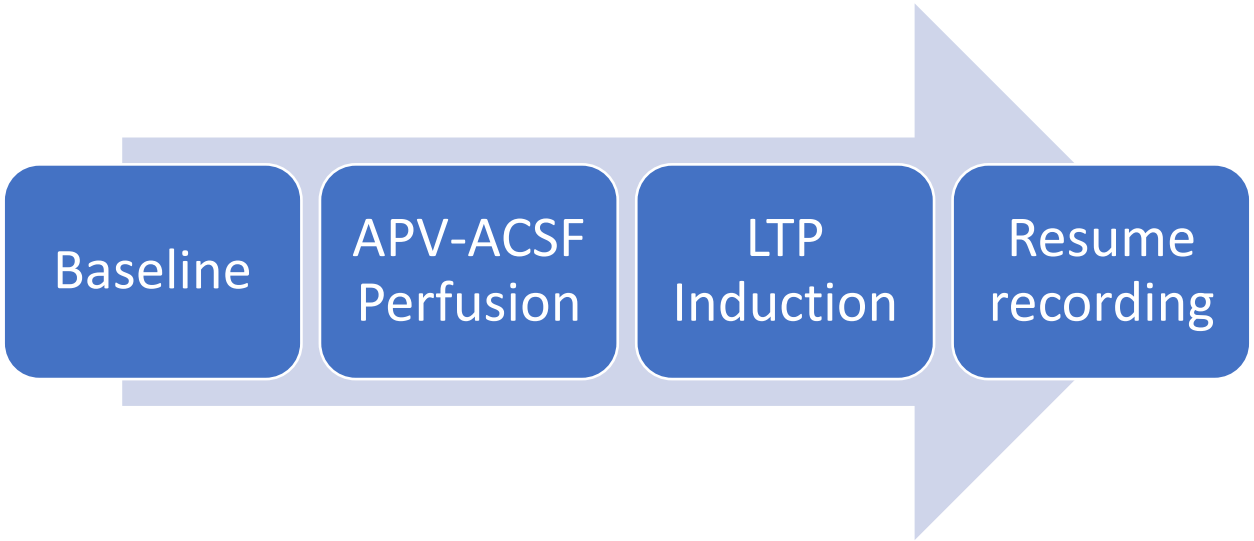

Figure 4.4. APV-Tetanus Experiment Flow. After establishing a 20-minute stable baseline recording, APV-ACSF perfusion began and persisted throughout the experiment. After 20 minutes of the start of APV perfusion, tetanus was applied and recording was resumed for 30 minutes.

4.2.7 Data Analysis

All data had been exported in csv (comma separated values) format and processed using python (3.2). To eliminate any fluctuations during pre-stimulations, all points of the waveform will be subtracted by the average of all points in the first 4 ms (pre-stimulus). Further analysis of the waveform will be conducted in python version 3.6 (Additional Packages: Matplotlib 2.1.0, NumPy 1.16, Pandas 0.24.2) or R version 3.5.0 (Additional Packages: emmeans 1.3.3, ggplot2 3.1.0, gridExtra 2.3, nlme 3.1-130)

4.2.7.1 Principal Component Analysis

In the current study, each evoked field potential waveform trace was composed of the following: i) 5 ms pre-stimulus baseline, ii) 1 ms stimulus artifact, and iii) a full waveform trace with the evoked response is illustrated figure 2.3. As seen in figure 2.3, the stimulus artifact is order of magnitudes larger than the evoked response. At the same time, it does not provide any physiological meaning. Due to its large magnitude, even slight changes in stimulus artifact variations will dominate PCA results and in turn mask other evoked responses variation in the principal component analysis. To eliminate the stimulus artifact, analysis was conducted using only the 6.5 to 300 ms interval of the waveform which resulted in 5880 points in each waveform trace. Furthermore, all waveforms were digitally down-sampled by 10-fold (to 2 kHz) to achieve data processing efficiency which resulted in 588 points in a single waveform. Visual inspection suggested that the down sampling did not alter the evoked waveform.

In brief, the PCA process first creates matrices of waveforms from each recording point on the MEA in a single experiment of a slice. The resultant data frame contained every trace of the evoked potential waveform as a column vector of p variables (p: number of points in the down sampled evoked response waveform trace) $x_{1\times p}$ representing a single observation among the n time points (n: row,1-50 minutes) of the tetanus experiment. Each waveform could be thought of as being defined by 588-coordinate position vector/ variables within a correlated coordinate space of time points (50 minutes). Using this notation, each recording point of a slice was a dataset that could be represented by the symbol $X_{n\times p}$ consisting of n observations with a vector of size of p. Principal components of a single recording point in a slice were then determined by computing the eigenvector (the principal components, directions of variability) of the correlation matrix $S_{p\times p}$ of a single dataset $X_{50\times 588}$. and the amount of variability in these directions were determined by the

corresponding eigenvalues. Each eigenvector is a linear combination of all points in the original signal and can be thought of as a feature. In order to locate mode of variation described by the principal component, corresponding principal component were computed and interpreted alongside the original waveform trajectory across the 50-minute duration of the tetanus experiment.

4.2.7.2 Linear Mixed Model Analysis

In this current study, the main effects of interest are sex, pole of origin, and recording distance to the soma. However, multiple values are not independent observations, which might distort the accuracy of statistical tests by increasing the chance of a false negative (West, Welch, Galecki, Welch, & Galecki, 2014). In biology, there is a belief that all observations from the same animal and same tissue have the possibility to have a co-variance structure, i.e. one observation can predict other observations of the same source (Carey, 2012). In the current structure, there are two levels in which a covariance structure may arise: 1. animal: the same animal can generate multiple slices, 2. slice: each slice generates 6 recording points for analysis.

A linear mixed model is a method that can account for underlying covariance structures by estimating these parameters as random effects. General linear models such as anovas and t-tests estimate experimental units of the same group to be a single line in an x-y coordinate in which all observations share the same intercept/baseline and slope/response. In contrast, a liner mixed model estimates each experimental unit to be a single line that may have different intercepts, or slopes. In other words, experimental units may have a unique slope and/or intercept when from the same animals and slices with prior covariance structure (Koerner & Zhang, 2017). Essentially, this resolves the issue of independence among repeated measures including temporal and spatial pseudo-replications. The model may shed light on how the independent variable impacts the outcome measurement when among co-existing variables.

In the tetanus experiment, fEPSP and PGA were separately fitted to a linear mixed model with main effects as: 1. sex (male, or female), 2. pole of origin (dorsal, or ventral), 3 recording distance to soma (1-6 10^2μm); and random effects as: 1. animal (1-13, total 13 animals in total) and 2. slice (1-3). In other words, sex, pole of origin and recording distance to soma were the main effects of interest tested. Slice and animal number were random effects to see if the response variables were affected. In the APV-tetanus experiment, fEPSP and PGA were separately fitted to a linear mixed model with main effects as: 1. Phase (Baseline, APV, or LTP), 2. Pole of origin (Dorsal or Ventral), 3 Recording distance to soma (1-6 x10^2μm); and random effects as:1. Animal (14-18, 5 animals in total) and 2. Slice (1-2). Random intercept only models were fitted in both experiments. The Tukey's test for post hoc comparisons was employed when a fixed effect, or interaction effect was found to be significant.

4.2.7.3 Linear Mixed Model Assumption

Although a linear mixed model allowed the bypass of independence assumption, the assumption of normality and homogeneity of variance were still needed. In all models, the homogeneity of variance assumption was not violated (Supplemental Figure A1). Similarly, the assumption of normality seems not to be violated in all models with the exception of fEPSP model in the tetanus experiment (Supplemental Figure A2). Even though skewedness and heavy tails are still observed, these should not pose a significant problem to the use of linear mixed models to compare means. As like ANOVAs, linear mixed models are relatively robust against non-normality related problems such as higher false positivity (Glass, Peckham, & Sanders, 1972; Lix, Keselman, & Keselman, 1996). Most importantly, there are currently no non-parametric alternatives for a 2 or 3-way ANOVA. To simplify the interpretations of the factors and their interaction, the linear mixed model was still used. Also, considering that the p-values observed in

the current study were often more than 10-fold lower than 0.01, the chance of a false positive should be considerably low.

4.3 Results

4.3.1 Principal Component Analysis

PCA results are best to interpret when the dataset can be mostly explained by only a few principal components (Jackson, 1991). Eigenvalues depict the amount of variation each principal component contributes in a numeric fashion. Through observing the eigenvalue of all recording points analyzed (126 in total) across all slices (n = 21 in total), two eigenvectors seem to dominate the majority of variance and have higher contribution to variation across the duration of experimental time than the remaining 586 eigenvectors. A sample normalized eigenvalue plot of all recording points within a given experiment is illustrated in Figure 8. It can be observed at minimum the first two eigenvectors can explain 76% of the overall variation, which also represents the overall information, across the tetanus experiment (Figure 4.5). This pattern seems to be also consistent among all channels recorded across all slices. Across all slices, the first two eigenvectors can explain on average 85% of the variation in the evoked responses across the tetanus experiment (Supplemental Table B1). Only in 6 of 126 channels, did the first eigenvector contribute less than 70% of the variation.

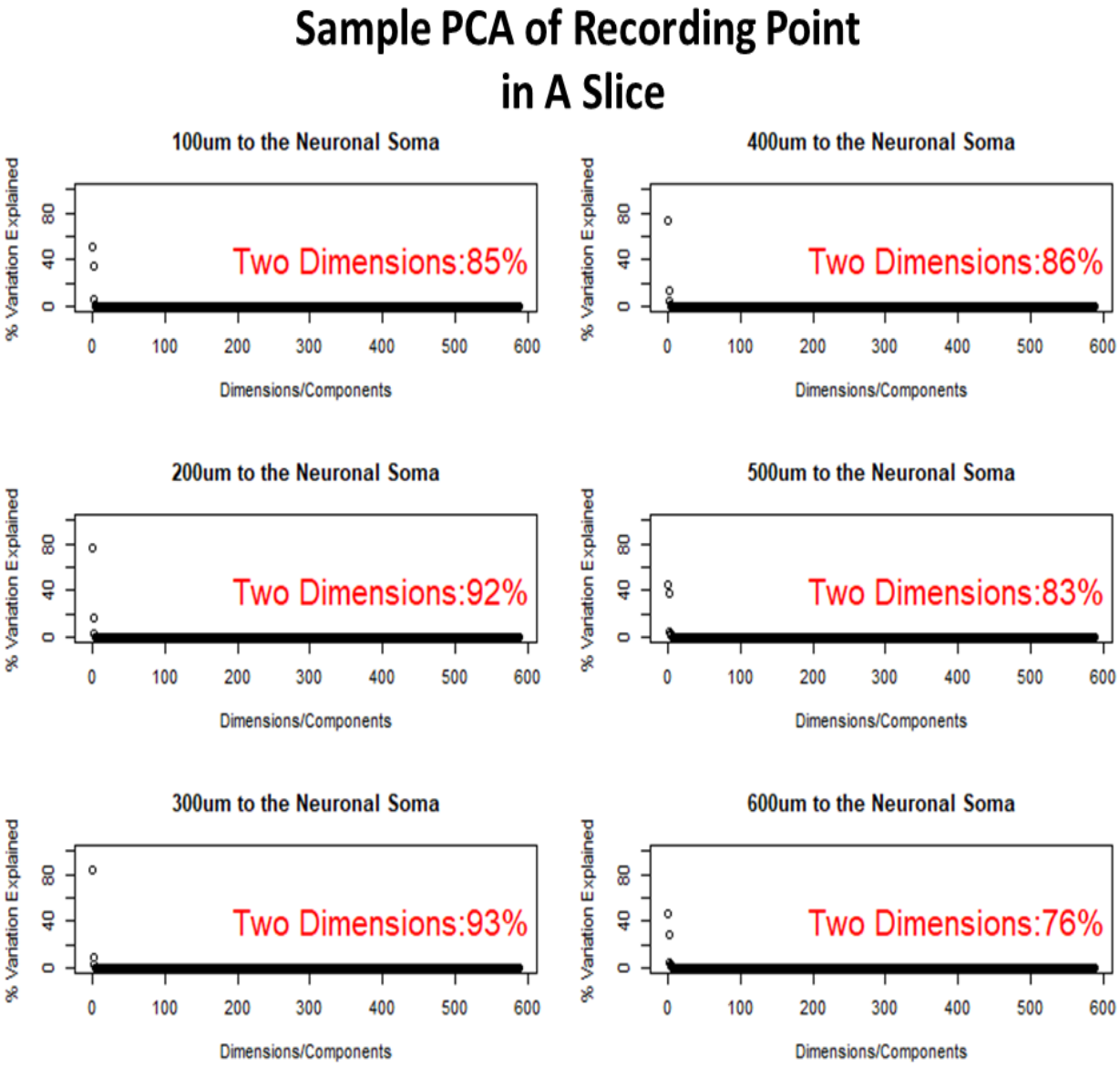

Figure 4.5 Sample PCA in a Slice. Sample principal component analysis of all recording distance within a slice with plotted normalized eigenvalues (in total 588). Each eigenvalue corresponds to a single eigenvector/principal component and shows the relative amount of variation contributed by the corresponding eigenvector. In this sample, it can be observed that there are two eigenvectors that contribute most of the variation across experimental time. Variation contributed by the two eigenvectors are listed in each channel. In all cases in the sample slice presented, the variation explained is more than 75%.

This process of determining where the principal component maybe present in the original data were conducted completely at the investigator's discretion with the help of statistical consultants. It is important to note that the process is solely determined by the analyst's interpretation and may vary between personnel (Vilenchik, Yichye, & Abutbul, 2019). Through observing the component scores and the trajectory of the evoked responses across time, the two modes of variation were located based on the analyzer's inference. An example of the analysis in one channel is illustrated in Figure 4.6. Figure 4.6A shows the trajectory of evoked response waveforms overlaid from a single recording point across the whole duration of the tetanus experiment. Through careful observation, the largest mode of variation of the principal component score 1 and 2 across the 50-minute tetanus experiment (Figure 4.6B and Figure 4.6C) were determined to best correspond to the initial negative component and later positive component, respectively, of the waveform. During baseline, the score is stable and peaks during post-synaptic potentiation and remains stably elevated from baseline during LTP. In the trajectory of the evoked responses, it seemed that this component score corresponds best with the negative aspect occurring from 6 to 15 ms. Principal component score 2 seems to be stable and has a notable change from baseline after tetanus as observed. It was determined that the principal component score 2 corresponds best with the positive going aspect occurring between 15.5 and 70 ms of the evoked response waveform.

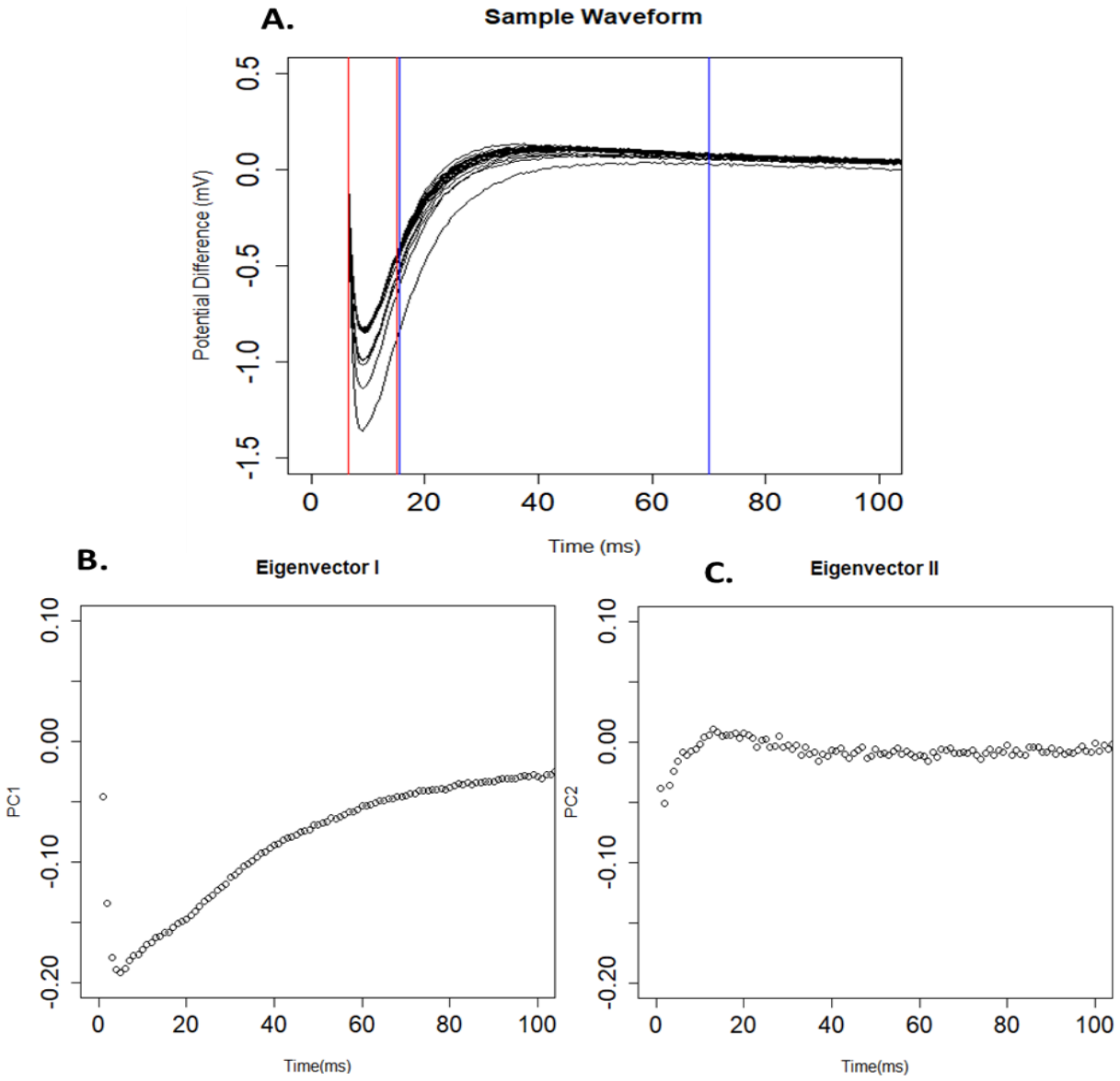

Figure 4.6 Locating Mode of Variation. A: Trajectory of waveforms overlaid at a recording point in a tetanus experiment. Red lines (6.5 ms and 15 ms) indicate where the estimated PC1 is. Blue lines (15.5 ms and 70 ms): where the estimated PC2 is. The estimated location of the principal components (PC) 1 and 2 are indicated in the graph. B: PC1 calculated component score changes across the tetanus experiment (50 minutes of recording). C. PC1 calculated component score changes across the tetanus experiment (50 minutes of recording).

4.3.2 Tetanus Induced Changes on Field Excitatory Post-Synaptic Potential

In total, there were 126 recording points analyzed from 21 slices (11 dorsal and 10 ventral) contributed by 8 male and 5 female rats.

In both male and female slices, a trend could be seen that the magnitude of potentiation in fEPSP, more commonly known as LTP, is inversely proportional to the recording distances from the neuronal soma as seen in Figure 4.7. In females (Figure 4.7B), this trend was less obvious, which may be due to the fact that there were more dorsal (N = 5) than ventral (N = 2) slices in the analysis. However, no effect of sex was detected ($p = 0.43$, $F = 0.64$) nor was there an interaction with recording distance to soma ($p = 0.97$, $F = 0.18$), or pole of origin ($p = 0.68$, $F = 0.17$). Results of linear mixed model analysis are summarized in Table 4.1.

Table 4.1 Tetanus Experiment Linear Mixed Model on fEPSP Results

Term	F-Value	p-Value
Sex	0.62	0.44
Recording Distance To Soma	14.87	<0.01
Pole of Origin	0.007	0.94
Sex: Recording Distance To Soma	0.56	0.73
Sex: Pole of Origin	0.17	0.72
Recording Distance To Soma: Pole of Origin	6.33	<0.01
Sex: Recording Distance To Soma: Pole of Origin	0.54	0.75

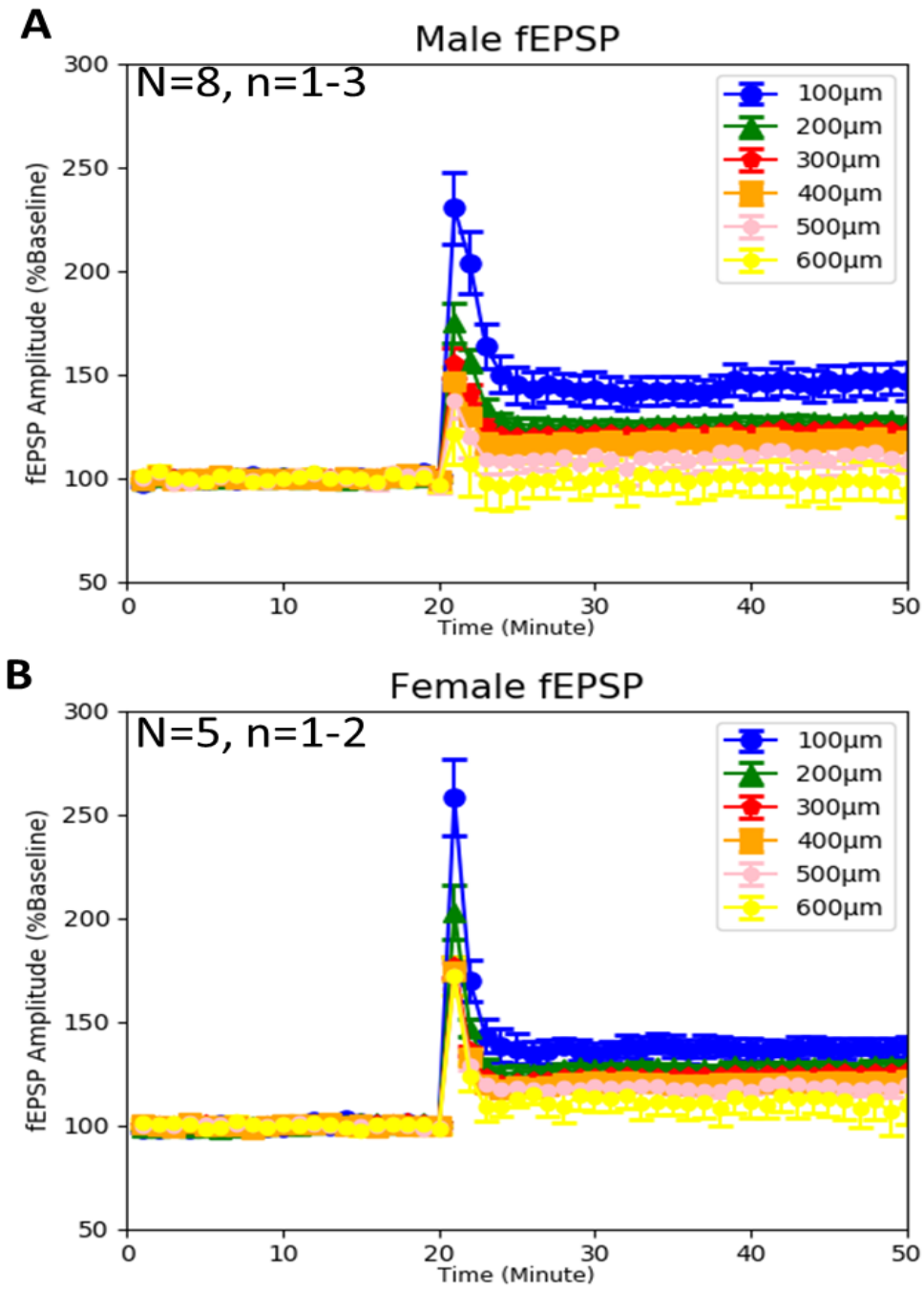

Figure 4.7 Male and Female fEPSP across Tetanus Experiment. A. Male fEPSP results across the tetanus experiment by recording distance to the neuronal soma. N = 8 animals, n = 1-3 slices per animal. B. Female fEPSP results across the tetanus experiment by recording distance to the neuronal soma. N = 5 animals, n = 1-2 slices per animal. Experimental results were pooled from both dorsal and ventral slices

Recording distance to soma had a significant effect on the potentiation of fEPSP after tetanus ($p < 0.01$, $F = 14.87$). Post hoc analysis with Tukey's pairwise comparisons between the LTP potentiation of the recording distance revealed that the majority of recording points are different to 100 μm and 600 μm away from the soma. Table 4.2 contains all significant pairwise comparisons on recording distance to soma. Specifically, it was found that fEPSP potentiation at the 100 μm recording point was statistically different than that at 300 μm ($p < 0.01$), 400 μm ($p < 0.01$), 500 μm ($p < 0.01$) and 600 μm ($p < 0.01$). No difference was found between that of 100 μm and 200 μm ($p = 0.09$). Similarly, it was found that fEPSP potentiation at the 600 μm recording point was statistically different from that at 100 μm ($p < 0.01$), 200 μm ($p < 0.01$), 300 μm ($p < 0.01$), 400 μm ($p = 0.01$). No difference was found between 600 μm and 500 μm ($p = 0.13$). Figure 4.8 shows the mean fEPSP potentiation across all recording points.

Table 4.2 Significant fEPSP Pairwise Comparison on Recording Distance to Soma in Tetanus Experiment. p value adjustment: Tukey method for comparing a family of 6 Estimates

Pairwise Comparisons (x10^2 μm)	**p-value**
1 - 3	0.0091
1 - 4	<0.001
1 - 5	<0.001
1 - 6	<0.001
2 - 6	<0.001
3 - 6	<0.001
4 - 6	0.0083

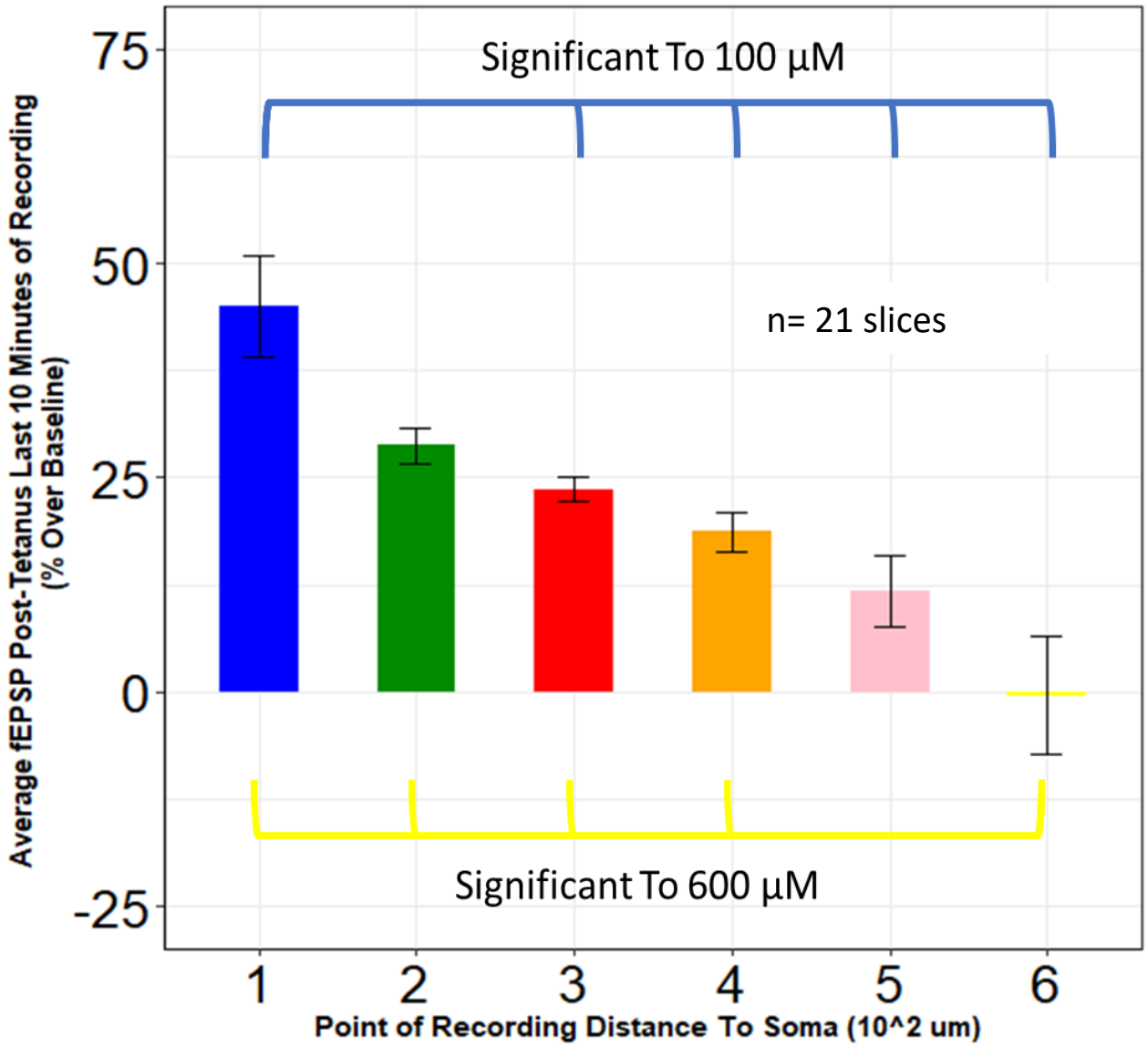

Figure 4.8 Potentiation in fEPSP by Recording Distance to Soma. Effect of recording distance to the neuronal soma was found to be significant. Post hoc analysis revealed that most points show a significant difference to recoding distances of 100 and 600 um away from the neuronal soma. Data generated from N=13 animals, which yielded 1-3 slices per animal. Data averaged over 21 slices for each recording point, Expressed in Mean+/-SEM

Pole of origin along the longitudinal did not affect fEPSP potentiation (p =0.96, F=0.0017), nor its interaction with sex had an effect on fEPSP potentiation (p = 0.68, F = 0.17). However, the interaction effect between pole of origin and recording distance to the soma was significant (p =< 0.01, F = 6.86). Figure 4.9 shows the interaction plot of recording distance between pole of origin on fEPSP. Figure 4.10 shows the fEPSP plots that are stratified by gender and pole of origin. In both sexes, the gradient of fEPSP potentiation induced by tetanus is more apparent in ventral hippocampal slices compared to dorsal hippocampal slices. Illustrative waveform traces are presented in Figure 4.11. Indeed, the same statistical significance of pairwise comparisons (100 µm and 600 µm being different from the most of the recording distances) is still present in ventral hippocampal slices, but absent in dorsal hippocampal slices as shown in Figure 4.12A. In dorsal hippocampal slices, there was no significant difference in fEPSP potentiation between the recording distances as seen in figure 4.13B. Summary of significant pairwise comparisons are shown in Table 4.3. All pairwise comparisons within dorsal slices were non-significant (p>0.5).

Table 4.3 Significant fEPSP Pairwise Comparison on Recording Distance to Soma. p value adjustment: Tukey method for comparing a family of 12 estimates.

Pairwise Comparison (Recording Distance 10^2 µm, Pole)	**p value**
1, Ventral - 3, Ventral	0.0133
1, Ventral - 4, Ventral	<0.001
1, Ventral - 5, Ventral	<0.001
1, Ventral - 6, Ventral	<0.001
2, Ventral - 6, Ventral	<0.001
3, Ventral - 6, Ventral	<0.001
4, Ventral - 6, Ventral	0.0061

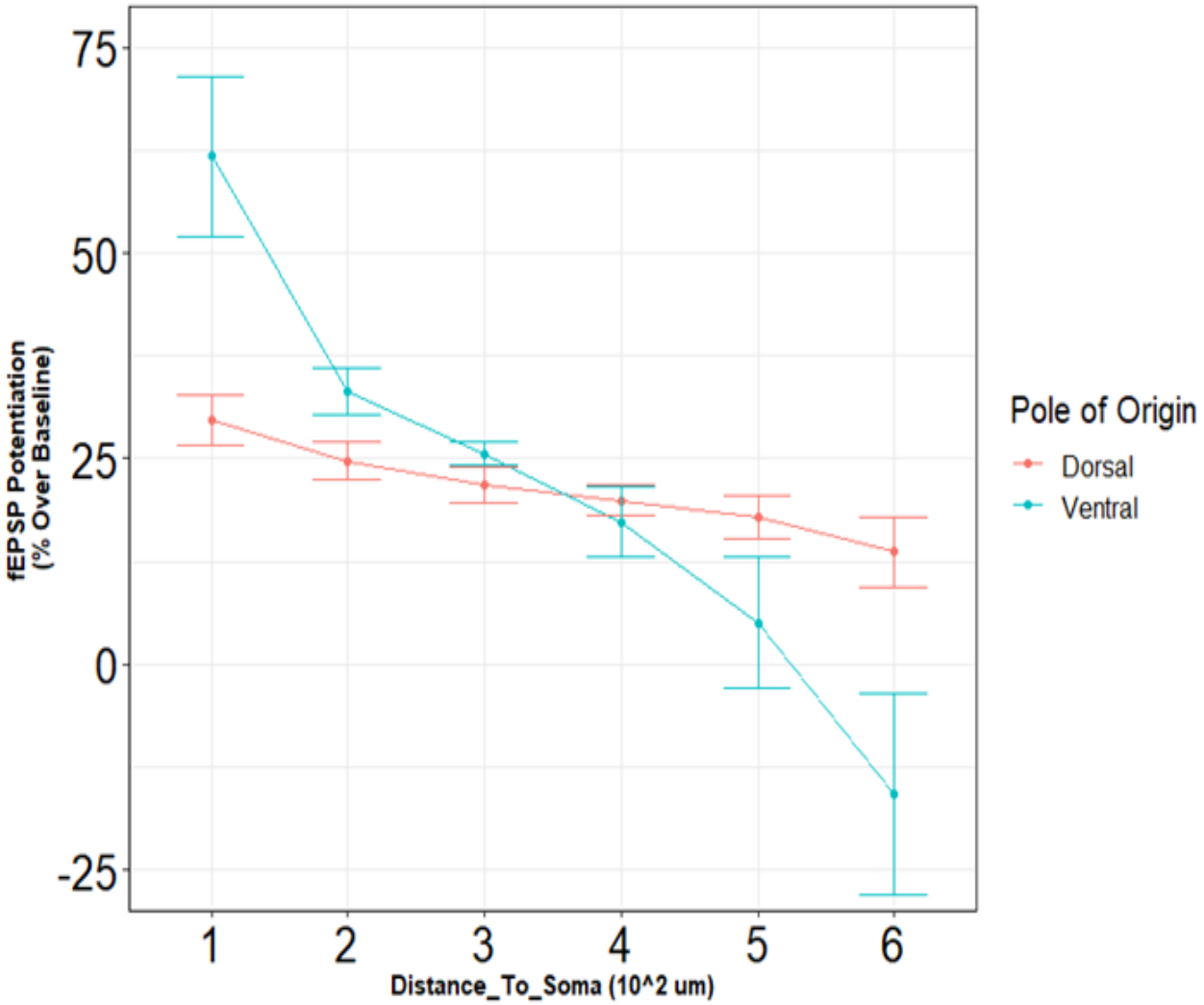

Figure 4.9 Interaction of Pole of Origin and Recording Distance on fEPSP potentiation. Data: Mean +/-SEM.

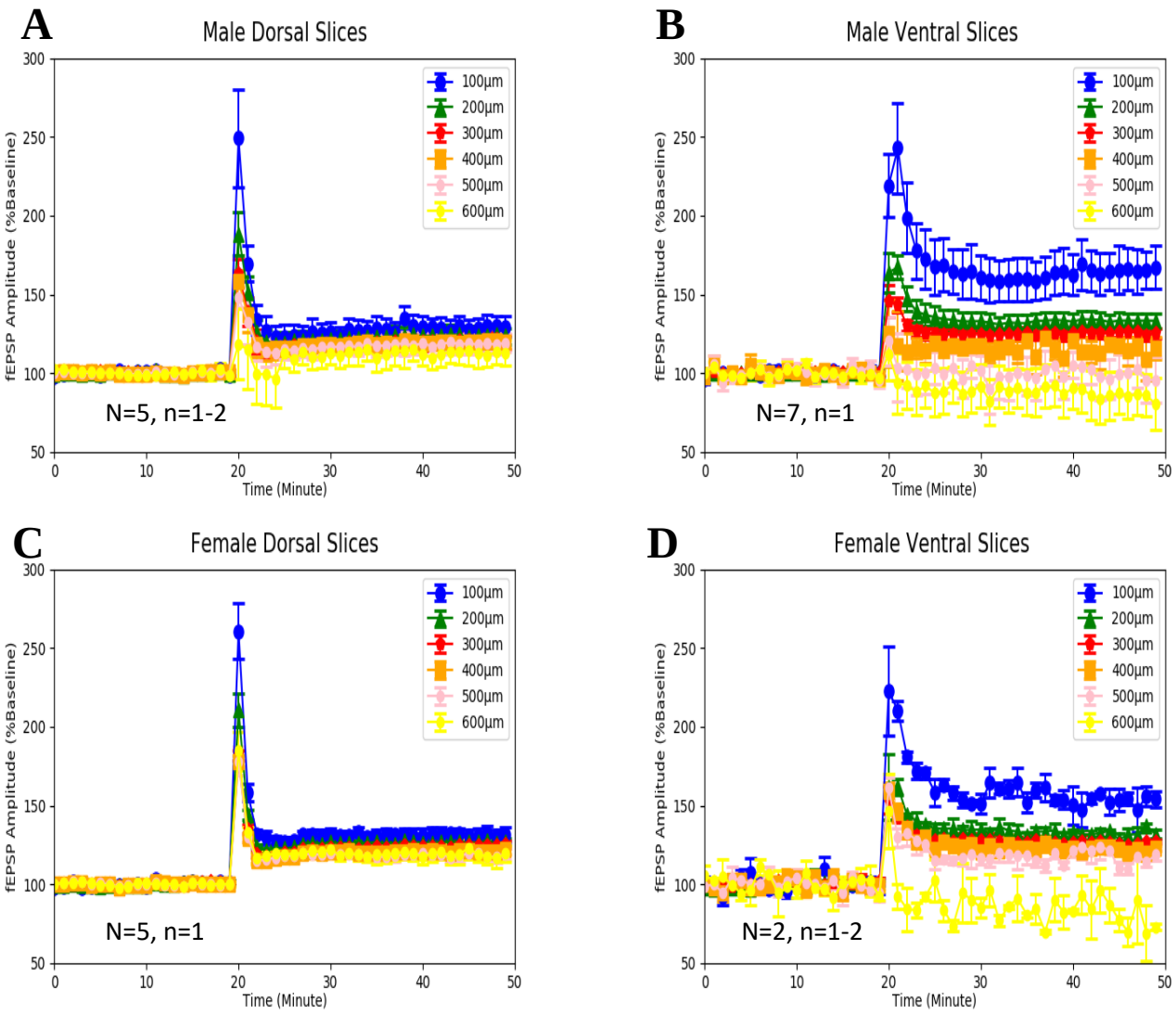

Figure 4.10 Tetanus fEPSP Plots: Sex and Pole A: fEPSP changes induced by tetanus in male dorsal slices. B: fEPSP changes induced by tetanus in male ventral slices. C: fEPSP changes induced by tetanus in female dorsal slices. D: fEPSP changes induced by tetanus in female ventral slices. Data: Mean +/- SEM

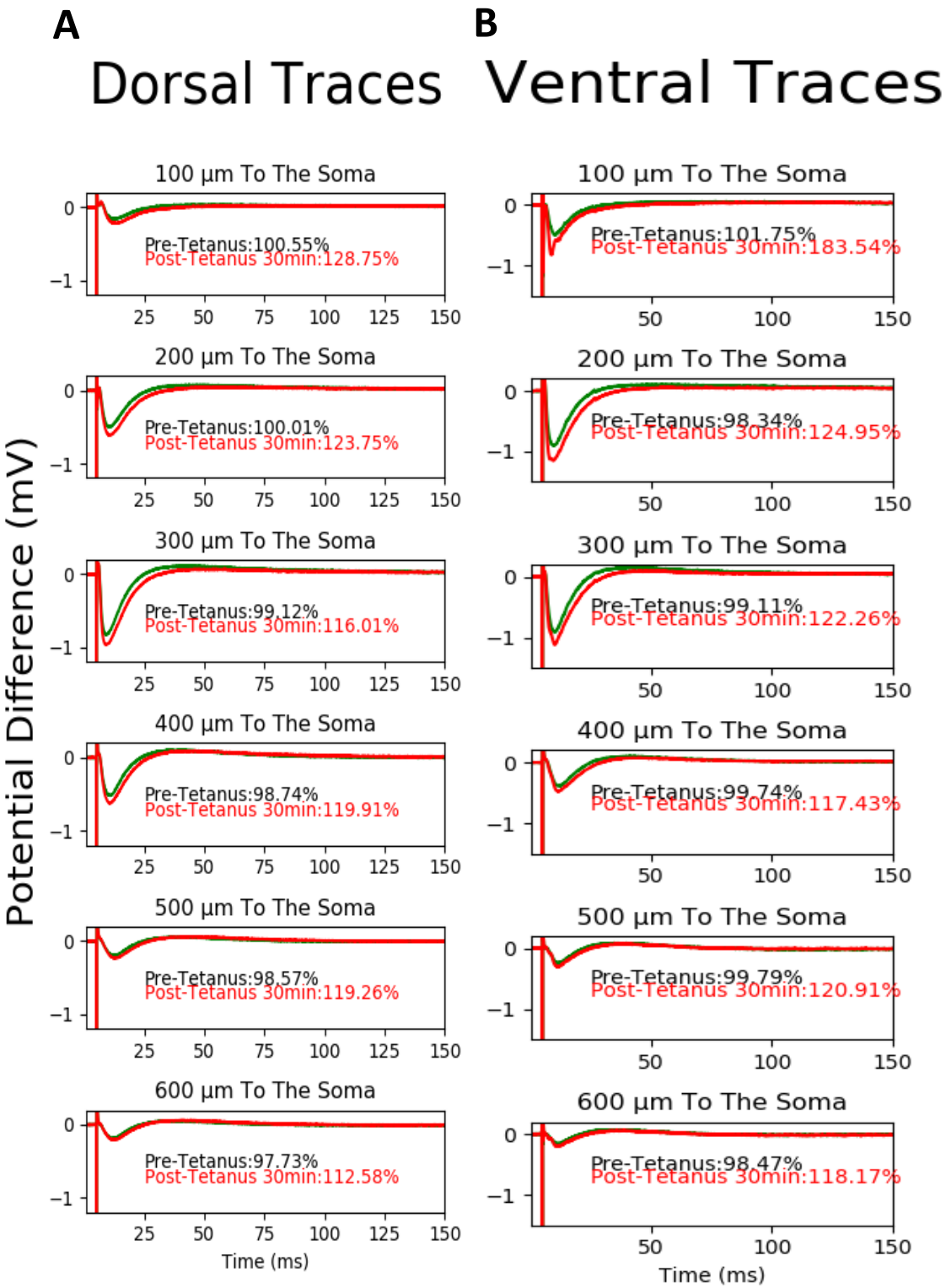

Figure 4.11 Illustrative Traces on Tetanus Induced fEPSP Changes A. Waveform traces from a dorsal hippocampal slice. B. Waveform traces from a ventral hippocampal slice.

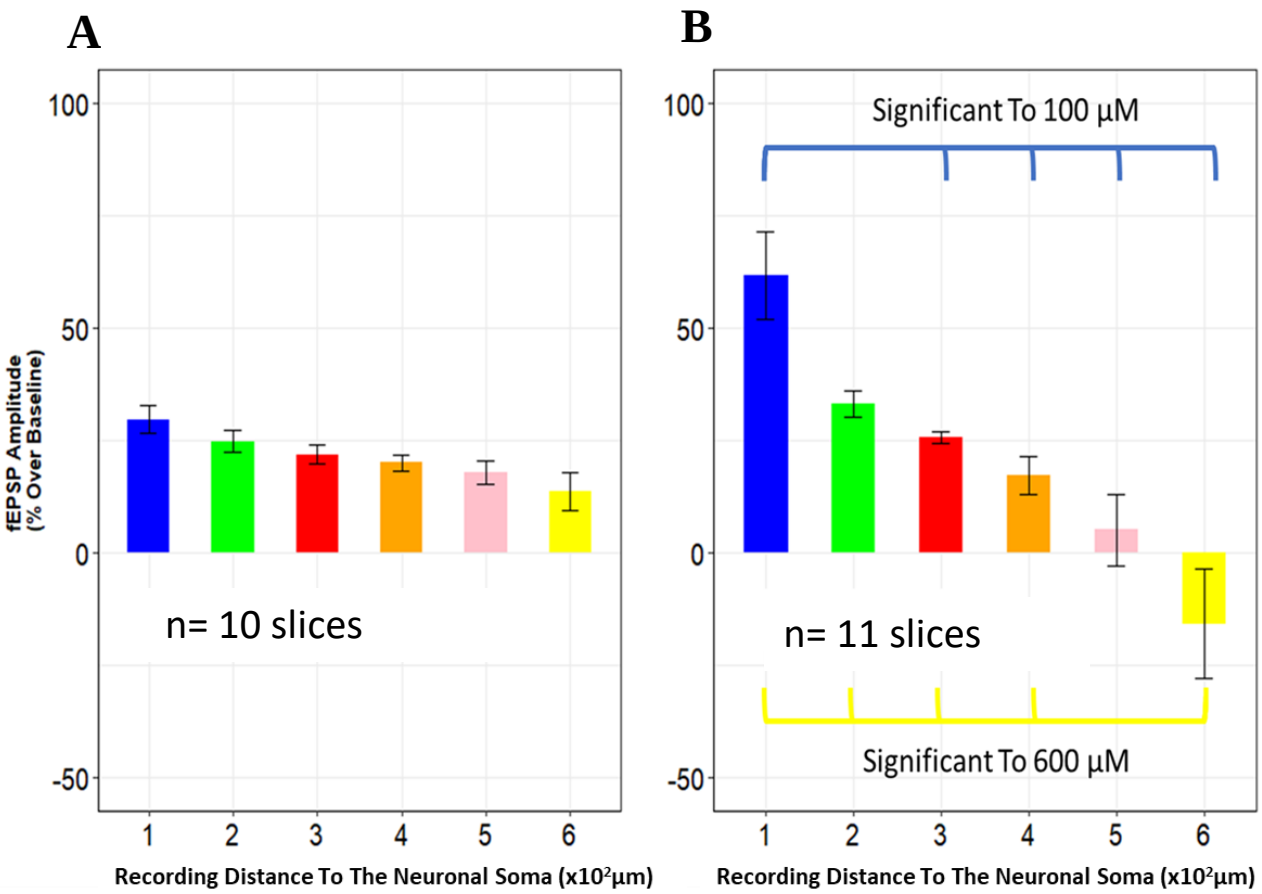

Figure 4.12 fEPSP Potentiation by Recording Distance x Pole A: fEPSP changes induced by tetanus at 100-600 µm recording points in dorsal hippocampal slices. B: fEPSP changes induced by tetanus at 100-600 µm recording points in ventral hippocampal slices. . Data generated from N=10(dorsal) or N=11(ventral) animals, which yielded 1-2 slices per animal. Data averaged over 10 or 11 slices for each recording point, Expressed in Mean+/- SEM

4.3.3 Tetanus Induced Changes on Field Inhibitory Post-Synaptic Potentials

As in fEPSP, there were 126 recording points analyzed from 21 slices contributed by 8 male and 5 female rats. In both male and female slices, a decrease in PGA magnitude can be seen at recording points more proximal to the neuronal soma, while at more distal recording points an increase can be observed as seen in Figure 4.13. Illustrative waveform traces with emphasis on PGA occurring between 15.5 and 70 ms are shown in Figure 4.14. No effect of sex on the last 10-minute average PGA magnitude was detected ($p= 0.98$, $F<0.001$) nor the interaction of sex with recording distance to soma ($p=0.71$, $F=0.59$). In addition, no sex to pole of origin interaction effect was detected ($p= 0.82$, $F=0.07$). Pole of origin along the longitudinal axis also did not affect PGA ($p=0.1608$, $F= 4.76$). Moreover, no significant interaction effect of pole with sex ($p=0.82$, $F=0.07$), or recording distance ($p=0.71$, $F=0.58$) was found. However, a significant effect of recording distance was detected ($p<0.001$, $F= 38.19$). Although a significant interaction effect was found between the three terms (sex X Pole X Recording Distance), no obvious trend can be found in the analysis. Results of linear mixed model analysis are summarized in Table 4.

Table 4.4 Tetanus Experiment Linear Mixed Model on PGA Results

Term	F-value	p-value
Sex	0.00066	0.98
Recording Distance To Soma	38.19	<0.001
Pole of Origin	4.76	0.16
Sex: Recording Distance To Soma	0.59	0.71
Sex: Pole of Origin	0.069	0.82
Recording Distance To Soma: Pole of Origin	2.037	0.082
Sex: Recording Distance To Soma: Pole of Origin	2.68	0.027

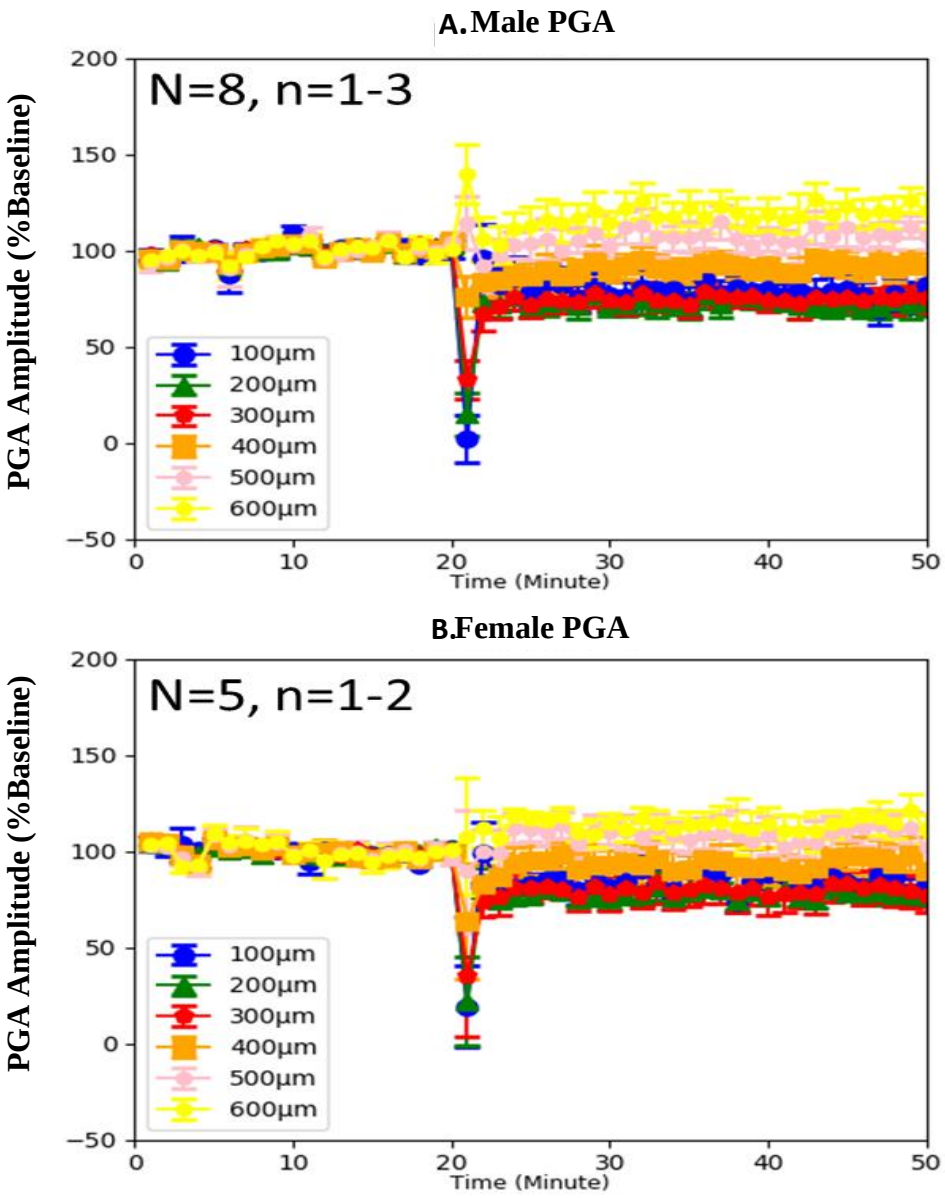

Figure 4. 13 Tetanus Induced Changes in PGA in Both Sexes. A. Male PGA results across the tetanus experiment by recording distance to the neuronal soma. N = 8 animals, n = 1-3 slices per animal. B. Female PGA results across the tetanus experiment by recording distance to the neuronal soma. N = 5 animals, n = 1-1 slice per animals.

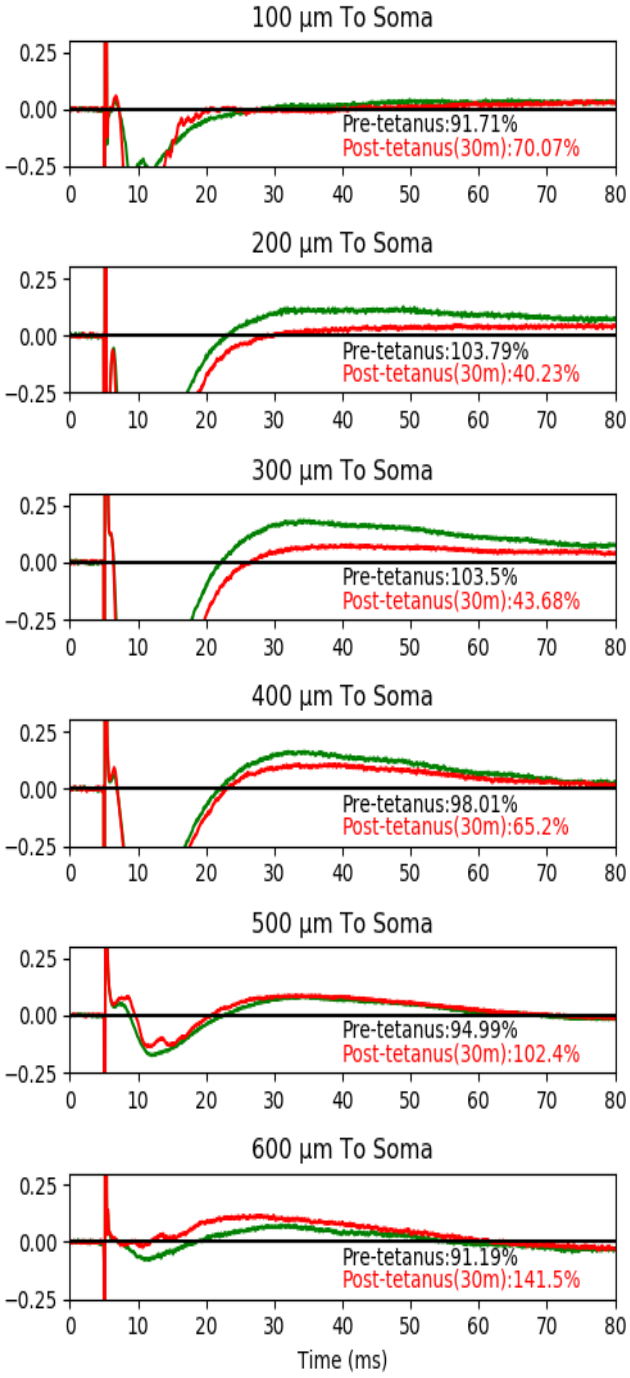

Figure 4.14 Illustrative Traces displaying the PGA. An emphasis is given to the positive going aspect of the waveform occurring between 15.5 and 70 ms. Green: Baseline traces. Red: Post-tetanus traces.

Looking specifically at the level of recording distances, post-hoc analysis revealed that there was no difference between the proximal recording points of 100 µm, 200 µm, and 300 µm to soma. However, there was a significant difference between the three most proximal points and the two most distal points 500 µm and 600 µm (all $p<0.01$). Interestingly, PGA at 400 µm was statistically different to all 5 other recording points. Summary of significant pairwise comparisons is shown in Table 4.5. Results are shown in Figure 4.15.

Table 4.5 Significant PGA Pairwise Comparison on Recording Distance to Soma in Tetanus Experiment. p value adjustment: Tukey method for comparing a family of 6 Estimates.

Pairwise Comparisons (x10^2 µm)	**p-value**
1 - 5	<0.001
1 - 6	<0.001
2 - 4	0.0059
2 - 5	<0.001
2 - 6	<0.001
3 - 4	0.011
3 - 5	<0.001
3 - 6	<0.001
4 - 5	0.0042
4 - 6	<0.001

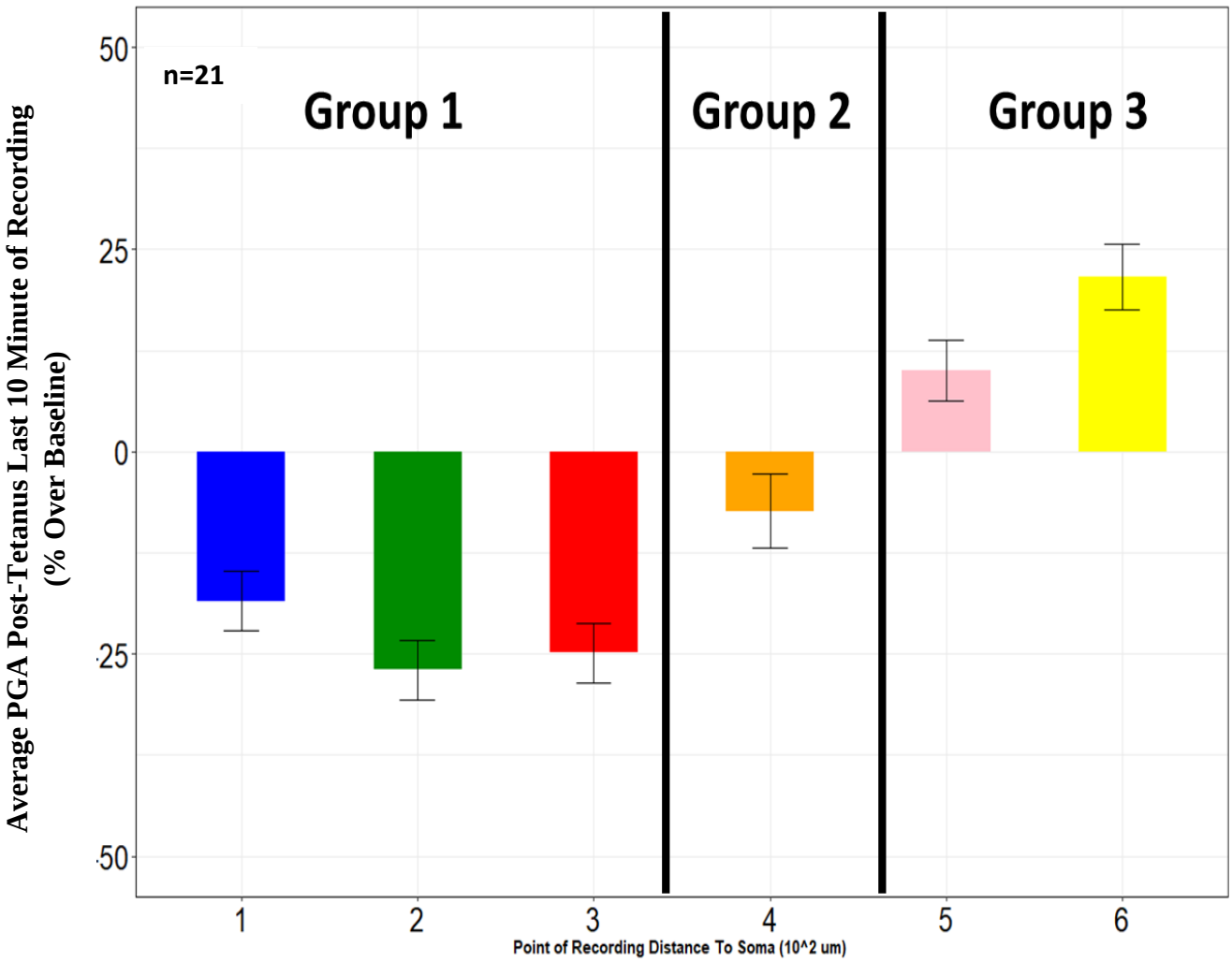

Figure 4.15 Tetanus Induced PGA Changes by Recording Distance. Effects of recording distance to the neuronal soma were found to be significant. Post hoc analysis shows that PGA changes at the recording distances of each group are statistically different than that of another group. Data generated from N=13 animals, which yielded 1-3 slices per animal. Data averaged over 21 slices for each recording point, Expressed in Mean+/-SEM

4.3.4 fEPSP and PGA Co-Analysis on Tetanus Induced Changes

The scatter plots of average fEPSPs and PGAs recorded during the last 10-minutes of the post-tetanus period in all ventral and dorsal slices are presented in Figure 4.16A and Figure 4.16B, respectively. An inverse relation between PGA and fEPSP changes can be seen in both figures with the pattern more robust in ventral slices. Indeed, the Pearson correlation coefficient was calculated to be -0.71 in ventral slices, while only -0.34 in dorsal slices. The correlation indicates that tetanus-induced changes in fEPSP are inversely proportional to tetanus-induced changes in PGA with the trend most robust in ventral slices.

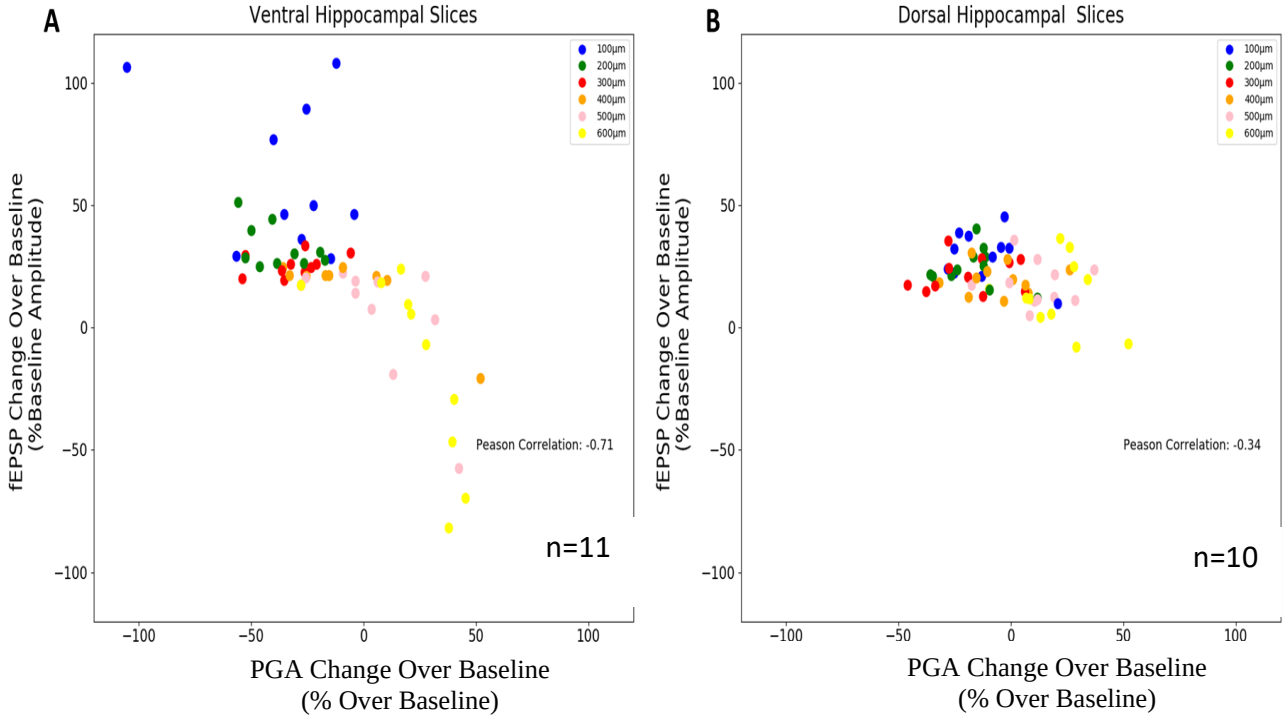

Figure 4.16. Tetanus Induced Changes in PGA vs fEPSP in Dorsal and Ventral Slices. A: Tetanus induced changes in PGA vs fEPSP in ventral slices. Data generated from 11 slices from 9 animals. Pearson correlation = -0.71 B: Tetanus Induced Changes in PGA vs fEPSP in Ventral Slices. Data generated from 10 slices from 10 animals. Pearson correlation = -0.34

4.3.5 APV Effects on Tetanus-Induced Changes in Field Excitatory Post-Synaptic Potentials

In total, there were 48 recording points analyzed from 8 (4 dorsal and 4 ventral) slices generated from 5 animals.

Figure 4.17 displays the normalized fEPSP values of the APV-tetanus experiment by pole of origin along the longitudinal axis. Little to no change can be observed after the start of APV-ACSF perfusion when compared to baseline. After tetanus application, fEPSP potentiation at all recording points seem to be greatly inhibited in the presence of APV compared those seen in the tetanus experiments. Interestingly, tetanus induced fEPSP potentiation shows slightly different patterns in dorsal vs ventral slices under APV. In dorsal slices, some degree of potentiation can still be observed at the most proximal layer. Whereas, in ventral slices, there is a decrease in fEPSP magnitude at the most distal recording point, which seems comparable to what was observed in the tetanus experiment.

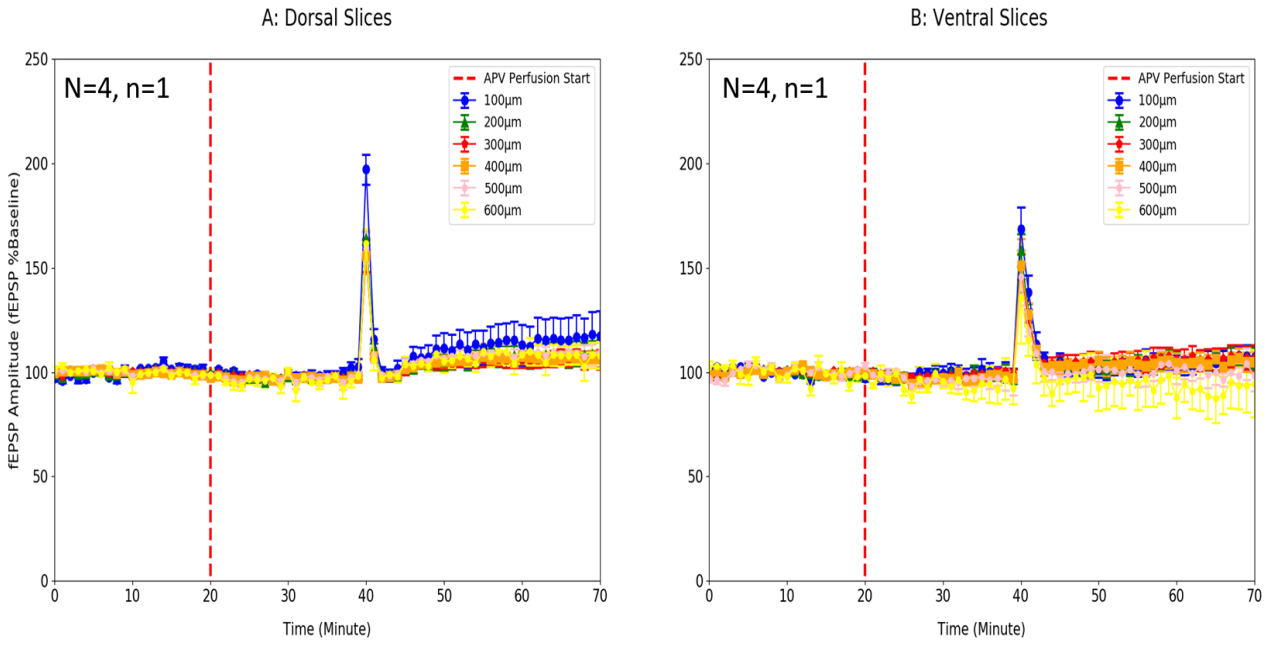

Figure 4.17. APV-Tetanus fEPSP Recording. A: APV-tetanus recording in dorsal hippocampal slices. B. APV-tetanus recording in ventral hippocampal slices. Red: Indicates the beginning of APV-ACSF perfusion.

A statistical significance was found in phase (Baseline, APV, and APV-LTP; $p<0.01$, $F=20.61$) and its interaction with pole of origin ($p=0.03$, $F=3.72$). No other significant main effects were found: 1. Recording Distance to Soma ($p=0.06$, $F=2.2$) or 2. Pole ($p=0.49$, $F=0.70$). Also, no other statistically significant interaction effect was found. Results are summarized in Table 4-6

Table 4.6 APV-Tetanus Experiment Linear Mixed Model on fEPSP Results

Term	F-Value	p-Value
Phase	20.61	<0.01
Recording Distance To Soma	2.2	0.06
Pole of Origin	0.69	0.49
Phase: Recording Distance To Soma	0.51	0.88
Phase: Pole of Origin	3.72	0.028
Recording Distance To Soma: Pole of Origin	1.04	0.4
Phase: Recording Distance To Soma: Pole of Origin	0.57	0.83

Looking into experimental phase, post-hoc pairwise Tukey's test analysis reveals that there were no significant differences in fEPSP 10-minute average during the last 10 minutes of recording between baseline and APV phase in both dorsal ($p=0.77$) and ventral slices ($p=0.87$). Moreover, it was found that the LTP phase in dorsal hippocampal slices was significantly different to both APV ($p<0.001$) and baseline ($p=0.001$) phases (Table 4-7). Similar differences were not found in ventral slices. A summary of the findings is illustrated in Figure 4.17. Results indicate that APV did not affect baseline synaptic transmission in both dorsal and ventral slices. However, APV is more effective at blocking fEPSP potentiation in ventral slices compared to dorsal slices.

Table 4.7 fEPSP Pairwise Comparison on Experiment Phase and Pole of Origin in APV-Tetanus Experiment. p value adjustment: Tukey method for comparing a family of 6 Estimates.

Pairwise Comparison (Experiment Phase, Pole)	p value
APV, Dorsal - LTP, Dorsal	<0.001
Baseline, Dorsal - LTP, Dorsal	<0.001
Baseline, Dorsal - APV, Ventral	0.94
Baseline, Dorsal - Baseline, Ventral	1.00
Baseline, Dorsal - LTP, Ventral	0.96
LTP, Dorsal - APV, Ventral	0.23
LTP, Dorsal - Baseline, Ventral	0.32
LTP, Dorsal - LTP, Ventral	0.53
APV, Ventral - Baseline, Ventral	0.88
APV, Ventral - LTP, Ventral	0.09
Baseline, Ventral - LTP, Ventral	0.62

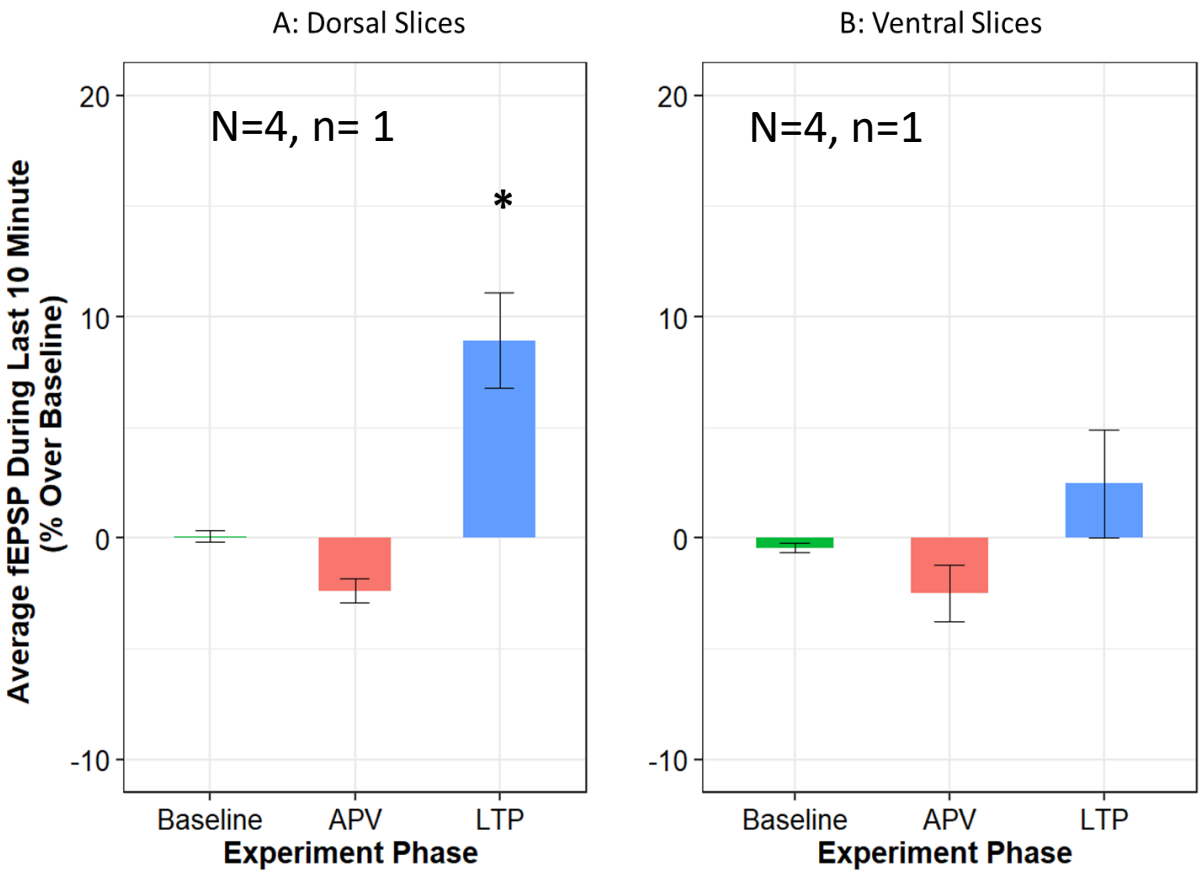

Figure 4.18. APV-Tetanus fEPSP: Phase x Pole. A: Average fEPSP during last 10 minutes of each experimental phase in dorsal hippocampal slices. B: Average fEPSP during last 10 minutes of each experimental phase in ventral hippocampal slices. Explain the meaning of the asterisk. Provide numbers of animals/slices, not recording points. Data generated from N=4 (dorsal) or N= 4 (ventral) animals, which yielded 1-2 slices per animal. Data averaged over 4 slices for each recording point in both dorsal and ventral slices, Expressed in Mean+/-SEM

4.3.6 APV Effects on Tetanus Induced Changes in Field Inhibitory Post-Synaptic Potentials

Figure 4.19 displays the normalized PGA values of the APV-tetanus experiment by pole of origin along the longitudinal axis. Similar to fEPSP, no notable changes in PGA amplitude can be seen upon the introduction of APV-ACSF in both dorsal and ventral slices. The decreases in PGA after tetanus seem to be directly proportional to the recording distance to the neuronal soma. The more proximal the recording point to the neuronal soma the larger the decrease in magnitude induced by the tetanus. Interestingly, no increases/potentiation in PGA can be

observed in the more distal recording points 500 µm and 600 µm, which appeared in the tetanus experiment.

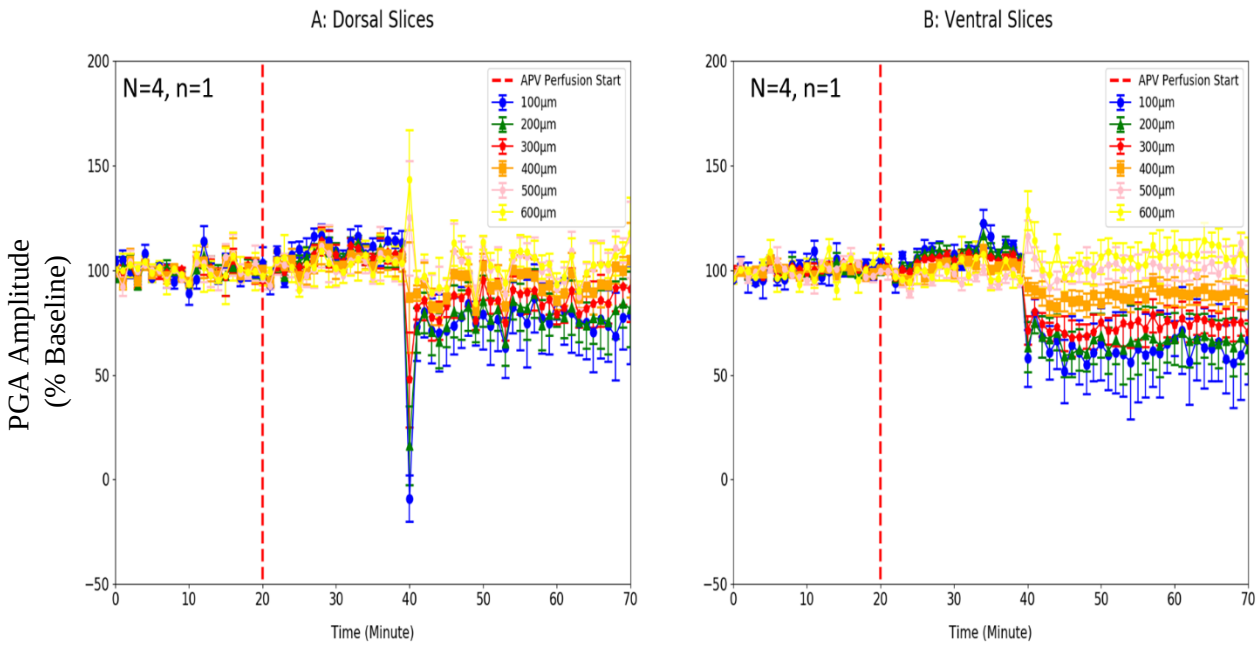

Figure 4.19.APV-Tetanus PGA Recording. A: APV-tetanus recording in dorsal hippocampal slices. B. APV-tetanus recording in ventral hippocampal slices. Red line: Indicates the beginning of APV-ACSF perfusion.

Statistical significance of main effects was detected in experiment phase ($p<0.001$, $F=44.67$) and recording distance to neuronal soma ($p<0.014$, $F=2.99$). The interaction between experiment phase and recording distance was found to be significant ($p<0.001$, $F=7.81$). No other mains or interaction effects were detected (Pole: $p=0.71$, $F=0.19$). All results of the linear mixed model analysis are presented in Table 4-8. Figure 4.20 shows the interaction plot between experimental phase and recording distances.

Table 4.8 APV-Tetanus Experiment Linear Mixed Model on PGA Results

Term	F-value	p-value
Phase	44.67	<0.001
Recording Distance To Soma	2.99	0.015
Pole of Origin	0.19	0.71
Phase: Recording Distance To Soma	7.81	<0.001
Phase: Pole of Origin	0.71	0.49
Recording Distance To Soma: Pole of Origin	0.32	0.9
Phase: Recording Distance To Soma: Pole of Origin	0.57	0.83

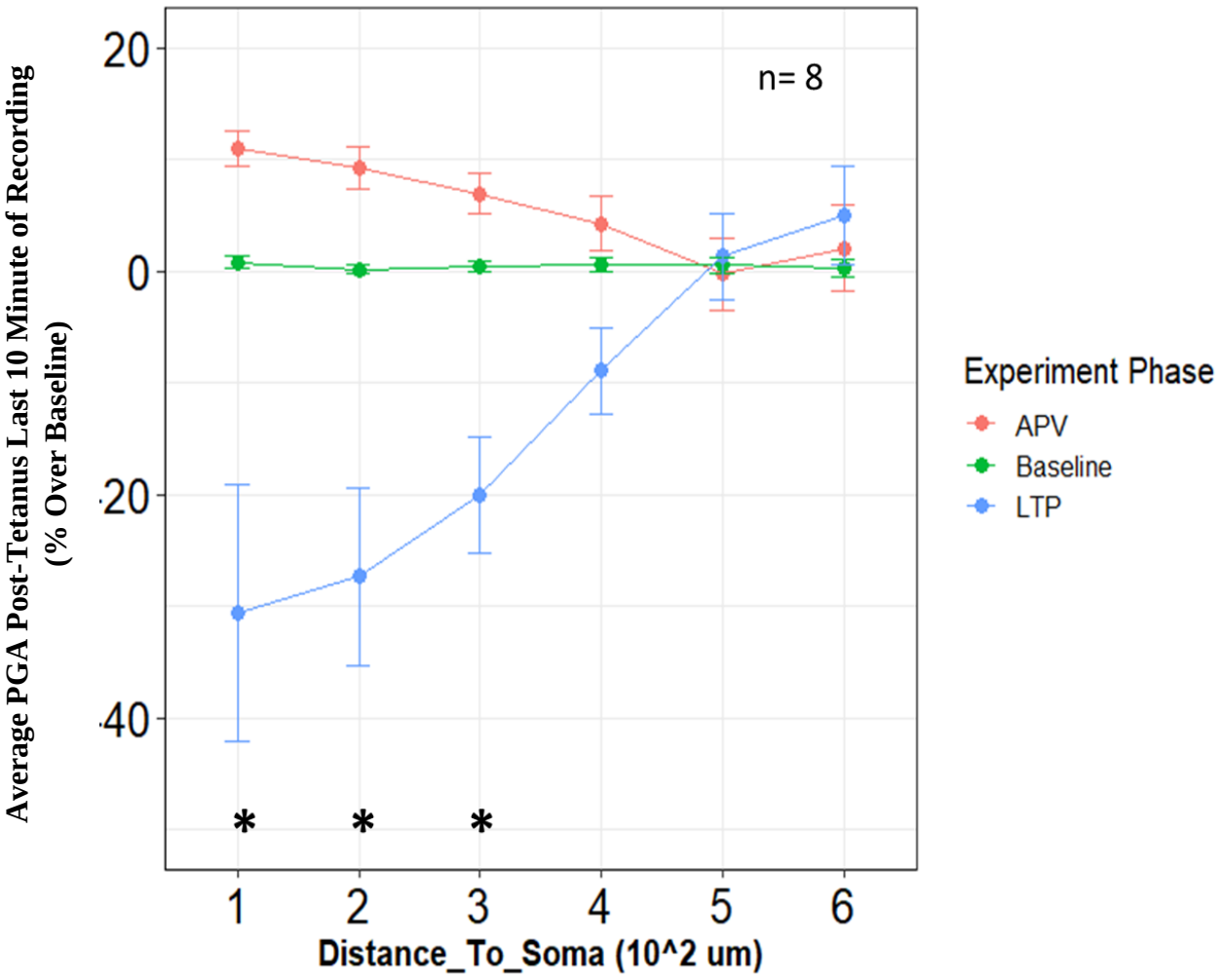

Figure 4.20. PGA Interaction Plot: Experiment Phase vs Recording Distance. * indicates statistical significance compared to Baseline and APV phase. Data generated from N= 5 animals, which yielded 1-2 slices per animal. Data averaged over n=8 slices for each recording point, Expressed in Mean+/-SEM

Looking at experimental phase, post hoc Tukey's test revealed that there was no significant difference in PGA changes over baseline in APV and Baseline phase across all experimental points. A difference in APV-LTP phase between the two other phases (APV and Baseline) was seen at recording distances 100, 200, 300 μm to the neuronal soma (all $p \leq 0.01$). Since the experimental phase and recording distance interaction was significant, while no differences were observed between Baseline and APV at all recording points, it is warranted to compared PGA values at APV-LTP phase between all recording points. A similar pattern to tetanus induced change in PGA of tetanus experiment can still be observed in the PGA of APV-LTP phase, i.e., a decrease in PGA at more proximal recording points while an increase at more distal points. Indeed, Tukey's pairwise comparison found significant differences between any recording points at 100-300 μm to those at 500-600 μm. Interestingly, a decrease in the degree of potentiation (the increase in PGA) at the most distal recording points (500-600 μm) can be observed compared to that of the tetanus experiment (no statistical tests). Complete pairwise results of recording points in APV-LTP phase reaching statistical significance are summarized in Table 4-9 and illustrated in Figure 4. 20.

Table 4.9. PGA Pairwise Comparison Between Recording Points in APV-LTP Phase. p value adjustment: Tukey method for comparing a family of 18 Estimates. 1-6: Recording Distance To Soma x10^2 μm

Pairwise Comparisons (Experiment Phase, Recording Distance To Soma x10^2 μm)	**p-value**
APV-LTP,1 – APV-LTP,2	1.00
APV-LTP,1 – APV-LTP,3	0.82
APV-LTP,1 – APV-LTP,4	0.0055
APV-LTP,1 – APV-LTP,5	<0.01
APV-LTP,1 – APV-LTP,6	<0.01
APV-LTP,2 – APV-LTP,3	0.99
APV-LTP,2 – APV-LTP,4	<0.01
APV-LTP,2 – APV-LTP,5	<0.01
APV-LTP,2 – APV-LTP,6	<0.01
APV-LTP,3 – APV-LTP,4	0.76
APV-LTP,3 – APV-LTP,5	0.007
APV-LTP,3 – APV-LTP,6	<0.01
APV-LTP,4 – APV-LTP,5	0.86
APV-LTP,4 – APV-LTP,6	0.37
APV-LTP,5 – APV-LTP,6	1.00

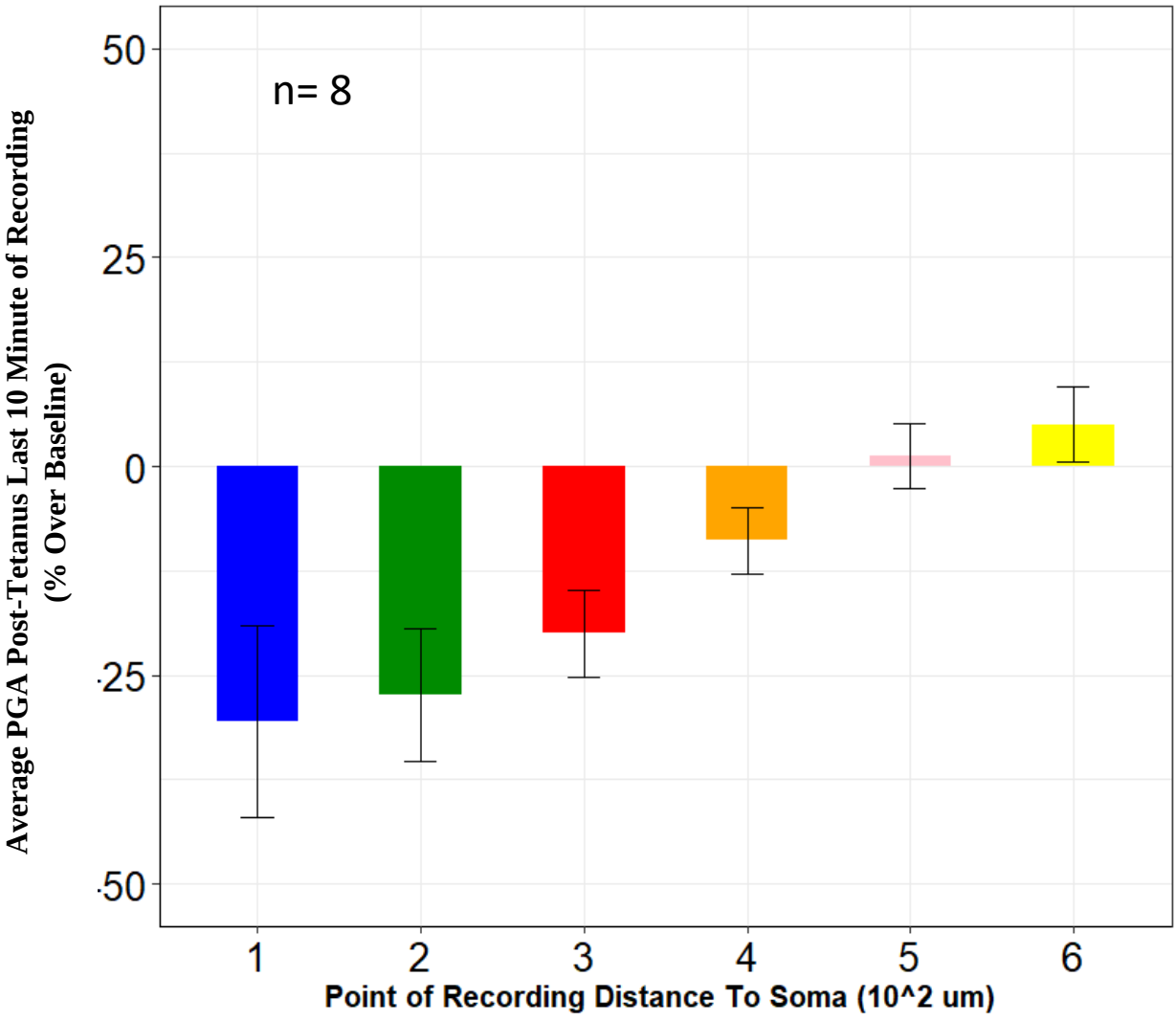

Figure 4.21. APV-Tetanus PGA at LTP Phase Data: Mean+/-SEM. Data generated from N=5 (ventral) animals, which yielded 1-2 slices per animal. Data averaged over 8 slices for each recording point, Expressed in Mean+/-SEM

4.4 Discussion

4.4.1 Principal Component Analysis

PCA revealed that there were two components in the waveforms that contribute to the overall variation induced by the tetanus protocol. In other words, collecting information on these two components will persevere the majority of information during tetanus protocol induces changes in the evoked response. Through observing and interpreting principal component scores with the waveform trajectory, the two main components seem to correspond best to the initial fast going negative deflection (appears between 6.5 ms – 15 ms) and the later slow positive going deflection (appears between 15.5-70 ms). However, it is important to note that the interpretation or locating where these principal components could be in the original data maybe biased by the analyst, i.e. different people may have different interpretations.

In the CA1 apical dendritic field, The negative-going component has been the primary interest in the majority of synaptic plasticity studies (Bliss & Collingridge, 2013; Bliss et al., 2018; Collingridge et al., 1983). This negative going aspect is believed to be reflective of glutamatergic transmission and has been dubbed field excitatory post-synaptic potential (fEPSP). During baseline, the fEPSP is mainly contributed by the activation of post-synaptic AMPA receptors by the pre-synaptic release of glutamate which is evident by the reversible blockage of the antagonist CNQX (Scharfman, 1993).

In comparison, there is very little information regarding the PGA that was identified. In 1995, Arai et al first isolated and examined a $GABA_A$ dependent later slow, positive going potential by recording the evoked field responses in the presence of NMDA and AMPA receptor antagonist. The isolated component was found to be more prominent in more distal point to the neuronal soma while being a negative deflation at the neuronal soma (Arai et al., 1995; Kolta et al., 1996). Now,

this component is believed to be a result of GABA release from interneurons from the activation of pre-synaptic glutamate release, or through this direct stimulation by the bipolar pulse given (Hulme et al., 2014). Some have speculated its prime purpose to act as feedforward inhibition to modulate the fEPSP (Colavita et al., 2016). Hence, this component has been dubbed field inhibitory post-synaptic potentiation (fIPSP) in 1995 by Arai et al. Recently, the existence of a non-uniform $GABA_A$ mediated fIPSP has been confirmed in the CA1 of rodent hippocampus through voltage sensitive dye imaging (Colavita et al., 2016). Hence, the laminar specific fIPSP expression maybe likely due to the different subtypes of interneurons distributed in the CA1 region. The PGA described in our current study shares many characteristics of the fIPSP such as time of occurrence (after the fEPSP), kinetics (slow going positive potential), and laminar response profile (negative at soma and most prominent when distal to soma). However, it is yet to be determined whether the PGA is also $GABA_A$ mediated which would completely equivalent the two phenomena once proven.

Overall, principal component analysis of evoked extracellular waveforms yielded two components of interest that can explain the majority of variation in the waveform across the tetanus experiment. Historically, much attention has been given to the study and analysis of the fEPSP component. However, current PCA results calls for the need to at least analyze two components in evoked field potential experiments to minimize information lost. Under our current inference, it was determined that in addition to the fEPSP the PGA should be included.

4.4.2 Effect of Recording Distance and Pole of Origin in fEPSP Potentiation

A main discovery of this study is that an LTP magnitude gradient phenomenon exists in ventral slices, while seemly to a lesser degree or even absent in dorsal slices. The LTP magnitude gradient observed is where the degree of potentiation was inversely proportional to recording

distance to the soma. Surprisingly, a decrease or depression like phenomenon in fEPSP was even observed at more distal points in ventral slices. Current results are consistent with a previous study by Kopanitsa et. al. (2006), the authors recorded LTP expression in relation to distance of the recording point to the neuronal soma. Earlier founding by Kolta et. al. (1995) also reported that more distal synapses were more difficult to potentiate compared to more proximal one. Although ignored, their results also showed that the most proximal recording point not only had the highest degree of potentiation, but also the highest degree of variability across all slices recorded. The variability observed in their study can roughly be estimated to be +/- 50% (standard error of mean), which might have been due to the fact that they ignored the origin of where the slice came from along the longitudinal axis. Indeed, current results also show that the highest degree of potentiation is observed at the most proximal recording point in ventral hippocampal slices which may give rise to the higher variability seen in their study, which combined dorsal and ventral slices

Despite evidence showing LTP magnitude is higher in dorsal hippocampal slices (Dubovyk & Manahan-Vaughan, 2018; Maggio & Segal, 2009), ventral hippocampal slices have an increased excitability. In theory, the increased excitability of ventral pole neurons should indicate an increased capacity to express higher magnitudes of LTP (Cohen et al., 1999). Biochemistry studies have shown ventral slices to express higher NMDA receptor levels, while simultaneously having lower expression of GABA-A receptors (Dubovyk & Manahan-Vaughan, 2018). Moreover, the ventral hippocampus contains a significantly higher density of Synaptopodin puncta, a binding protein positively associated with expression of synaptic plasticity, than the dorsal (Vlachos et al., 2008). Accordingly, multiple studies have found that ventral hippocampal CA1 pyramidal neurons are more excitable, including higher probability to elicit action potential, a more polarized membrane potential and a lower input resistance compared to their dorsal counterparts (Dougherty

et al., 2012; Kim & Johnston, 2015; Milior et al., 2016). Contrary to this evidence, majority of studies show that dorsal hippocampal slices express a higher degree of LTP.

Reasons for the contradiction between higher excitability and lower LTP expression in ventral hippocampal slices in previous studies maybe due to an increased threshold/ restriction. The increased threshold are likely to be due to post-synaptic mechanisms as previously it was shown that although ventral pyramidal neurons have higher excitability when directly injected with current, stronger afferent stimulations were needed to elicit action potentiation firing compared to dorsal neurons (Dubovyk & Manahan-Vaughan, 2018). The increased threshold for LTP expression is also further supported by the fact that basal release probability of neurotransmitters is the same in dorsal and ventral hippocampal slices (Babiec et al., 2017). Possible mechanisms for higher threshold for LTP expression in the ventral hippocamps may include the recruitment of SK channels by NMDA activation (Babiec et al., 2017) and activation of extra synaptic GluN2B receptors by presynaptic glutamate spill over (Delgado et al., 2018), all of which would produce an opposing hyperpolarising current to oppose LTP induction, during tetanus.

The majority of previous studies in dorsal and ventral hippocampal slices have only used relatively weaker LTP induction protocols such as a single tetanus, or theta burst to induce LTP. Therefore, it can then be hypothesized that a stronger stimulus (2 x tetanus) can evoke a stronger LTP expression in ventral hippocampal slices as seen in the current study. In accordance to this assumption, increased trains of theta burst have been shown to induce similar magnitude of LTP expression in both dorsal and ventral slices (Kouvaros & Papatheodoropoulos, 2016). The theory of a higher threshold for LTP induction in ventral slices is also supported by stress inducing higher LTP expression in only ventral hippocampal slices (Grigoryan et al., 2015; Keralapurath et al., 2014). The underlying mechanisms of stress induction of LTP expression has been proposed to be

due to an increased excitatory state in pyramidal neurons through decreases in GABA current or action of corticosterone stress hormone (Maggio & Segal, 2012). Regardless, there is evidence suggesting additional mechanism at play that would increase the threshold (stronger stimulus pattern needed) for LTP expression in CA1 ventral hippocampus.

Ventral hippocampal LTP expression is currently shown to be more dependent on NMDA receptors compared to dorsal hippocampal slices. Our current results show that APV does not affect basal synaptic transmission in both dorsal and ventral hippocampal slices at all recording distances, which is consistent with previous findings. Interestingly, it was observed that LTP can still be expressed to some degree in dorsal slices in the presence of NMDA receptor antagonist carboxypiperazin propyl phosphonic acid. Papatheodoropoulos and Kouvaros (2016) found that ventral slices expressed only NMDA-dependent LTP whereas dorsal hippocampal slices also expressed NMDA-independent LTP. It was found that the L-type voltage-gated channels, the main molecular mechanism for NMDA-independent LTP, was more effective/ involved in LTP expression in dorsal hippocampal slices (Papatheodoropoulos & Kouvaros, 2016).

4.4.3 Effect of Recording Distance on Tetanus Induced PGA Changes

Current results indicate that PGA after tetanus shows a decrease in amplitude (depression like phenomenon) at more proximal layers while an increase (potentiation) at more distal recording points. In contrast to the fEPSP, this pattern is consistent in both dorsal and ventral hippocampus. Sadly, there are very few studies on the PGA in the current literature. To date, there has only been one study that investigated the changes induced by tetanus on the fIPSP (Arai et al., 1995). Similar to fIPSP, a temporary depression can be observed in the current study at most recording points, except distal points, after the application of tetanus. However, Arai et al. (1995) did not observe any lasting changes after the initial depression. Two main reasons can be speculated for the

differences in the PGA observed in the current study and the fIPSP by Arai et. al. (1995). One reason may be due to the fact that Arai et al (1995) applied CNQX, an AMPA and NMDA receptor antagonist as there has been evidence suggesting both NMDA and AMPA receptors play a crucial role in interneuron synaptic plasticity (Pelkey et al., 2017). Another reason, similar to most LTP studies on fEPSP, may be the disregard for where the PGA change was recorded. Our current results show that there are recording positions which have minimal change in PGA after tetanus induction (PGA 400 μm in tetanus experiment).

Synapses of interneurons in the CA1 region can express both LTP and long-term depression (LTD). In 1995, it was first shown through intracellular recordings that tetanus stimulation on excitatory synapses can potentiate interneurons in CA1 of the hippocampus (Ouardouz & Lacaille, 1995). Later, it was also shown that the same tetanus stimulation pattern could induce LTD in the hands of another group (McMahon & Kauer, 1997). Indeed, it is now clear that interneurons can express both LTP and LTD under similar electric conditioning protocols (Cowan et al., 1998; Laezza & Dingledine, 2004). One reason is that, with our increasing understanding, there are multiple interneuron types in the CA1 region, which were not previously known (NyÍri et al., 2003; Pelkey et al., 2017). Moreover, there is some laminar specificity to the housing of specific interneuron populations (Pelkey et al., 2017). At different laminar, the different interneurons can express different forms of plasticity in response to one stimulus. In consistent with this notion, results of this study show that tetanus can induce depression of PGA at proximal recording points to the soma whereas a potentiation in PGA at more distal recording points. The complexity of interneuron distributions is well beyond the scope of this project and even to this day, the distribution and composition of all types of interneurons in the CA1 of the hippocampus is not fully understood.

Both NMDA dependent and independent synaptic plasticity expression have been found in interneurons (Pelkey et al., 2017). Although some evidence and speculation exist in the literature, the exact mechanism and contribution of NMDA receptors to interneuron plasticity is unknown. Regardless, this would not hinder the interpretation of our results. In the APV-tetanus study, NMDA receptors does not seem not to affect the PGA gradient as a whole and that the same pattern of potentiation at proximal recording points whereas depression like phenomenon at distal points. Through observatory comparison to the tetanus experiments, it can be observed that NMDA receptors do not contribute much to the depression like phenomenon at the proximal recording points. In contrast, a notable decrease in the degree of PGA potentiation at distal recording points in the presence of APV can be seen. Therefore, it can be speculated that NMDA receptors may play a significant role in tetanus-induced potentiation of PGA at distal recording points.

4.4.4 fEPSP and PGA

Current results suggest an inverse relationship between tetanus-induced changes in fEPSP and PGA at all recording points. At more proximal recording points, the fEPSP is potentiated while the PGA is decreased/depressed. In contrast, fEPSP is depressed while PGA is potentiated at more distal recording points. Although this relationship is less robust in dorsal slices, this pattern can be observed in slices from both poles. At recording points where the fEPSP shows potentiation, the decrease/depression in IPSP has been speculated as a duel mechanism to facilitate the LTP phenomenon (McMahon & Kauer, 1997). Interestingly, the reverse seems to also be true, i.e. the decrease/depression in fEPSP seem to be facilitated by a potentiation in PGA.

4.6 Conclusion

The current study is the first to record and analyze evoked waveforms in acute hippocampal slices stratified by distance of recording point to soma and origin of the slice along

the longitudinal axis. First, fEPSP potentiation gradient is inversely proportional to the distance of the recording point to the neuronal soma. It was also observed that dorsal, but not ventral, slices can exhibit NMDA-independent potentiation. In regards to PGA, a potentiation gradient that is directly proportional to distance of the recording point to the soma which has a NMDA dependent component in both poles. Furthermore, this study describes an inverse relation where if the fEPSP potentiates, the PGA depresses and vice versa along the apical dendritic field. In summary, current results indicate the importance of: 1. Stratifying by pole of slice origin along the longitudinal axis and distance of the point of recording to the neuronal soma when studying evoked potentials in hippocampal slices and 2. Documenting and analyzing the positive component PGA of the evoked response.

Appendix A

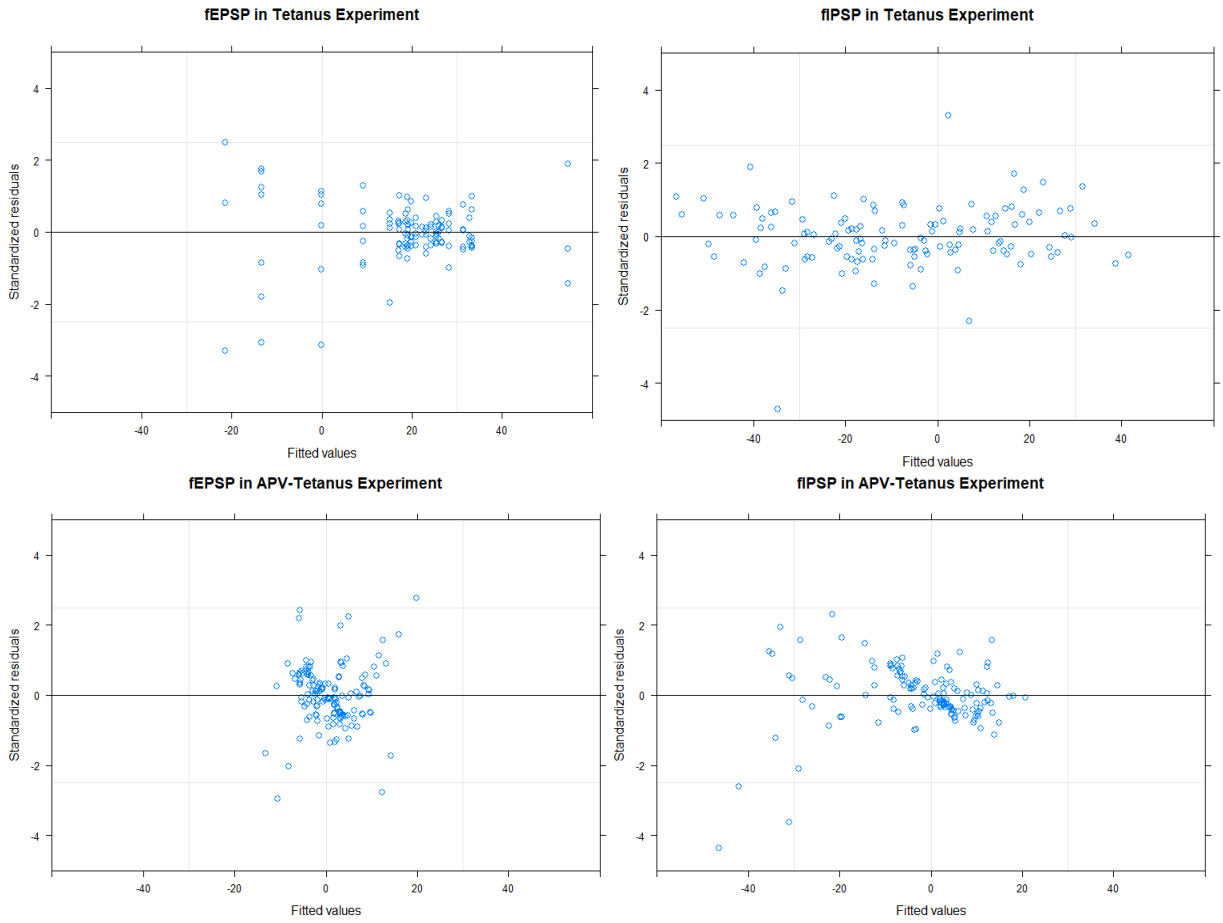

Supplementary Figure A1. Fitted Values vs Standard Residual Plot for All Models. The plots show that the assumption of homogeneity is not violated in all models

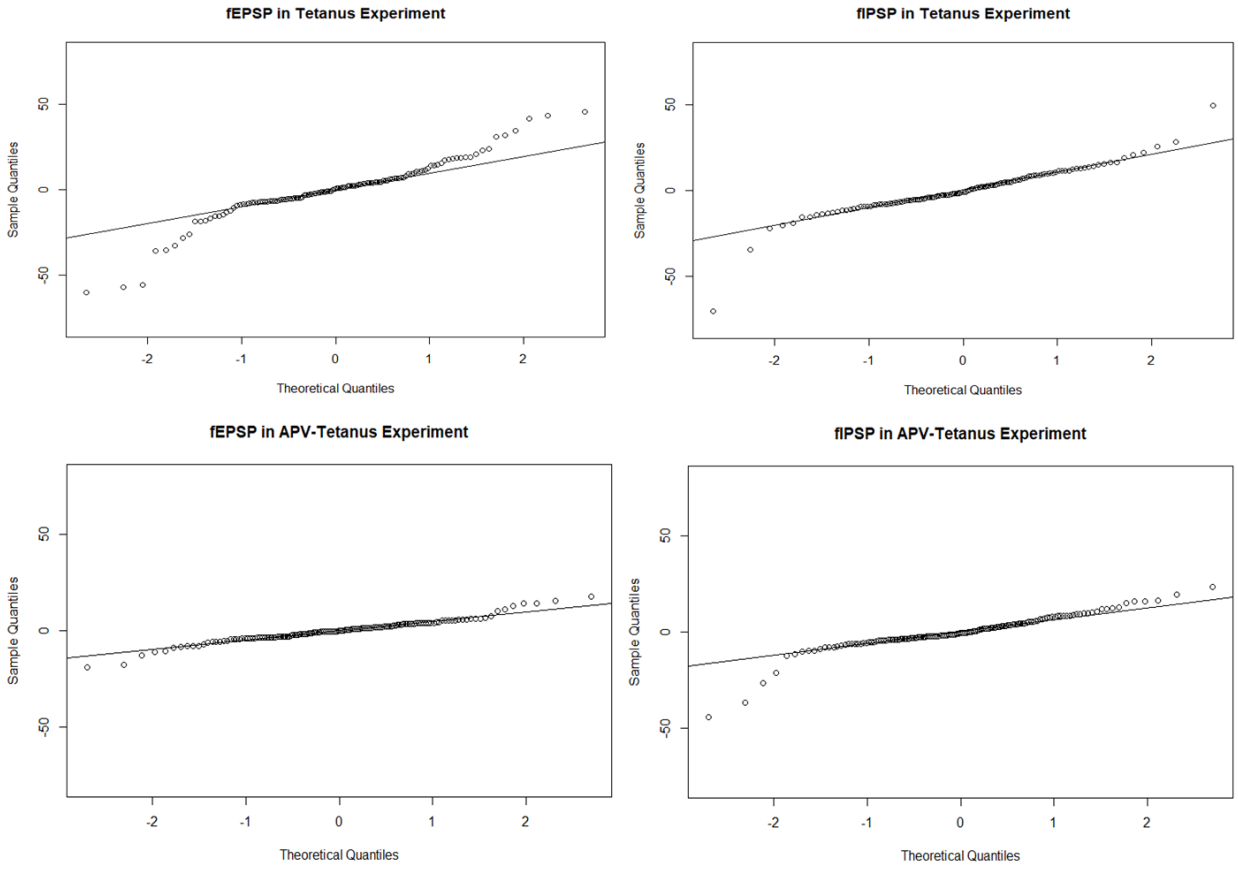

Supplementary Figure A2. Normal Q-Q Plot for All Models Used It can be observed that all models do not violate the assumption of independence with the exception of the fEPSP in tetanus experiment mode. It is noted that slight/limited degrees of skewness can be observed in the other models.

Supplementary Table B 1. Table of %Variation Contribution by The First Two Components at Each Recording Point

			% Variation Contribution by The First Two Components at Each Recording Point					
Animal#	**Gender**	**Pole**	**100 µm**	**200 µm**	**300 µm**	**400 µm**	**500 µm**	**600 µm**
1	Male	Dorsal	62	86	92	89	84	59
1	Male	Ventral	91	96	96	92	78	63
2	Male	Ventral	81	87	91	76	82	82
3	Male	Ventral	88	95	97	89	80	64
4	Male	Dorsal	85	92	93	86	83	76
4	Male	Ventral	91	96	97	94	84	74
5	Male	Ventral	95	98	95	87	69	65
6	Male	Dorsal	87	96	94	89	92	81
6	Male	Ventral	80	86	86	76	92	92
7	Male	Dorsal	93	97	94	89	78	70
8	Male	Dorsal	91	96	95	89	82	71
8	Male	Ventral	95	96	84	88	78	78
8	Male	Ventral	84	93	92	84	85	73
10	Female	Dorsal	88	94	96	93	85	80
11	Female	Dorsal	95	97	97	93	86	79
12	Female	Dorsal	93	93	86	79	72	64
12	Female	Ventral	78	83	85	82	63	56
13	Female	Dorsal	86	92	94	93	88	84
14	Female	Dorsal	80	89	94	88	79	73
14	Female	Ventral	83	93	94	92	79	49
14	Female	Ventral	94	97	97	92	72	77

5.0 Effects of Methylmercury on Tetanus-Induced Changes in fEPSP and PGA

5.1 Overview

The main purpose of the current chapter is to investigate the effects of MeHg on synaptic plasticity in the CA1 region of acute hippocampal slices using the tools developed in Chapter 4. Specifically, the goal is to investigate the effects of MeHg on the fEPSP and PGA, which may reflect excitatory glutamate and inhibitory GABA transmission, to a certain extent. MeHg effects would be investigated at levels: 1. that are seen in the brains or regular populations and 2. doses that do not affect basal transmission.

5.2 Materials and Methods

5.2.1 Electrophysiology Experiments

Female and Male SD rats (12-20 weeks old) were purchased from Envigo™ and anaesthetized with CO_2. After decapitation, brains were quickly removed and placed in ice cold oxygenated (95% O_2:5% CO_2) artificial cerebrospinal fluid (ACSF). ACSF composition was as follows: 127.0 mM NaCl, 2.0 mM KCl, 1.2 mM KH_2PO_4, 26.0 mM $NaHCO_3$, 2.0 mM $MgSO_4$, 2.0 mM $CaCl_2$, 10.0 mM glucose (pH 7.4; osmolality 300-320 mOsm). The right hippocampus was extracted and 350 μm thick transverse slices were prepared using a McIlwain tissue chopper, sectioning the hippocampus from dorsal to ventral along the longitudinal axis. Slices generated from the approximate first 2 mm were defined as dorsal slices. Ventral slices were generated from tissue that was at least 4.55 mm away from the first 2 mm (dorsal) portion. Slices would then be transferred to a custom holding chamber filled with oxygenated ACSF (35°C) and allowed to recover at interface (95 % O_2:5 %CO_2) for a minimum of 2 hours.

5.2.2 Field Excitatory Postsynaptic Potential Recording

Evoked responses were recorded using an 8 x 8 multi-electrode array probe (electrode size 20 x 20 μm, interelectrode distance of 100 μm). Responses were evoked and sampled at 0.167 Hz using the MED64 system (Alpha MED Scientific Inc., Osaka). The first row of the electrode probe was consistently placed at the SP layer or approximately 100 – 200 um away from the neuronal soma. Warmed and oxygenated ACSF (32°C) was perfused at a rate of 1-1.5 mL/min. Slices were allowed to rest on the probe for a minimum of 20 minutes following placement. Subsequently, points of stimulation in the SR would be selected in the CA1 region of each slice. Points of recording were up to 600 μm from the soma that are 100 μm away from the stimulating electrode on the horizontal axis, i.e. 6 points were recorded per slice. If electrical noise was present, the adjacent channel that was 100 μm away along the horizontal axis was analyzed.

The fEPSP amplitude were extracted as the minimum value located between 6 to 15 ms of the evoked response. The field inhibitory post-synaptic potential (PGA) amplitude were extracted as the maximum value located between 15.5 to 70 ms. In other word, the fEPSP and PGA represent absolute amplitude differences to zero at 6 to 15 ms and 15.5 to 70 ms, respectively. For each slice, an average of the first twenty minutes served as a baseline to which all values were normalized for both fEPSP and PGA. The average increase over baseline in the last 10 minutes of recording after tetanus was taken as the degree of potentiation.

N indicates the number of animals whereas n indicates the number of slices.

5.2.3 Imaging and Determination of Electrode Position in the CA1

Placement of the hippocampal slices on the multi-electrode array was recorded with a light microscope. Illustrative images of dorsal and ventral hippocampal slices are in Figure 4A and Figure 4B. However, evoked waveform shapes was used as a gold standard to determine the

location of the first row of electrodes, the 100 μm recording point to the neuronal soma. It has been revealed that the evoked responses can be identified according to distance to soma depending on the shape of the waveform (A. Kolta et al., 1995). Previous current-source density analysis study revealed observations that the negative deflection of the evoked responses will decrease when approaching the soma and that at the soma the response will become a positive peak when an electrical stimulation is applied to the SR (Arlette Kolta et al., 1996). Methods to determine the location of the 100 μm are as described in details in chapter 4.3.3.

5.2.4 Input/Output Curve

An input-output curve was made to determine the test stimulation intensity needed to evoke a response eliciting 30-60% of the maximal fEPSP at the channel that was 100 μm horizontally from the point of stimulus towards the subiculum. To measure the input-output (IO) relationship, fEPSP amplitudes was recorded against increasing stimulation intensities at increments of 5 μA. Maximum fEPSP amplitude would be defined as occurring immediately before the waveform shows contamination from other sources.

5.3.5 Methylmercury-Tetanus Experiment Flow

Stable baseline activity was recorded for a minimum of 20 minutes before perfusion with either 0, 0.1, 1, or 5 μM MeHg (Sigma-Aldrich) containing ACSF, which would last for the remainder of the experiment. Tetanus was applied 10 minutes after MeHg ACSF perfusion. Recordings were continued for at least 30 minutes. Evoked responses were recorded for another 30 minutes post-tetanus. As a result, the experiment was divided into three phases in the proceeding order: 1. Baseline, 2. MeHg (0, 0.1, 1, or 5 μM) 3. MeHg-LTP (0, 0.1, 1, or 5 μM). A schematic representation is illustrated in Figure 5.1. The average change over baseline in the last

10 minutes of baseline, MeHg (0, 0.1, 1, or 5 µM), and recording was taken as baseline, MeHg (0, 0.1, 1, or 5 µM), and LTP phase.

Phase: Baseline	Phase: MeHg	Phase: None	Phase: MeHg-LTP
20 Min	20 Min	Apply Tetanus	30 Min

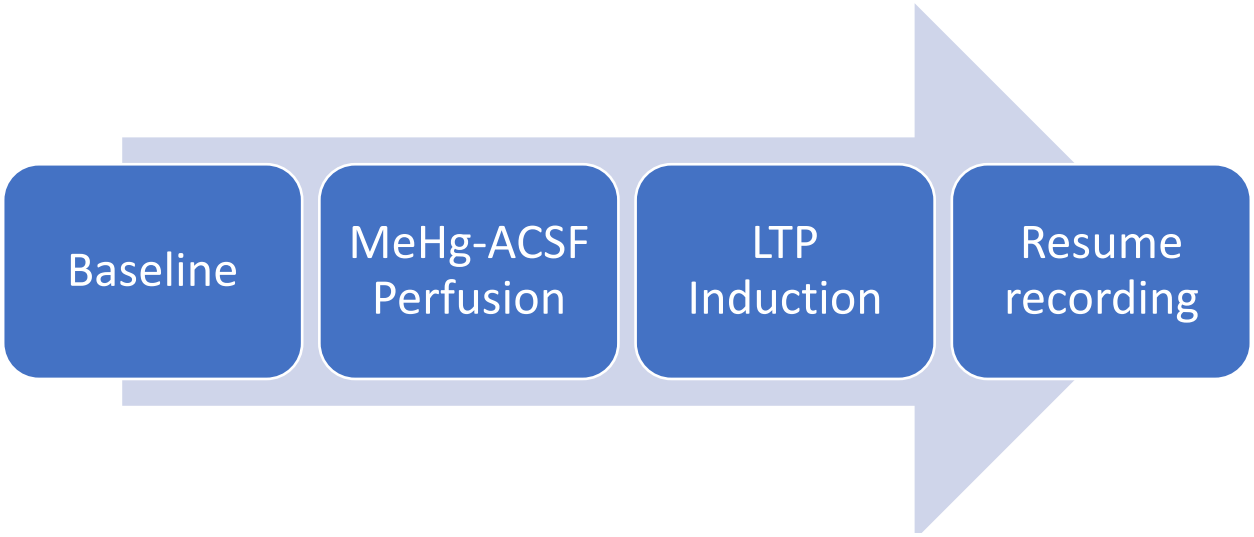

Figure 5.1. MeHg-Tetanus Experiment Flow. Overall flow of an individual MeHg tetanus experiment. After establishing 20 minutes of stable baseline, MeHg-ACSF perfusion began and persisted throughout the experiment. After 20 minutes of MeHg perfusion, tetanus was applied and recording was resumed for 30 minutes.

5.3.6 Data Analysis

All data was be exported in csv (comma separated values) format and processed using python (3.2). To eliminate any fluctuations during pre-stimulations, all points of the waveform was subtracted by the average of all points in the first 4 ms (pre-stimulus). Further analysis of the waveform were conducted in python version 3.6 (Additional Packages: Matplotlib 2.1.0, NumPy 1.16, Pandas 0.24.2) or R version 3.5.0 (Additional Packages: emmeans 1.3.3, ggplot2 3.1.0, gridExtra 2.3, nlme 3.1-130).

5.4 Results

Currently, an N of 1 for most doses and no control (MeHg 0 μM) was collected. Hence, no statistical analysis was conducted. Instead, only observations from the available data were made.

5.4.1 Effects of Methylmercury on fEPSP Results

The results of fEPSP in dorsal and ventral are illustrated Figure 5.2 and Figure 5.3, respectively. In both poles and at all recording distances, no obvious change in basal synaptic fEPSP transmission can be observed during the MeHg perfusion at all doses before the application of tetanus. Since no control (MeHg 0 μM) was present in the current results, 0.1 μM was considered as a reference point. Compared to ventral slices, it would seem that 1 μM is able to inhibit the expression of LTP in dorsal slices. This effect is particularly notable when compared at the more proximal recording points (100-300 μm to soma). In contrast, 5 μM would seem to increase potentiation in both ventral and dorsal slices. Moreover, this increase in potentiation seems to present at more distal recording points (300-600 μm). Most importantly, it can be observed that MeHg effects on fEPSP is directly proportional do dose, i.e. higher MeHg levels, higher LTP levels in both ventral and dorsal hippocampal slices.

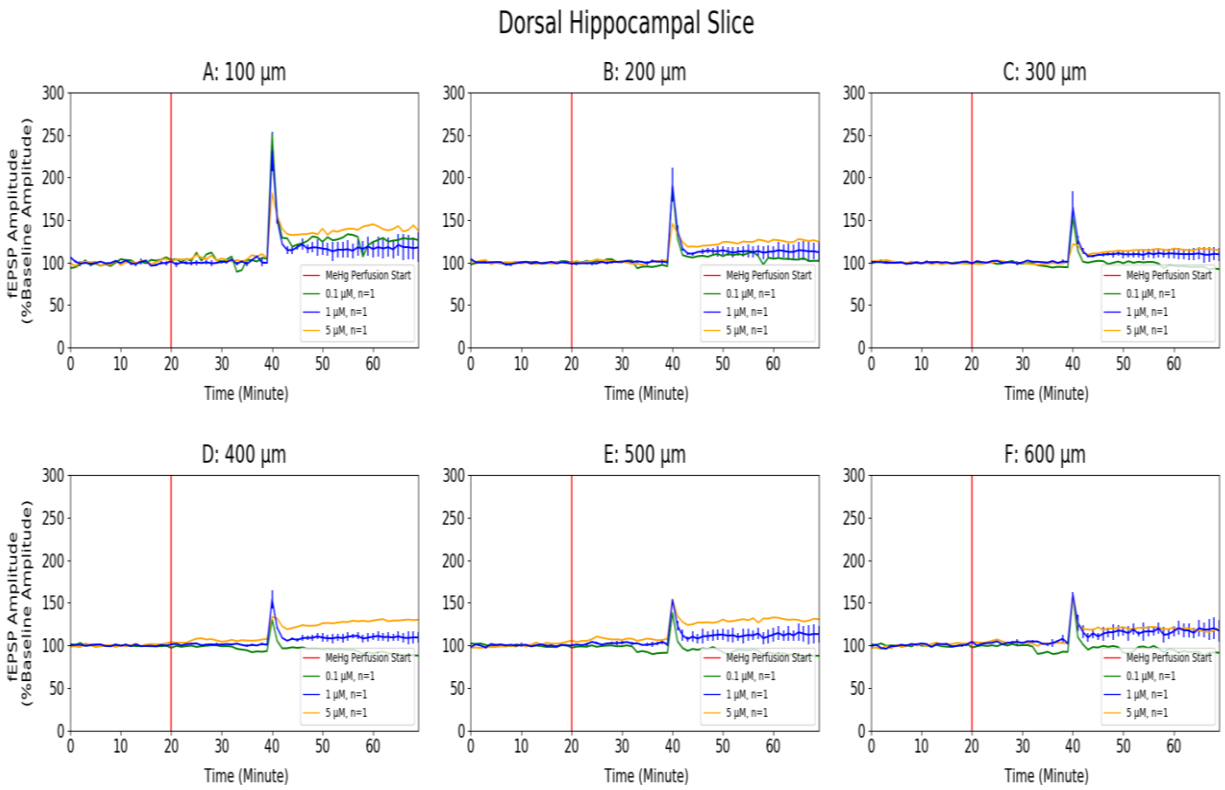

Figure 5.2 MeHg fEPSP Experiment Recording Across Time in Dorsal Hippocampal Slices
A: fEPSP at 100 µm. B: fEPSP at 200 µm/ C: fEPSP at 300 µm. D: fEPSP at 400 µm. E. fEPSP at 500 µm. F: fEPSP at 600 µm. Data: Mean+/SEM

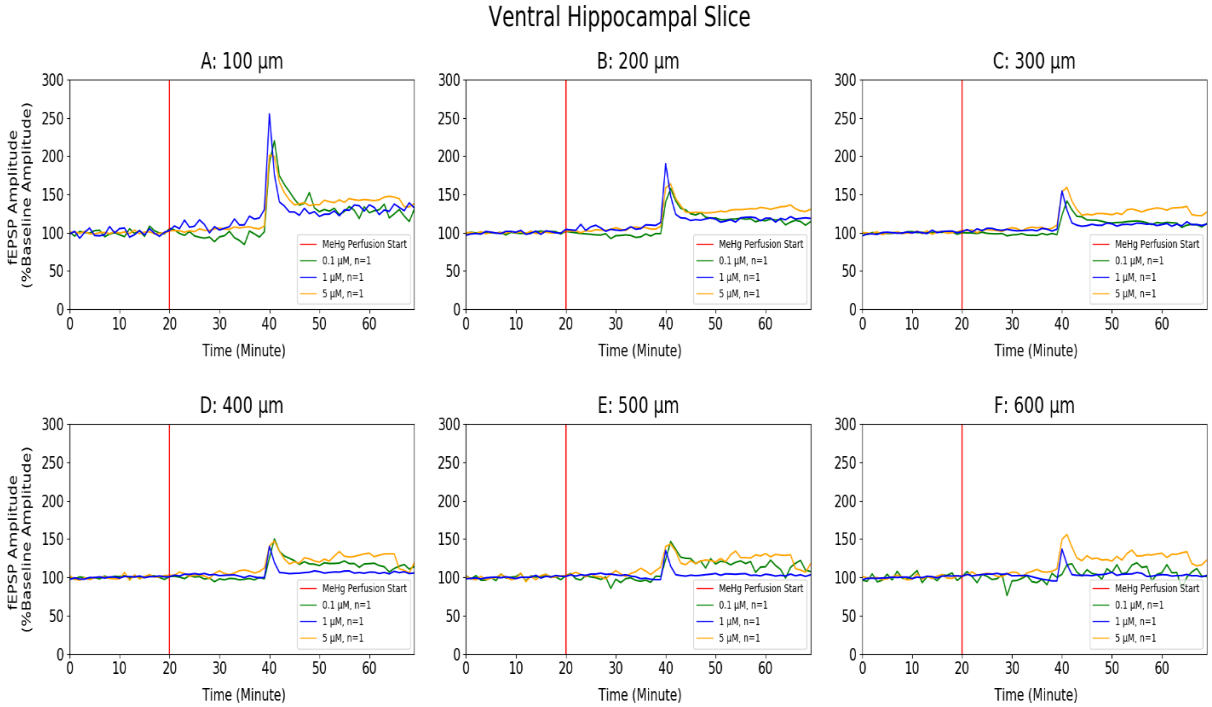

Figure 5.3 MeHg fEPSP Experiment Recording Across Time in Ventral Hippocampal Slices
A: fEPSP at 100 µm. B: fEPSP at 200 µm C: fEPSP at 300 µm. D: fEPSP at 400 µm. E. fEPSP at 500 µm. F: fEPSP at 600 µm

5.4.2 Effects of Methylmercury on PGA Results

The results of PGA in dorsal and ventral are illustrated Figure 5.3 and Figure 5.4, respectively. In both poles and at all recording distances, no obvious change in basal synaptic PGA transmission can be observed during the MeHg perfusion at all doses before the application of tetanus. Since no control (MeHg 0 μM) is present in the current results, 0.1 μM would be considered as a reference point. No obvious effect of MeHg at all doses can be observed in the dorsal hippocampal slice. In contrast, there was a trend of increased PGA potentiation at more distal recording points, namely the 400 and 500 μm point, by 5 μM MeHg treatment.

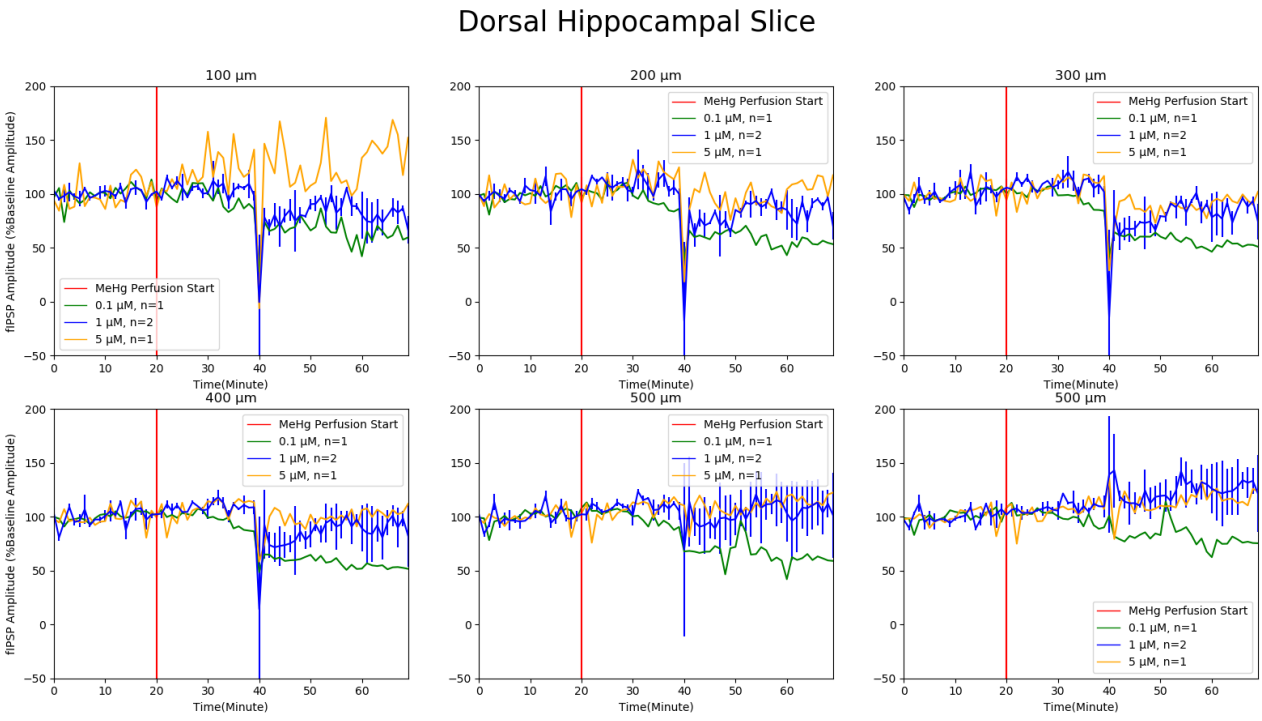

Figure 5.4 MeHg PGA Experiment Recording Across Time in Dorsal Hippocampal Slices A: PGA at 100 μm. B: PGA at 200 μm C: PGA at 300 μm. D: PGA at 400 μm. E. PGA at 500 μm. F: PGA at 600 μm. Data: Mean+/SEM

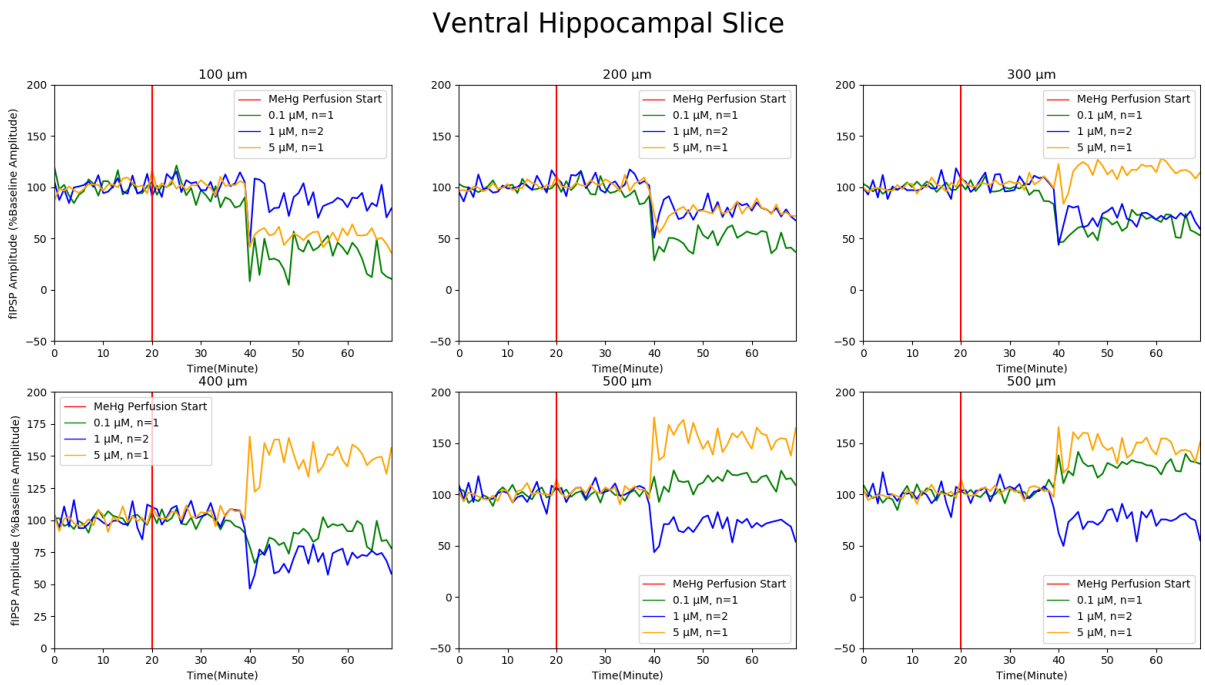

Figure 5.5 MeHg PGA Experiment Recording Across Time in Ventral Hippocampal Slices A: PGA at 100 µm. B: PGA at 200 µm C: PGA at 300 µm. D: PGA at 400 µm. E. PGA at 500 µm. F: PGA at 600 µm

5.5 Discussion

Although previous studies have paved the way for understanding MeHg toxicity, the majority of evoked response studies in acute hippocampal slices were difficult to interpret due to limitation of physiological knowledge and technical capabilities of the time when conducting experiments. First, these studies only described effects of MeHg at high physiological irrelevant levels, the minimum being 20 μM, which is hundreds of folds above normal levels observed in most populations (Fountain & Rowan, 2000; Gutiérrez et al., 2018; Yuan & Atchison, 1995; Yuan & Atchison, 1993). From a technical perspective, some of these studies also suffered from problematic recording methods as a lot of electrical noise can be seen in their representative evoked waveform traces (Yuan & Atchison, 1995; Yuan & Atchison, 1993). Most importantly, it is very difficult to interpret the effects of MeHg on synaptic plasticity expression, namely LTP, due to the use of non-standard experimental procedures. To my knowledge, all studies induced LTP either when no stable baseline was established (Yuan & Atchison, 1993), or at increased magnitudes of electrical stimulation compared to baseline (Gutiérrez et al., 2018). Therefore, it is nearly impossible to differentiate the effects of MeHg on synaptic plasticity from: 1. Existing effects on basal synaptic transmission and 2. Increased basal stimulation magnitude. The role of MeHg on fEPSP and PGA was evaluated using nominal concentrations. Future work should investigate the extent to which MeHg was absorbed into the tissue slices during the tissue exposure protocol.

Although the current study suffers from having a single point of observation at each dose level, these preliminary results show that basal synaptic transmission does not seem to be affected by the application of MeHg at all dose levels. Most importantly, the newly developed method may allow for the detection of MeHg effects on GABA mediated action on the post-

synaptic membrane. Compared to APV treatment, some degree of fEPSP potentiation is still maintained and that the magnitude of potentiation seems to be proportional to MeHg levels while within 0.1-5 μM range. Excitingly, there is a trend that indicates 5 μM can increase potentiation of GABA transmission/PGA at distal recording points to neuronal soma in both dorsal and ventral hippocampal slices.

5.6 Conclusion

In summary, a larger sample size is needed to make any conclusion regarding the effects of MeHg on synaptic plasticity. However, this study provides a practical means of investigating the prime targets of MeHg action: 1. Glutamate and 2. GABA transmission in a cellar model of memory and learning which are presumed to be affected at lower levels of MeHg exposure. Some degrees of evidence for increased excitability of GABA transmission post-tetanus can be observed. At least in the current study, the level of fEPSP inhibition observed at 1 μM MeHg appeared greater than observed at 5 μM. Further, previous evidence has shown little to no effect at higher does (5 μM and 10 μM), This suggests that MeHg effects on fEPSP inhibition could be non-monotonic. This underscores the importance of running the experiments at several intermediary MeHg concentrations in order to better describe the dose response curve. Only after this dose response curve has been established for MeHg could this model be used for assessing the ability of nutrients (e.g., selenium, omega-3 fatty acids) to alter the slope or threshold of the dose response curve.

6.0 Thesis Conclusion

In summary, the current study has accomplished two goals: i) establish a standard experimental protocol and analytical methodology using MEA to investigate LTP in acute hippocampal CA1 region and ii) showed preliminary evidence of MeHg actions on synaptic plasticity.

6.1 Basic electrophysiology/ MEA Protocol Development

To knowledge, this thesis document is the first to show that LTP (fEPSP potentiation) expression varies as a function of both recording distance to soma and tissue of origin along the longitudinal axis. Moreover, in addition to analyzing fEPSP (initial negative aspect in apical dendritic evoked response), it was also found that PGA (later and long acting positive going component) contributes significantly to the overall variation of the evoked response during LTP induction and expression. Some interesting observation were also made. An fEPSP potentiation gradient that is inversely proportional to the distance of the recording point to the neuronal soma was found in the CA1 region of ventral hippocampal slices. In contrast, this gradient is less noticeable in CA1 region of dorsal slices. Although great effort has been made to ensure the electrode locations in each experiment, it is important to recognize that there may be overlap of the location of one recording point in one experiment to another. Despite this limitation, the gradient phenomena in post-tetanus fEPSP and PGA amplitude was still robust enough to be observed. Most importantly, it is still yet to be determined if the phenomenon is of biological origin or an experimental artifact such as cells at distal recording points receiving less stimulation.

Interesting observation and interpretation were also made in the APV-LTP experiment. It was observed that dorsal as opposed to ventral slices, dorsal slices can exhibit NMDA-independent potentiation to some degree. In regards to PGA, a potentiation gradient that is directly proportional to distance of the recording point to the soma which has a NMDA dependent component in both poles. Furthermore, an inverse relation where if fEPSP potentiates, PGA depresses and vice reverse along the apical dendritic field is observed. Interestingly, APV further demonstrated that the expression of LTP in slices of different origin along the longitudinal axis may be altered to different degree by different drugs or toxicants. All related questions proposed including effects of recording distance, pole of origin, sex and effects of APV on LTP were sufficiently answered.

Overall, the basic physiology/ MEA protocol development section established a more standard and sensitive procedure to record and analyze LTP studies of acute hippocampal slices. Mainly, there is a need to stratify recording and analysis by pole of origin and recording distance to the neuronal soma. Furthermore, these findings can also be applied in investigating cultured hippocampal evoked or spontaneous field potentials. The importance of recording distance to the neuronal soma can also be extended to evoked potential investigating other slice tissue types such cortical or cerebellum.

For future directions, a control level, i.e., 0 μM APV, should be added to the APV-Tetanus experiments which can further ensure that no artificial effect (mainly mechanical) were present in the result. Most importantly, the study would benefit greatly from testing the effects of a GABA antagonist, such as bicuculline, on PGA changes during basal transmission and tetanus application.

6.2 Preliminary Results of Methylmercury Effects on Synaptic Plasticity

Using the developed MEA protocol for studying LTP in acute hippocampal slices, the current study shows preliminary results describing the effects of MeHg on synaptic plasticity. Current results suggest that at levels regularly seen in North American populations, MeHg does not affect basal synaptic transmission, fEPSP or PGA, of evoked responses in the CA1 region hippocampus. Moreover, MeHg does not seem to impede or block tetanus induced potentiation (LTP) at the doses used. Most importantly, there is evidence indicating that MeHg can affect both fEPSP and PGA of the evoked response. Taken into account previous studies that have shown complete decay of the evoke response, the effects of MeHg on fEPSP and PGA may not be monotonic. Several additional intermediary dose levels less than 5 μM MeHg to describe the shape of the dose-response curve. Moreover, the use of absorbed tissue concentrations (rather than nominal dose levels) may shed light on these observations.

However, the current results cannot fully describe MeHg effects on synaptic plasticity with confidence. An improvement in the sample size is needed, ideally to N = 3 for each concentration across the longitudinal axis, for conclusive statements to be made about the effects of MeHg on synaptic plasticity. Furthermore, a negative control (0 μM MeHg) is urgently needed to exclude any artificial effect induced by switching the solution perfused. Most importantly, it would be advised in the future to measure the actual MeHg concentration in the tissue after perfusion as the nominal concentration (applied dose levels) may not correlate linearly with tissue MeHg concentrations.

Bibliography

Albrecht, J., Talbot, M., Kimelberg, H. K., & Aschner, M. (1993). The role of sulfhydryl groups and calcium in the mercuric chloride-induced inhibition of glutamate uptake in rat primary astrocyte cultures. *Brain Research*, *607*(1), 249–254. https://doi.org/10.1016/0006-8993(93)91513-R

Amaral, D. G., Scharfman, H. E., & Lavenex, P. (2007). The dentate gyrus: Fundamental neuroanatomical organization (dentate gyrus for dummies). *Progress in Brain Research*, *163*, 3–22. https://doi.org/10.1016/S0079-6123(07)63001-5

Andersen, P., Bliss, T. V. P., & Skrede, K. K. (1971). Lamellar organization of hippocampal excitatory pathways. *Experimental Brain Research*, *13*(2), 222–238. https://doi.org/10.1007/BF00234087

Arai, A., Silberg, J., & Lynch, G. (1995). Differences in the refractory properties of two distinct inhibitory circuitries in field CA1 of the hippocampus. *Brain Research*, *704*(2), 298–306. https://doi.org/10.1016/0006-8993(95)01137-4

Araki, K., Wakabayashi, M., Sakimura, K., Kushiya, E., Ozawa, H., Kumamoto, T., & Takahashi, Y. (1981). Decreased uptake of GABA by dorsal ganglia in methylmercury-treated rats. *Neurotoxicology*, *2*(3), 557–566.

Ashton, D., Van Reempts, J., Haseldonckx, M., & Willems, R. (1989). Dorsal-ventral gradient in vulnerability of CA1 hippocampus to ischemia: A combined histological and electrophysiological study. *Brain Research*, *487*(2), 368–372. https://doi.org/10.1016/0006-8993(89)90842-1

Astrelin, A. V., Sokolov, M. V., Behnisch, T., Reymann, K. G., & Voronin, L. L. (1998). Principal component analysis of minimal excitatory postsynaptic potentials. *Journal of Neuroscience Methods, 79*(2), 169–186.

Babiec, W. E., Jami, S. A., Guglietta, R., Chen, P. B., & O'Dell, T. J. (2017). Differential regulation of NMDA receptor-mediated transmission by SK channels underlies dorsal-ventral differences in dynamics of Schaffer collateral synaptic function. *The Journal of Neuroscience*, *37*(7), 1950–1964. https://doi.org/10.1523/JNEUROSCI.3196-16.2017

Berger-Sweeney, J., Arnold, A., Gabeau, D., & Mills, J. (1995). Sex differences in learning and memory in mice: Effects of sequence of testing and cholinergic blockade. *Behavioral Neuroscience*, *109*(5), 859–873.

Björklund, O., Kahlström, J., Salmi, P., Ogren, S. O., Vahter, M., Chen, J.-F., … Daré, E. (2007). The effects of methylmercury on motor activity are sex- and age-dependent, and modulated by genetic deletion of adenosine receptors and caffeine administration. *Toxicology*, *241*(3), 119–133. https://doi.org/10.1016/j.tox.2007.08.092

Bliss, T. V., & Collingridge, G. L. (2013). Expression of NMDA receptor-dependent LTP in the hippocampus: Bridging the divide. *Molecular Brain*, *6*, 5. https://doi.org/10.1186/1756-6606-6-5

Bliss, T. V. P., & Collingridge, G. L. (1993). A synaptic model of memory: Long-term potentiation in the hippocampus. *Nature*, *361*(6407), 31. https://doi.org/10.1038/361031a0

Bliss, Tim V.P., Collingridge, G. L., Morris, R. G. M., & Reymann, K. G. (2018). Long-term potentiation in the hippocampus: Discovery, mechanisms and function. *Neuroforum*, *24*(3), A103–A120. https://doi.org/10.1515/nf-2017-A059

Bradford, A. B., Mancini, J. D., & Atchison, W. D. (2016). Methylmercury-dependent increases in Fluo4 fluorescence in neonatal rat cerebellar slices depend on granule cell migrational stage and GABAA receptor modulation. *Journal of Pharmacology and Experimental Therapeutics*, *356*(1), 2–12. https://doi.org/10.1124/jpet.115.226761

Bunsey, M., & Eichenbaum, H. (1996). Conservation of hippocampal memory function in rats and humans. *Nature*, *379*(6562), 255–257. https://doi.org/10.1038/379255a0

Cahill, L. (2006). Why sex matters for neuroscience. *Nature Reviews Neuroscience*, *7*(6), 477–484. https://doi.org/10.1038/nrn1909

Carey, G. (2012). *Quantitative Methods In Neuroscience*. University of Colorado.

Chapman, R. M., & Mccrary, J. W. (1995). EP component identification and measurement by principal components-analysis. *Brain and Cognition*, *27*(3), 288–310. https://doi.org/10.1006/brcg.1995.1024

Cohen, A. S., Coussens, C. M., Raymond, C. R., & Abraham, W. C. (1999). Long-lasting increase in cellular excitability associated with the priming of LTP induction in rat hippocampus. *Journal of Neurophysiology*, *82*(6), 3139–3148. https://doi.org/10.1152/jn.1999.82.6.3139

Colavita, M., Terral, G., Lemercier, C. E., Drago, F., Marsicano, G., & Massa, F. (2016). Layer-specific potentiation of network GABAergic inhibition in the CA1 area of the hippocampus. *Scientific Reports*, *6*. https://doi.org/10.1038/srep28454

Collingridge, G. L., Kehl, S. J., & McLennan, H. (1983). The antagonism of amino acid-induced excitations of rat hippocampal CA1 neurones in vitro. *The Journal of Physiology*, *334*, 19–31.

Cowan, A. I., Stricker, C., Reece, L. J., & Redman, S. J. (1998). Long-term plasticity at excitatory synapses on Aspinous interneurons in area CA1 lacks synaptic specificity. *Journal of Neurophysiology*, *79*(1), 13–20. https://doi.org/10.1152/jn.1998.79.1.13

Crump, K. S., Kjellström, T., Shipp, A. M., Silvers, A., & Stewart, A. (1998). Influence of prenatal mercury exposure upon scholastic and psychological test performance: benchmark analysis of a new zealand cohort. *Risk Analysis*, *18*(6), 701–713. https://doi.org/10.1023/B:RIAN.0000005917.52151.e6

Dasari, S., & Yuan, Y. (2010). In vivo methylmercury exposure induced long-lasting epileptiform activity in layer II/III neurons in cortical slices from the rat. *Toxicology Letters*, *193*(2), 138–143. https://doi.org/10.1016/j.toxlet.2009.12.017

Debes, F., Weihe, P., & Grandjean, P. (2016). Cognitive deficits at age 22 years associated with prenatal exposure to methylmercury. *Cortex*, *74*, 358–369. https://doi.org/10.1016/j.cortex.2015.05.017

Delgado, J. Y., Fink, A. E., Grant, S. G. N., O'Dell, T. J., & Opazo, P. (2018). Rapid homeostatic downregulation of LTP by extrasynaptic GluN2B receptors. *Journal of Neurophysiology*, *120*(5), 2351–2357. https://doi.org/10.1152/jn.00421.2018

Derks, N. A. V., Krugers, H. J., Hoogenraad, C. C., Joëls, M., & Sarabdjitsingh, R. A. (2016). effects of early life stress on synaptic plasticity in the developing hippocampus of male and female Rats. *PloS One*, *11*(10), e0164551. https://doi.org/10.1371/journal.pone.0164551

dos Santos, A. A., Hort, M. A., Culbreth, M., López-Granero, C., Farina, M., Rocha, J. B., & Aschner, M. (2016). Methylmercury and brain development: A review of recent literature. *Journal of Trace Elements in Medicine and Biology : Organ of the Society for*

Minerals and Trace Elements (GMS), *38*, 99–107. https://doi.org/10.1016/j.jtemb.2016.03.001

Dougherty, K. A., Islam, T., & Johnston, D. (2012). Intrinsic excitability of CA1 pyramidal neurones from the rat dorsal and ventral hippocampus. *The Journal of Physiology*, *590*(Pt 22), 5707–5722. https://doi.org/10.1113/jphysiol.2012.242693

Dougherty, K. A., Nicholson, D. A., Diaz, L., Buss, E. W., Neuman, K. M., Chetkovich, D. M., & Johnston, D. (2013). Differential expression of HCN subunits alters voltage-dependent gating of h-channels in CA1 pyramidal neurons from dorsal and ventral hippocampus. *Journal of Neurophysiology*, *109*(7), 1940–1953. https://doi.org/10.1152/jn.00010.2013

Dubovyk, V., & Manahan-Vaughan, D. (2018). Less means more: The magnitude of synaptic plasticity along the hippocampal dorso-ventral axis is inversely related to the expression levels of plasticity-related neurotransmitter receptors. *Hippocampus*, *28*(2), 136–150. https://doi.org/10.1002/hipo.22816

Edelmann, E., Cepeda-Prado, E., & Leßmann, V. (2017). Coexistence of multiple types of synaptic plasticity in individual hippocampal CA1 pyramidal neurons. *Frontiers in Synaptic Neuroscience*, *9*. https://doi.org/10.3389/fnsyn.2017.00007

Ekino, S., Susa, M., Ninomiya, T., Imamura, K., & Kitamura, T. (2007). Minamata disease revisited: An update on the acute and chronic manifestations of methyl mercury poisoning. *Journal of the Neurological Sciences*, *262*(1), 131–144. https://doi.org/10.1016/j.jns.2007.06.036

Falluel-Morel, A., Sokolowski, K., Sisti, H. M., Zhou, X., Shors, T. J., & DiCicco-Bloom, E. (2007). Developmental mercury exposure elicits acute hippocampal cell death, reductions

in neurogenesis, and severe learning deficits during puberty. *Journal of Neurochemistry*, *103*(5), 1968–1981. https://doi.org/10.1111/j.1471-4159.2007.04882.x

Fanselow, M. S., & Dong, H.-W. (2010). Are the dorsal and ventral hippocampus functionally distinct structures? *Neuron*, *65*(1), 7–19. https://doi.org/10.1016/j.neuron.2009.11.031

Fountain, S. B., & Rowan, J. D. (2000). Effects of sequential exposure to multiple concentrations of methylmercury in the rat hippocampal slice. *Ecotoxicology and Environmental Safety*, *47*(2), 130–136. https://doi.org/10.1006/eesa.2000.1941

Gao, Y., Ding, Y., Shi, R., & Tian, Y. (2008). Effects of methylmercury on postnatal neurobehavioral development in mice. *Neurotoxicology and Teratology*, *30*(6), 462–467. https://doi.org/10.1016/j.ntt.2008.07.004

Glass, G. V., Peckham, P. D., & Sanders, J. R. (1972). Consequences of failure to meet assumptions underlying the fixed effects analyses of variance and covariance. *Review of Educational Research*, *42*(3), 237–288. https://doi.org/10.3102/00346543042003237

Gonçalves, J. T., Schafer, S. T., & Gage, F. H. (2016). Adult neurogenesis in the hippocampus: from stem cells to behavior. *Cell*, *167*(4), 897–914. https://doi.org/10.1016/j.cell.2016.10.021

Grandjean, P., & Herz, K. T. (2011). Brain development and methylmercury: underestimation of neurotoxicity. *The Mount Sinai Journal of Medicine, New York*, *78*(1), 107–118. https://doi.org/10.1002/msj.20228

Grigoryan, G., Ardi, Z., Albrecht, A., Richter-Levin, G., & Segal, M. (2015). Juvenile stress alters LTP in ventral hippocampal slices: Involvement of noradrenergic mechanisms. *Behavioural Brain Research*, *278*, 559–562. https://doi.org/10.1016/j.bbr.2014.09.047

Gutiérrez, J., Baraibar, A. M., Albiñana, E., Velasco, P., Solís, J. M., & Hernández-Guijo, J. M. (2018). Methylmercury reduces synaptic transmission and neuronal excitability in rat hippocampal slices. *Pflügers Archiv - European Journal of Physiology*, *470*(8), 1221–1230. https://doi.org/10.1007/s00424-018-2144-x

Hansen, N., & Manahan-Vaughan, D. (2014). Dopamine D1/D5 receptors mediate informational saliency that promotes persistent hippocampal long-term plasticity. *Cerebral Cortex (New York, N.Y.: 1991)*, *24*(4), 845–858. https://doi.org/10.1093/cercor/bhs362

Harada, M. (1995). Minamata disease: methylmercury poisoning in Japan caused by environmental pollution. *CRC Critical Reviews in Toxicology*, *25*(1), 1–24. https://doi.org/10.3109/10408449509089885

Hebb, D. (n.d.). Drives and the c.n.s (conceptual nervous system). *Psychological Review*, *62*, 243–254.

Hong, Y.-S., Kim, Y.-M., & Lee, K.-E. (2012). Methylmercury exposure and health effects, methylmercury exposure and health effects. *Journal of Preventive Medicine and Public Health, Journal of Preventive Medicine and Public Health*, *45*(6), 353–363. https://doi.org/2012.45.6.353

Huang, C. S., & Narahashi, T. (1997). The role of phosphorylation in the activity and mercury modulation of GABA-induced currents in rat neurons. *Neuropharmacology*, *36*(11–12), 1631–1640.

Hulme, S. R., Jones, O. D., Raymond, C. R., Sah, P., & Abraham, W. C. (2014). Mechanisms of heterosynaptic metaplasticity. *Philosophical Transactions of the Royal Society of London. Series B, Biological Sciences*, *369*(1633), 20130148. https://doi.org/10.1098/rstb.2013.0148

Hwang, L.-L., Wang, C.-H., Li, T.-L., Chang, S.-D., Lin, L.-C., Chen, C.-P., … Chiou, L.-C. (2010). Sex differences in high-fat diet-induced obesity, metabolic alterations and learning, and synaptic plasticity deficits in mice. *Obesity (Silver Spring, Md.)*, *18*(3), 463–469. https://doi.org/10.1038/oby.2009.273

Hyer, M. M., Phillips, L. L., & Neigh, G. N. (2018). Sex differences in synaptic plasticity: Hormones and Beyond. *Frontiers in Molecular Neuroscience*, *11*. https://doi.org/10.3389/fnmol.2018.00266

Jackson, J. E. (1991). *A User's Guide to Principal Components*. Retrieved from https://www.springer.com/gp/book/9781475771077

Jain, A., Huang, G. Z., & Woolley, C. S. (2019). Latent sex differences in molecular signaling that underlies excitatory synaptic potentiation in the hippocampus. *Journal of Neuroscience*, *39*(9), 1552–1565. https://doi.org/10.1523/JNEUROSCI.1897-18.2018

Kakita, A., Wakabayashi, K., Su, M., Yoneoka, Y., Sakamoto, M., Ikuta, F., & Takahashi, H. (2000). Intrauterine methylmercury intoxication: Consequence of the inherent brain lesions and cognitive dysfunction in maturity. *Brain Research*, *877*(2), 322–330. https://doi.org/10.1016/S0006-8993(00)02717-7

Karpova, N. N., Lindholm, J. S. O., Kulesskaya, N., Onishchenko, N., Vahter, M., Popova, D., … Castrén, E. (2014). TrkB overexpression in mice buffers against memory deficits and depression-like behavior but not all anxiety- and stress-related symptoms induced by developmental exposure to methylmercury. *Frontiers in Behavioral Neuroscience*, *8*. https://doi.org/10.3389/fnbeh.2014.00315

Keralapurath, M. M., Clark, J. K., Hammond, S., & Wagner, J. J. (2014). Cocaine- or stress-induced metaplasticity of LTP in the dorsal and ventral hippocampus. *Hippocampus*, *24*(5), 577–590. https://doi.org/10.1002/hipo.22250

Kim, C. S., & Johnston, D. (2015). A1 adenosine receptor-mediated GIRK channels contribute to the resting conductance of CA1 neurons in the dorsal hippocampus. *Journal of Neurophysiology*, *113*(7), 2511–2523. https://doi.org/10.1152/jn.00951.2014

Knowles, W. D. (1992). Normal anatomy and neurophysiology of the hippocampal formation. *Journal of Clinical Neurophysiology*, *9*(2), 253–263.

Ko, M. C., Lee, M. C., Amstislavskaya, T. G., Tikhonova, M. A., Yang, Y.-L., & Lu, K.-T. (2014). Inhibition of NKCC1 attenuated hippocampal LTP formation and inhibitory Avoidance in Rat. *PLOS ONE*, *9*(11), e106692. https://doi.org/10.1371/journal.pone.0106692

Koerner, T. K., & Zhang, Y. (2017). Application of linear mixed-effects models in human neuroscience research: A comparison with pearson correlation in two auditory electrophysiology studies. *Brain Sciences*, *7*(3). https://doi.org/10.3390/brainsci7030026

Kolta, A., Larson, J., & Lynch, G. (1995). Comparison of long-term potentiation in the proximal versus distal stratum radiatum of hippocampal field CA1. *Neuroscience*, *66*(2), 277–289. https://doi.org/10.1016/0306-4522(94)00565-M

Kolta, Arlette, Ambros-Ingerson, J., & Lynch, G. (1996). Early and late components of AMPA-receptor mediated field potentials in hippocampal slices. *Brain Research*, *737*(1), 133–145. https://doi.org/10.1016/0006-8993(96)00721-4

Kopanitsa, M. V., Afinowi, N. O., & Grant, S. G. (2006). Recording long-term potentiation of synaptic transmission by three-dimensional multi-electrode arrays. *BMC Neuroscience*, *7*, 61. https://doi.org/10.1186/1471-2202-7-61

Kouvaros, S., & Papatheodoropoulos, C. (2016). Theta burst stimulation-induced LTP: Differences and similarities between the dorsal and ventral CA1 hippocampal synapses. *Hippocampus*, *26*(12), 1542–1559. https://doi.org/10.1002/hipo.22655

Kung, M. P., Kostyniak, P. J., Olson, J. R., Sansone, F. M., Nickerson, P. A., Malone, M. A., … Roth, J. A. (1989). Cell specific enzyme markers as indicators of neurotoxicity: Effects of acute exposure to methylmercury. *Neurotoxicology*, *10*(1), 41–52.

Laezza, F., & Dingledine, R. (2004). Voltage-controlled plasticity at GluR2-deficient synapses onto hippocampal interneurons. *Journal of Neurophysiology*, *92*(6), 3575–3581. https://doi.org/10.1152/jn.00425.2004

Lapham, L. W., Cernichiari, E., Cox, C., Myers, G. J., Baggs, R. B., Shamlaye, C. F., … Clarkson, T. W. (1995). An analysis of autopsy brain tissue from infants prenatally exposed to methymercury. *Neurotoxicology*, *16*(4), pp.689-704.

Lei, M., Xu, H., Li, Z., Wang, Z., O'Malley, T. T., Zhang, D., … Li, S. (2016). Soluble Aβ oligomers impair hippocampal LTP by disrupting glutamatergic/GABAergic balance. *Neurobiology of Disease*, *85*, 111–121. https://doi.org/10.1016/j.nbd.2015.10.019

Lein, P. J., Barnhart, C. D., & Pessah, I. N. (2011). Acute hippocampal slice preparation and hippocampal slice cultures. In *Methods in Molecular Biology*. *In Vitro Neurotoxicology* (pp. 115–134). https://doi.org/10.1007/978-1-61779-170-3_8

Lindström, H., Luthman, J., Oskarsson, A., Sundberg, J., & Olson, L. (1991). Effects of long-term treatment with methyl mercury on the developing rat brain. *Environmental Research*, *56*(2), 158–169.

Liu, W., Xu, Z., Yang, T., Xu, B., Deng, Y., & Feng, S. (2017). Memantine, a low-affinity NMDA receptor antagonist, protects against methylmercury-induced cytotoxicity of rat primary cultured cortical neurons, involvement of C^{2+} dyshomeostasis antagonism, and indirect antioxidation effects. *Molecular Neurobiology*, *54*(7), 5034–5050. https://doi.org/10.1007/s12035-016-0020-2

Lix, L. M., Keselman, J. C., & Keselman, H. J. (1996). Consequences of assumption violations revisited: A quantitative review of alternatives to the one-way analysis of variance "F" test. *Review of Educational Research*, *66*(4), 579–619. https://doi.org/10.2307/1170654

Maggio, N., & Segal, M. (2007). Unique regulation of long-term potentiation in the rat ventral hippocampus. *Hippocampus*, *17*(1), 10–25. https://doi.org/10.1002/hipo.20237

Maggio, N., & Segal, M. (2009). Differential corticosteroid modulation of inhibitory synaptic currents in the dorsal and ventral hippocampus. *Journal of Neuroscience*, *29*(9), 2857–2866. https://doi.org/10.1523/JNEUROSCI.4399-08.2009

Maggio, N., & Segal, M. (2012). Cellular basis of a rapid effect of mineralocorticosteroid receptors activation on LTP in ventral hippocampal slices. *Hippocampus*, *22*(2), 267–275. https://doi.org/10.1002/hipo.20893

Maggio, N., Stein, E. S., & Segal, M. (2015). Ischemic LTP: NMDA-dependency and dorso/ventral distribution within the hippocampus. *Hippocampus*, *25*(11), 1465–1471. https://doi.org/10.1002/hipo.22467

Maren, S. (1995). Sexually dimorphic perforant path long-term potentiation (LTP) in urethane-anesthetized rats. *Neuroscience Letters, 196*(2), 177–180. https://doi.org/10.1016/0304-3940(95)11869-X

McMahon, L. L., & Kauer, J. A. (1997). Hippocampal interneurons express a novel form of synaptic plasticity. *Neuron, 18*(2), 295–305. https://doi.org/10.1016/S0896-6273(00)80269-X

Menon, V., Musial, T. F., Liu, A., Katz, Y., Kath, W. L., Spruston, N., & Nicholson, D. A. (2013). Balanced synaptic impact via distance-dependent synapse distribution and complementary expression of AMPARs and NMDARs in hippocampal dendrites. *Neuron, 80*(6), 1451–1463. https://doi.org/10.1016/j.neuron.2013.09.027

Milior, G., Castro, M. A. D., Sciarria, L. P., Garofalo, S., Branchi, I., Ragozzino, D., … Maggi, L. (2016). Electrophysiological properties of CA1 pyramidal neurons along the longitudinal axis of the mouse hippocampus. *Scientific Reports, 6*. https://doi.org/10.1038/srep38242

Myers, G. J., Thurston, S. W., Pearson, A. T., Davidson, P. W., Cox, C., Shamlaye, C. F., … Clarkson, T. W. (2009). Postnatal exposure to methyl mercury from fish consumption: A review and new data from the Seychelles Child Development Study. *NeuroToxicology, 30*(3), 338–349. https://doi.org/10.1016/j.neuro.2009.01.005

Neves, G., Cooke, S. F., & Bliss, T. V. P. (2008). Synaptic plasticity, memory and the hippocampus: A neural network approach to causality. *Nature Reviews Neuroscience, 9*(1), 65–75. https://doi.org/10.1038/nrn2303

Nicholson, D. A., Trana, R., Katz, Y., Kath, W. L., Spruston, N., & Geinisman, Y. (2006). Distance-dependent differences in synapse number and AMPA receptor expression in

hippocampal CA1 pyramidal neurons. *Neuron*, *50*(3), 431–442. https://doi.org/10.1016/j.neuron.2006.03.022

Nicoll, R. A. (2017). A brief history of long-term potentiation. *Neuron*, *93*(2), 281–290. https://doi.org/10.1016/j.neuron.2016.12.015

NyÍri, G., Stephenson, F. A., Freund, T. F., & Somogyi, P. (2003). Large variability in synaptic n-methyl-d-aspartate receptor density on interneurons and a comparison with pyramidal-cell spines in the rat hippocampus. *Neuroscience*, *119*(2), 347–363. https://doi.org/10.1016/S0306-4522(03)00157-X

Oken, E., Rifas-Shiman, S. L., Amarasiriwardena, C., Jayawardene, I., Bellinger, D. C., Hibbeln, J. R., … Gillman, M. W. (2016). Maternal prenatal fish consumption and cognition in mid childhood: Mercury, fatty acids, and selenium. *Neurotoxicology and Teratology*, *57*, 71–78. https://doi.org/10.1016/j.ntt.2016.07.001

O'Kusky, J. R., & McGeer, E. G. (1989). Methylmercury-induced movement and postural disorders in developing rat: high-affinity uptake of choline, glutamate, and γ-aminobutyric acid in the cerebral cortex and caudate-putamen. *Journal of Neurochemistry*, *53*(4), 999–1006. https://doi.org/10.1111/j.1471-4159.1989.tb07386.x

Onishchenko, N., Tamm, C., Vahter, M., Hökfelt, T., Johnson, J. A., Johnson, D. A., & Ceccatelli, S. (2007). Developmental exposure to methylmercury alters learning and induces depression-like behavior in male mice. *Toxicological Sciences*, *97*(2), 428–437. https://doi.org/10.1093/toxsci/kfl199

Ouardouz, M., & Lacaille, J. C. (1995). Mechanisms of selective long-term potentiation of excitatory synapses in stratum oriens/alveus interneurons of rat hippocampal slices. *Journal of Neurophysiology*, *73*(2), 810–819. https://doi.org/10.1152/jn.1995.73.2.810

Papatheodoropoulos, C. (2015a). Higher intrinsic network excitability in ventral compared with the dorsal hippocampus is controlled less effectively by GABAB receptors. *BMC Neuroscience*, *16*. https://doi.org/10.1186/s12868-015-0213-z

Papatheodoropoulos, C. (2015b). Higher intrinsic network excitability in ventral compared with the dorsal hippocampus is controlled less effectively by GABAB receptors. *BMC Neuroscience*, *16*, 75. https://doi.org/10.1186/s12868-015-0213-z

Papatheodoropoulos, C., & Kostopoulos, G. (2000). Decreased ability of rat temporal hippocampal CA1 region to produce long-term potentiation. *Neuroscience Letters*, *279*(3), 177–180. https://doi.org/10.1016/S0304-3940(99)01002-2

Papatheodoropoulos, C., & Kouvaros, S. (2016). High-frequency stimulation-induced synaptic potentiation in dorsal and ventral CA1 hippocampal synapses: The involvement of NMDA receptors, mGluR5, and (L-type) voltage-gated calcium channels. *Learning & Memory*, *23*(9), 460–464. https://doi.org/10.1101/lm.042531.116

Pelkey, K. A., Chittajallu, R., Craig, M. T., Tricoire, L., Wester, J. C., & McBain, C. J. (2017). Hippocampal GABAergic inhibitory interneurons. *Physiological Reviews*, *97*(4), 1619–1747. https://doi.org/10.1152/physrev.00007.2017

Petroni, D., Tsai, J., Mondal, D., & George, W. (2013). Attenuation of low dose methylmercury and glutamate induced-cytotoxicity and tau phosphorylation by an N-methyl-D-aspartate antagonist in human neuroblastoma (SHSY5Y) cells. *Environmental Toxicology*, *28*(12), 700–706. https://doi.org/10.1002/tox.20765

Qi, X., Zhang, K., Xu, T., Yamaki, V. N., Wei, Z., Huang, M., … Cai, X. (2016). Sex differences in long-term potentiation at temporoammonic-ca1 synapses: potential implications for

memory consolidatio. *PloS One*, *11*(11), e0165891. https://doi.org/10.1371/journal.pone.0165891

Reich, B., Zhou, Y., Goldstein, E., Srivats, S. S., Contoreggi, N. H., Kogan, J. F., … Gray, J. D. (2019). Chronic immobilization stress primes the hippocampal opioid system for oxycodone-associated learning in female but not male rats. *Synapse (New York, N.Y.)*, *73*(5), e22088. https://doi.org/10.1002/syn.22088

Reynolds, I. J., & Hastings, T. G. (1995). Glutamate induces the production of reactive oxygen species in cultured forebrain neurons following NMDA receptor activation. *Journal of Neuroscience*, *15*(5), 3318–3327.

Rizk-Jackson, A. M., Acevedo, S. F., Inman, D., Howieson, D., Benice, T. S., & Raber, J. (2006). Effects of sex on object recognition and spatial navigation in humans. *Behavioural Brain Research*, *173*(2), 181–190. https://doi.org/10.1016/j.bbr.2006.06.029

Rothenberg, S. E., Windham-Myers, L., & Creswell, J. E. (2014). Rice methylmercury exposure and mitigation: a comprehensive review. *Environmental Research*, *0*, 407–423. https://doi.org/10.1016/j.envres.2014.03.001

Rothenberg, S. E., Yu, X., Liu, J., Biasini, F. J., Hong, C., Jiang, X., … Korrick, S. A. (2016). Maternal methylmercury exposure through rice ingestion and offspring neurodevelopment: a prospective cohort study. *International Journal of Hygiene and Environmental Health*, *219*(8), 832–842. https://doi.org/10.1016/j.ijheh.2016.07.014

Ruchi, M., Ann, D. K., Komal, P., Connor, B., & Daniel, J. (2016). Mapping the electrophysiological and morphological properties of CA1 pyramidal neurons along the longitudinal hippocampal axis. *Hippocampus*, *26*(3), 341–361. https://doi.org/10.1002/hipo.22526

Ruszkiewicz, J. A., Bowman, A. B., Farina, M., Rocha, J. B. T., & Aschner, M. (2016). Sex- and structure-specific differences in antioxidant responses to methylmercury during early development. *Neurotoxicology*, *56*, 118–126. https://doi.org/10.1016/j.neuro.2016.07.009

Sakamoto, M., Kakita, A., Bezerra de Oliveira, R., Sheng Pan, H., & Takahashi, H. (2004). Dose-dependent effects of methylmercury administered during neonatal brain spurt in rats. *Developmental Brain Research*, *152*(2), 171–176. https://doi.org/10.1016/j.devbrainres.2004.06.016

Scharfman, H. E. (1993). Characteristics of spontaneous and evoked epsps recorded from dentate spiny hilar cells in rat hippocampal slices. *Journal of Neurophysiology*, *70*(2), 742–757.

Shah, D. S., Prados, J., Gamble, J., De Lillo, C., & Gibson, C. L. (2013). Sex differences in spatial memory using serial and search tasks. *Behavioural Brain Research*, *257*, 90–99. https://doi.org/10.1016/j.bbr.2013.09.027

Sokolowski, K., Poku, M., Robinson, K., McCandlish, E., Buckley, B., & DiCicco-Bloom, E. (2013). Neural stem cell apoptosis after low methylmercury (MeHg) exposures in postnatal hippocampus produce persistent cell loss and adolescent memory deficits. *Developmental Neurobiology*, *73*(12). https://doi.org/10.1002/dneu.22119

Spruston, N. (2008). Pyramidal neurons: dendritic structure and synaptic integration. *Nature Reviews Neuroscience*, *9*(3), 206. https://doi.org/10.1038/nrn2286

Stabel, J., Wil3kirchen, T., & Heinemann, U. (1990). Laminar profiles of N-methyl-D-aspartate- and quisqualate-induced Na+ changes in rat hippocampus. *Brain Research*, *520*, 215–221.

Stern, A. H. (2005). A review of the studies of the cardiovascular health effects of methylmercury with consideration of their suitability for risk assessment. *Environmental Research*, *98*(1), 133–142. https://doi.org/10.1016/j.envres.2004.07.016

Strange, B. A., Witter, M. P., Lein, E. S., & Moser, E. I. (2014). Functional organization of the hippocampal longitudinal axis. *Nature Reviews Neuroscience*, *15*(10), 655–669. https://doi.org/10.1038/nrn3785

Suárez, L. M., Bustamante, J., Orensanz, L. M., Martín del Río, R., & Solís, J. M. (2014). Cooperation of taurine uptake and dopamine D1 receptor activation facilitates the induction of protein synthesis-dependent late LTP. *Neuropharmacology*, *79*, 101–111. https://doi.org/10.1016/j.neuropharm.2013.10.035

Tian, J., Luo, Y., Chen, W., Yang, S., Wang, H., Cui, J., … Bi, Y. (2016). Mehg suppressed neuronal potency of hippocampal Nscs contributing to the puberal spatial memory deficits. *Biological Trace Element Research*, *172*(2), 424–436. https://doi.org/10.1007/s12011-015-0609-8

Vilenchik, D., Yichye, B., & Abutbul, M. (2019). To interpret or not to interpret PCA? this is our question. *Proceedings of the International AAAI Conference on Web and Social Media*, *13*, 655–658.

Vlachos, A., Maggio, N., & Segal, M. (2008). Lack of correlation between synaptopodin expression and the ability to induce LTP in the rat dorsal and ventral hippocampus. *Hippocampus*, *18*(1), 1–4. https://doi.org/10.1002/hipo.20373

Volianskis, A., France, G., Jensen, M. S., Bortolotto, Z. A., Jane, D. E., & Collingridge, G. L. (2015). Long-term potentiation and the role of N-methyl-d-aspartate receptors. *Brain Research*, *1621*, 5–16. https://doi.org/10.1016/j.brainres.2015.01.016

Wakabayashi, K., Kakita, A., Sakamoto, M., Su, M., Iwanaga, K., & Ikuta, F. (1995). Variability of brain lesions in rats administered methylmercury at various postnatal development phases. *Brain Research*, *705*(1), 267–272. https://doi.org/10.1016/0006-8993(95)01208-7

West, B. T., Welch, K. B., Galecki, A. T., Welch, K. B., & Galecki, A. T. (2014). *Linear Mixed Models: A Practical Guide Using Statistical Software, Second Edition*. https://doi.org/10.1201/b17198

Xu, B., Xu, Z., Deng, Y., Liu, W., Yang, H., & Wei, Y.-G. (2013). MK-801 Protects against Intracellular Ca2+ Overloa ding an d Improves N-methyl- d-aspartate Receptor Expression in Cerebral Cortex of Methylmercury-Poisone d Rats. *Journal of Molecular Neuroscience*, *49*(1), 162–171. https://doi.org/10.1007/s12031-012-9926-y

Xu, X., Kang, C., & Guo, T. (2014). The Effects of Gender and Self-Insight on Early Semantic Processing. *PLoS ONE*, *9*(12). https://doi.org/10.1371/journal.pone.0114421

Yang, D.-W., Pan, B., Han, T.-Z., & Xie, W. (2004). Sexual dimorphism in the induction of LTP: Critical role of tetanizing stimulation. *Life Sciences*, *75*(1), 119–127. https://doi.org/10.1016/j.lfs.2003.12.004

Yang, T., Xu, Z., Liu, W., Xu, B., & Deng, Y. (2016). Protective effects of Alpha-lipoic acid on MeHg-induced oxidative damage and intracellular Ca2+ dyshomeostasis in primary cultured neurons. *Free Radical Research*, *50*(5), 542–556. https://doi.org/10.3109/10715762.2016.1152362

Yonker, J. E., Nilsson, L.-G., Herlitz, A., & Anthenelli, R. M. (2005). Sex differences in spatial visualization and episodic memory as a function of alcohol consumption. *Alcohol and Alcoholism*, *40*(3), 201–207. https://doi.org/10.1093/alcalc/agh141

Yuan, Y., & Atchison, W. D. (1995). Methylmercury acts at multiple sites to block hippocampal synaptic transmission. *Journal of Pharmacology and Experimental Therapeutics, 275*(3), 1308–1316.

Yuan, Y. K., & Atchison, W. D. (1993). Disruption by methylmercury of membrane excitability and synaptic transmission of ca1 neurons in hippocampal slices of the rat. *Toxicology and Applied Pharmacology*, *120*(2), 203–215. https://doi.org/10.1006/taap.1993.1104

Yuan, Yukun, & Atchison, W. D. (2003). Methylmercury differentially affects Gabaa receptor-mediated spontaneous IPSCS in purkinje and granule cells of rat cerebellar slices. *The Journal of Physiology*, *550*(1), 191–204. https://doi.org/10.1113/jphysiol.2003.040543

Yuan, Yukun, & Atchison, W. D. (2007). Methylmercury-induced increase of intracellular ca2+ increases spontaneous synaptic current frequency in rat cerebellar slices. *Molecular Pharmacology*, *71*(4), 1109–1121. https://doi.org/10.1124/mol.106.031286

Yuan, Yukun, & Atchison, W. D. (2016). Multiple sources of Ca^{2+} contribute to methylmercury-induced increased frequency of spontaneous inhibitory synaptic responses in cerebellar slices of rat. *Toxicological Sciences*, *150*(1), 117–130. https://doi.org/10.1093/toxsci/kfv314